MEMORANDUM REPORT NO. 2458

SOME AERODYNAMIC CHARACTERISTICS OF SUPERSONIC LIFTING BODIES

Charles J. Nietubicz

March 1975

USA BALLISTIC RESEARCH LABORATORIES
ABERDEEN PROVING GROUND, MARYLAND

UNCLASSIFIED

SECURITY CLASSIFICATION OF THIS PAGE *(When Data Entered)*

REPORT DOCUMENTATION PAGE		READ INSTRUCTIONS BEFORE COMPLETING FORM
1. REPORT NUMBER BRL Memorandum Report No. 2458	2. GOVT ACCESSION NO.	3. RECIPIENT'S CATALOG NUMBER
4. TITLE *(and Subtitle)* SOME AERODYNAMIC CHARACTERISTICS OF SUPERSONIC LIFTING BODIES		5. TYPE OF REPORT & PERIOD COVERED Final 6. PERFORMING ORG. REPORT NUMBER
7. AUTHOR(s) Charles J. Nietubicz		8. CONTRACT OR GRANT NUMBER(s)
9. PERFORMING ORGANIZATION NAME AND ADDRESS USA Ballistic Research Laboratories Aberdeen Proving Ground, Maryland 21005		10. PROGRAM ELEMENT, PROJECT, TASK AREA & WORK UNIT NUMBERS RDT&E 1T362301A201
11. CONTROLLING OFFICE NAME AND ADDRESS US Army Materiel Command 5001 Eisenhower Avenue Alexandria, Virginia 22304		12. REPORT DATE MARCH 1975 13. NUMBER OF PAGES 83
14. MONITORING AGENCY NAME & ADDRESS *(if different from Controlling Office)*		15. SECURITY CLASS. *(of this report)* UNCLASSIFIED 15a. DECLASSIFICATION/DOWNGRADING SCHEDULE

16. DISTRIBUTION STATEMENT *(of this Report)*

Approved for public release; distribution unlimited.

17. DISTRIBUTION STATEMENT *(of the abstract entered in Block 20, if different from Report)*

18. SUPPLEMENTARY NOTES

19. KEY WORDS *(Continue on reverse side if necessary and identify by block number)*

Wave Rider
Lifting Bodies
Wedge Shapes
Supersonic Wind Tunnel Tests

20. ABSTRACT *(Continue on reverse side if necessary and identify by block number)* (1ca)

Aerodynamic characteristics are presented for various lifting body configurations. Data were collected for an angle of attack sweep of -10° to +10° throughout a Mach number range of 1.5 to 4.0. The test Reynolds number per meter was 15.7×10^6. The data are presented as standard force coefficients which have additionally been transformed about a tunnel axis coordinate system to obtain lift and drag data. The normal force center of pressure was found to be invariant with angle of attack and Mach number for all configurations.

DD FORM 1 JAN 73 1473 EDITION OF 1 NOV 65 IS OBSOLETE

UNCLASSIFIED

SECURITY CLASSIFICATION OF THIS PAGE *(When Data Entered)*

TABLE OF CONTENTS

LIST OF ILLUSTRATIONS

LIST OF ILLUSTRATIONS (Continued)

APPENDIX ILLUSTRATIONS

LIST OF ILLUSTRATIONS (Continued)

LIST OF ILLUSTRATIONS (Continued)

I. INTRODUCTION

A series of wind tunnel tests to determine the aerodynamic characteristics of several lifting body configurations has been conducted at the Ballistic Research Laboratories (BRL). This experimental investigation was initiated by the Aerodynamics Research Branch of Edgewood Arsenal. The basic data obtained from these tests will be used as input for calculations of projectile range and altitude based on given initial conditions and aerodynamic loads. The program concept is to design a model with low overall drag and sufficient aerodynamic lift to slightly offset the effect of gravity, thereby contributing to a greater range and a flattened trajectory. Therefore, the models tested were designed with reference to the wave-rider concept, which describes a lifting body supported by a unique shock system[1]. The wind tunnel tests were conducted in three phases which covered a period from April 1972 through April 1973.

II. EXPERIMENTAL INVESTIGATION

A six component force test which included roll moment data for two configurations and base pressure data for all configurations was conducted. The test data covered a Mach number range of 1.5 through 4.0 and, with the exception of one configuration, all were tested at a constant Reynolds number per meter of 15.7×10^6. The tests were conducted in Supersonic Wind Tunnel No. 1[2] of the U.S. Army Ballistic Research Laboratories.

A. Equipment

The wind tunnel is a continuous, closed circuit, variable throat tunnel with Mach capability from 1.5 through 5.0 calibrated in 1/4 Mach number increments. The supply pressure can be varied from 5.33 to 68.9×10^4 Newton/m^2. The free stream Reynolds number has a range of 1.64×10^6 to 27.9×10^6 per meter (m) for a stagnation temperature of 311° Kelvin (K). The test section is 33 centimeters (cm) wide by 38 centimeters high and the standard angle of attack range is from +15° to -10°. An automatic roll head allows the model to be positioned throughout 270° with no interruption of air flow.

---

1. *L. F. Crabtree and D. A. Treadgold, "Experiments on Hypersonic Lifting Bodies," International Council of the Aeronautical Sciences Paper No. 66-24, September 1966.*

2. *J. C. McMullen, "Wind Tunnel Testing Facilities at the Ballistic Research Laboratories," U.S. Army Ballistic Research Laboratories Memorandum Report No. 1292, Aberdeen Proving Ground, Maryland, July 1960. AD 244180.*

The unique configuration design which follows from the wave rider concept prohibits the balance from being located within the model and near the center of pressure. Therefore, the balance was installed externally and connected to the models and strut by means of specially designed adapters. A windshield was attached to the strut and protected the balance from all extraneous forces. A sketch of this arrangement is shown in Figure 1.

The balance used to measure the aerodynamic forces and moments was a six component strain gage balance. The maximum allowable normal and side force acting between the gages are 890 Newtons (N) and 445 N respectively. The balance capacity in axial force is 334 N and the maximum roll moment is 6.77 Newton-meter (Nm).

The models are shown in Figure 2 and are identified as follows:

Model Description	Configuration No.
60° Wedge	972.0
90° Wedge	972.1
60° Wedge With Boundary Layer Trip	972.5
Flat Undersurface	972.6
Boattail	972.7
Cone Shape	972.8
Caret Shape	972.9

B. Test Procedure

Phase I involved tests of configurations 972.0 and 972.1. Phase II was an extension of the first phase and included a boundary layer trip on configuration 972.0. Phase III resulted from an evaluation of the previous data and involved testing four additional configurations.

All configurations were tested at Mach numbers 1.5, 2.0, 2.5, 3.0, 3.5 and 4.0. Configuration 972.1 was tested at the maximum allowable Reynolds number, based on load limitations, while the remaining configurations were tested at a constant Reynolds number per meter of 15.7×10^6. Most configurations covered an angle of attack range of +10° to -10° with some limitations due to excessive loads. Base pressures were measured with three 0.159 cm diameter tubes located near the model base. Roll data were determined during Phase I only. Schlieren pictures were taken at the following conditions: alpha = maximum, 0° and trim ($C_m = 0$). Color schlieren movies showing the

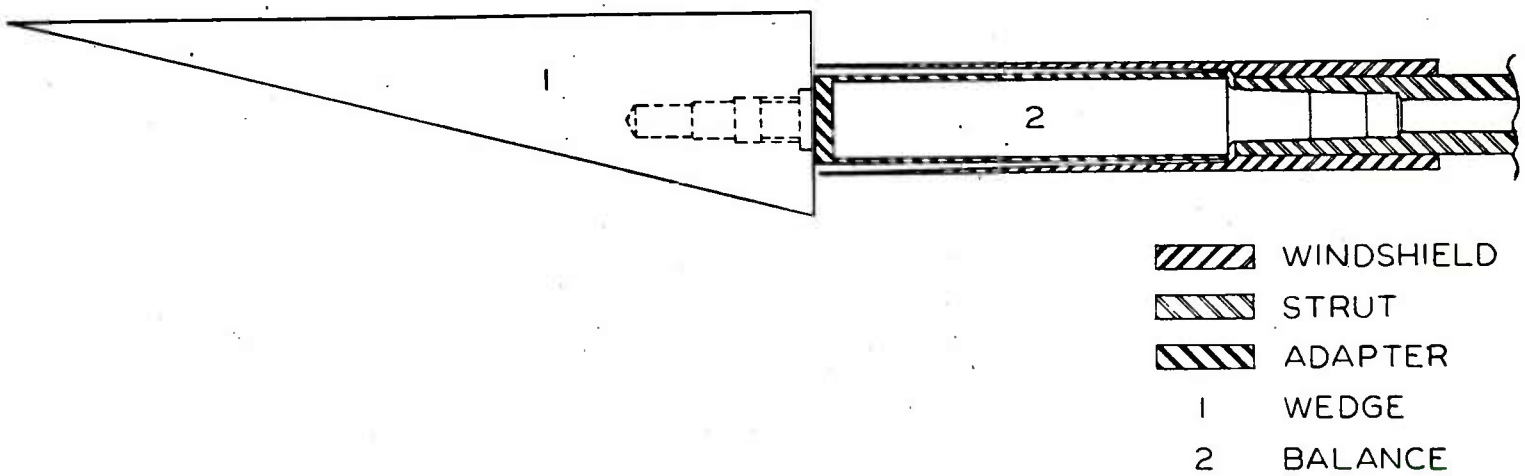

Figure 1. Model-Balance-Strut Assembly

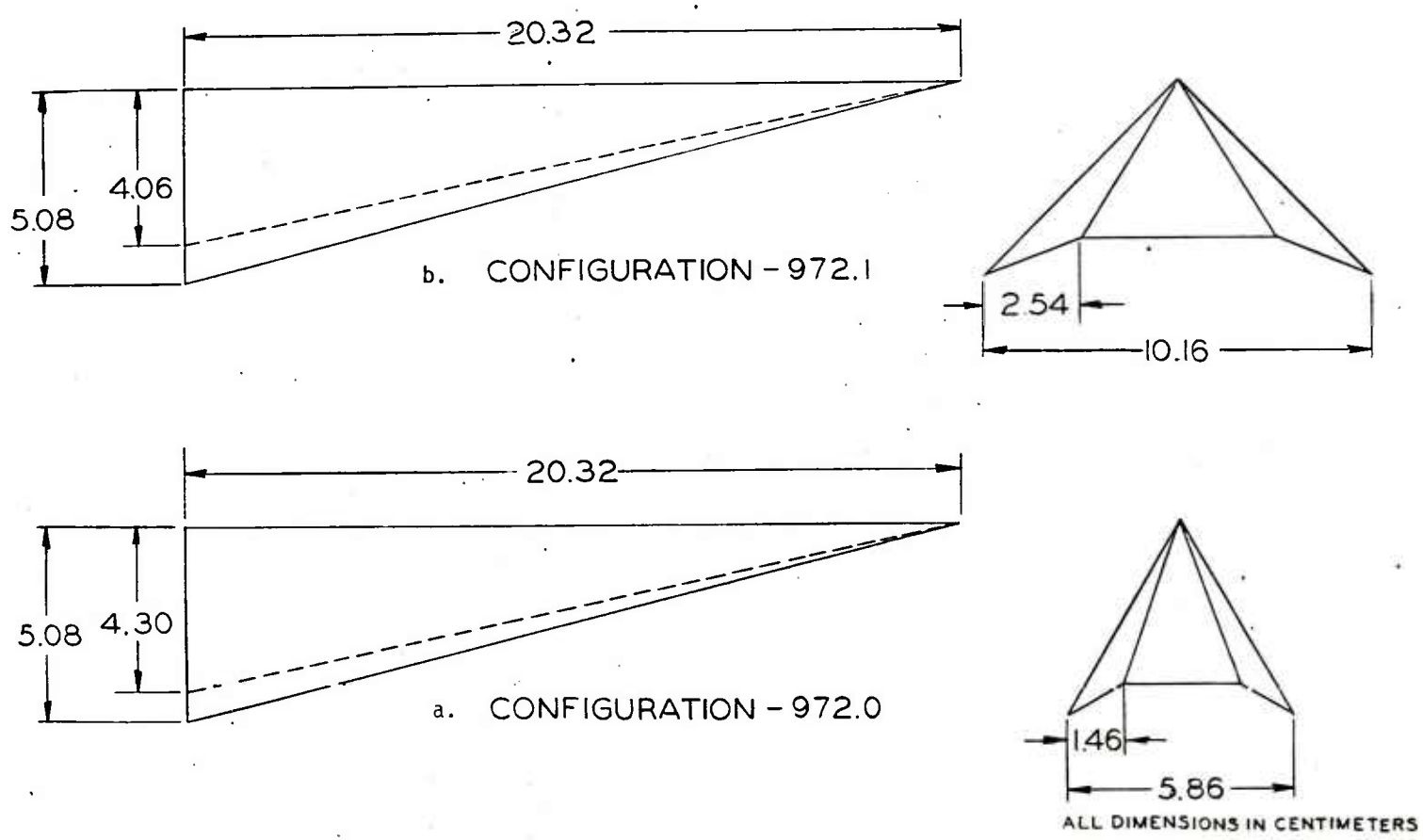

Figure 2. Model Details

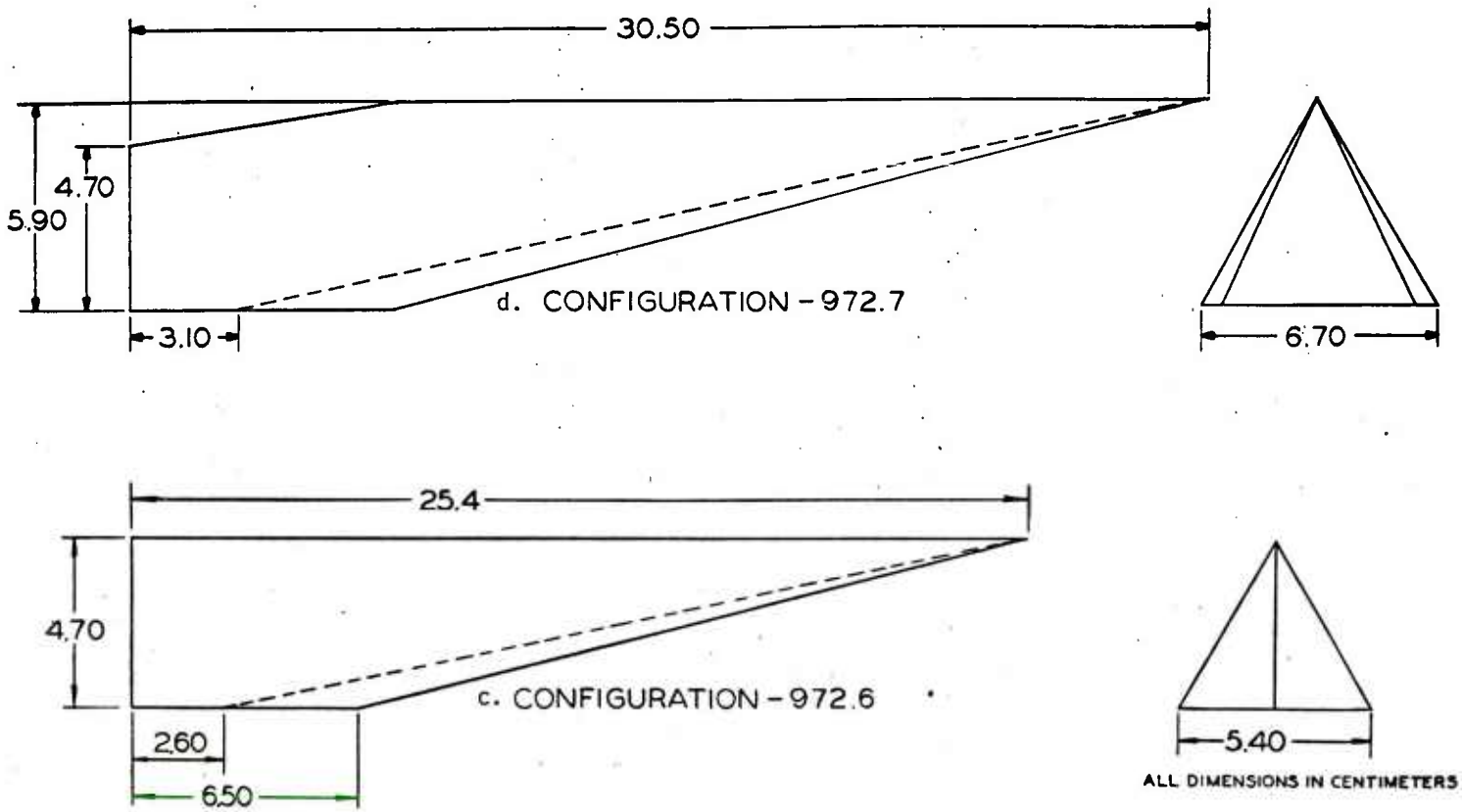

Figure 2. Continued

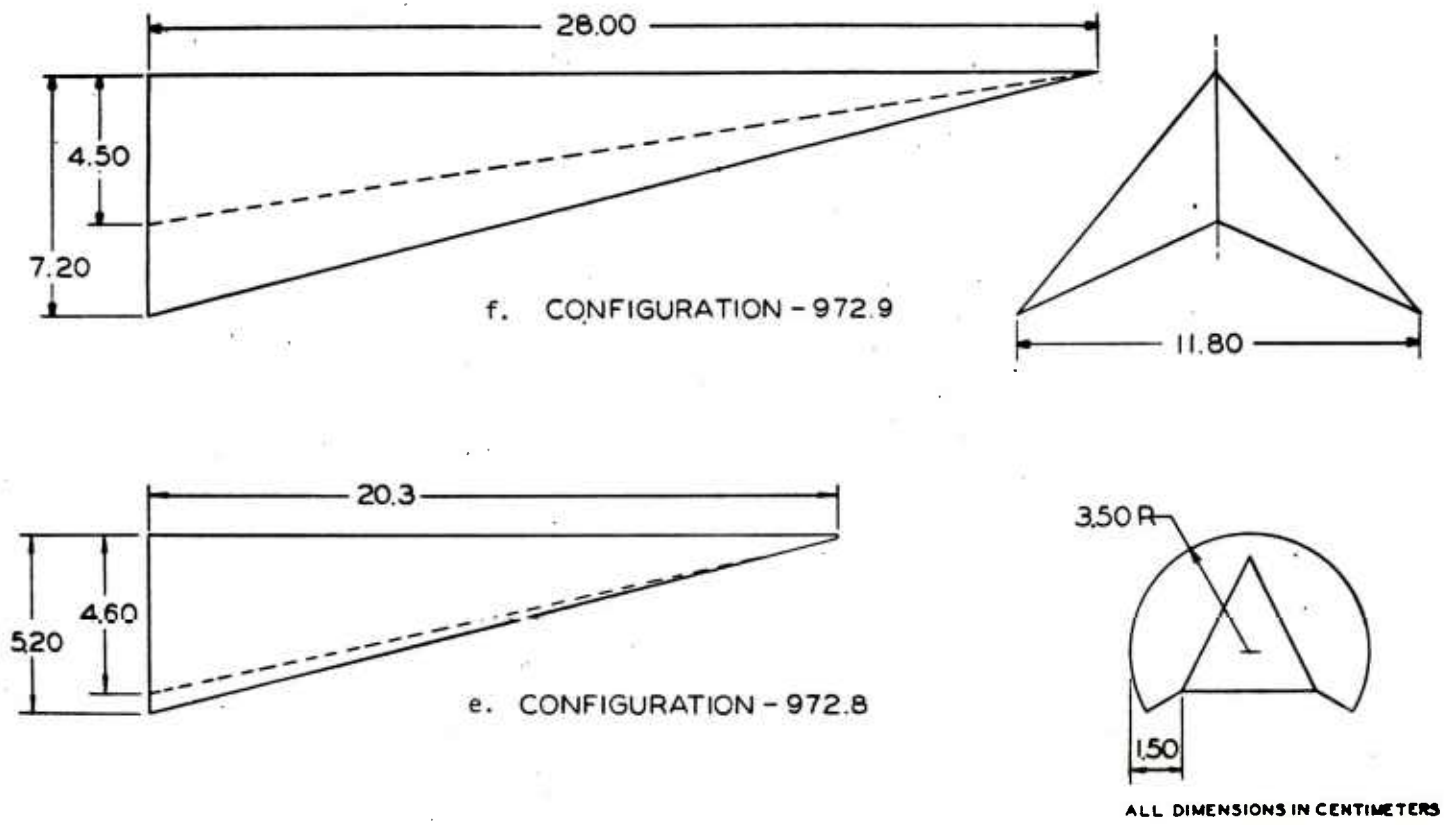

Figure 2. Concluded

effect of angle of attack variation were taken at selected Mach numbers. Vapor screen pictures[3] of selected configurations were taken during Phase III in an attempt to view the wave-rider shock pattern. Tunnel installation of configuration 972.6 is shown in Figure 3.

All data were reduced on the Ballistic Research Laboratories BRLESC computer using a standard force reduction program. The data for each phase was added sequentially to the original data tape and enhanced comparison of data between phases. Due to non-symmetry of the configurations in the pitch plane, flow inclination corrections were not applied to the data. The configurations are symmetrical in the yaw plane and flow corrections were, therefore, applied to the side force data. Strut deflections for pitch and yaw were subtracted from the appropriate data. The coefficients were reduced about a body axis system which was allowed to roll with the model.

C. Presentation of Data

The data are presented in the appendix (Figures A1 thru A7) for the following coefficients: normal force (C_N), pitching moment (C_m), axial force (C_A), normal force center of pressure (X_{CP}), side force (C_Y), yawing moment (C_n), side force center of pressure (Y_{CP}), roll moment (C_ℓ), lift (C_L), drag (C_D), and lift/drag (C_L/C_D). The data have been grouped to show the effects of Mach number variation and configuration changes on most coefficients.

Limited testing was accomplished at Edgewood Arsenal for configuration 972.0. The data are compared with BRL's results in Figures 4 through 6 for C_L, C_D, and C_L/C_D.

A subsequent pressure program was conducted at BRL for configuration 972.9. Comparison of base axial force data between the force and pressure test are presented in Figure 7.

A selected vapor screen photograph is shown in Figure 8. Figure 9 presents a schlieren photograph of configuration 972.7.

III. DISCUSSION

The results shown in Figure A1(a) are typical of the data obtained. The normal force data, C_N, are effectively nonlinear over

---

3. *C. J. Nietubicz, "Vapor Screen Technique Development at the Ballistic Research Laboratories," U.S. Army Ballistic Research Laboratories Memorandum Report No. 2387, Aberdeen Proving Ground, Maryland, June 1974. AD 784077.*

Figure 3. Model Installation of Configuration 972.6 in Tunnel No. 1

the entire range of alpha and non-symmetric with respect to alpha = 0 (top surface of model is parallel to tunnel floor; as seen in Figure 3). The largest magnitude of C_N is obtained for configurations 972.0, 979.9 and 972.1, above alpha of -6°. As the Mach number increases (Figures A1(a) through A1(f)) the effect of configuration on C_N decreases. Expectedly, configuration 972.8 shows the largest magnitude in axial force at all angles of attack. This is due to the increased base drag of the cone shaped configuration.

The normal force centers of pressure, X_{CP}, are seen in Figure A1(a) to remain constant throughout the angle of attack range and are comparable in magnitude with the exception of configurations 972.6 and 972.7. These two configurations exhibit a slight variation with angle of attack and the apparent discontinuity ($-8 \leqslant \alpha \leqslant -4$) is a result of the present method used in calculating X_{CP}. The forward shift of X_{CP} is apparently due to the square base and boattail shapes of configurations 972.6 and 972.7. The A2 series of figures show additionally X_{CP} to be invariant with respect to changing Mach number. The magnitude of X_{CP} as seen in Figure A2(a) and typical of all configurations (again, with the exception of configurations 972.6 and 972.7) has a value of approximately .33 ℓ where ℓ is the model length.

The pyramid like shape of the configurations tested suggests that the center of gravity is located at .25 ℓ. A transfer of the moment reference (presently at the model base) to the center of gravity location would rotate the present C_m curves (Figure series A1 and A2) about the point $C_m = 0$. The resultant C_{m_α} would still be positive (center of pressure forward of the center of gravity) and a slightly unstable condition, therefore, exists for all configurations. A forward movement of the center of gravity is presently required to achieve static stability. Additionally, the data show the normal force to be effectively zero at the trim condition ($C_m = 0$). Thus, the present configurations act as lifting bodies only at angles of attack other than α_{trim}.

The side force, C_Y, yawing moment, C_{YM}, and side force center of pressure, Y_{CP}, data are shown in Figures A3(a) through A3(f) as a function of yaw angle. These figures represent the variation due to configuration changes at constant Mach number. The C_Y and C_{YM} data are symmetrical with respect to $\psi = 0°$ and nonlinear over the entire angle of yaw range. Figures A4(a) through A4(f) show the effect of Mach number variation on each configuration. Again, it is interesting to note that the side force center of pressure, Y_{CP}, is independent of both Mach number and angle of yaw.

Roll moment data were obtained for configuration 972.0 and are shown in Figures A5(a) through A5(g) for various roll angles. The resultant data reveal a lack of roll stability for alpha < +4° and only a slight restoring moment for angles of attack greater than +4°. This problem area is basic to the wedge shaped configuration and necessitates the use of some type of control surface.

The initial objective of this program was to determine which configuration exhibited the highest lift over drag ratios. Therefore, the normal force data were further reduced to present lift, drag and lift/drag data which are shown in Figure series A6 and A7. Figure A6(d), which is typical of the data presented, shows configurations 972.0, 972.1 and 972.9 to have the highest magnitude of C_L/C_D above $\alpha = 0°$. However, for $\alpha < -2°$ configurations 972.7 and 972.0 exhibit the largest value of C_L/C_D. This is further represented in Figures A7(a) and A7(d) which shows additionally the maximum C_L/C_D occurring at M = 4.0.

Comparison of BRL's data to Edgewood Arsenal's results for configuration 972.0 at $\alpha = 0°$ (for purpose of comparison only) shows reasonable agreement for lift data. Figure 4(a) shows a 10% difference in lift at $\alpha = 0°$; however, the greatest difference is found in the drag data (Figure 5(a)) which shows a 50% difference at $\alpha = 0°$. Therefore, a substantial decrease in the lift to drag ratio results and is shown in Figure 6(a). Since the lift data compared favorably, both with and without boundary layer trip, attention is then focused on the base area; more specifically base pressure drag. However, the ratio of model base area to sting area was comparable for both tests and implies similar base flow conditions existed. More recently a pressure test was conducted at BRL for configuration 972.9. A comparison of base axial force data from the pressure test and force test is shown in Figure 7. Due to different ratios of base to strut diameter and different methods of acquiring the base pressure data the results differ by about 9%. However, the trends with angle of attack are comparable and the pressure test, which should be considered the more accurate of the two, shows an expected, higher base axial force. Based on this comparison the axial force data obtained from the Edgewood test are felt to be in error.

The existence of a planar shock pattern, characteristic of wave-rider configurations[4,5], has not been experimentally verified for the models tested. A vapor screen photograph shown in Figure 8 for configuration 972.0 at $\alpha = 0°$ establishes only the existence of a conical

4. *C. T. Nardo, "Aerodynamic Characteristics of Two-Dimensional Wave-rider Configurations," AIAA Journal, Vol. 10, No. 9, September 1972, pp. 1258-1261.*

5. *K. Kipe, "Experimental Investigations of Wave Riders in the Mach Number Range From 8 to 15," AGARD CP No. 30, May 1968.*

bow shock. The light sheet was positioned approximately 1-1/2 inches aft of the model and normal to the air flow. The light source was located on the far side of the tunnel and causes the strut to form a shadow within the vapor screen. Also visible in this photograph are the wing tip vortices which appear as dark triangular regions. After completion of the test program and analysis of the data, the model geometry was reviewed. At that time, it was learned that the design Mach number, i.e., the Mach number at which the planar shock would form, was actually 8.3; therefore, no planar shock should have been seen at M = 2.5 and this was verified by the vapor screen results.

The lift producing mechanism, typical of all configurations tested can be seen in the schlieren photograph (Figure 9). The strong vertical asymmetry of the bow shock indicates a region of high pressure on the models lower surface.

IV. CONCLUSION

The models tested have been shown to produce moderate lift/drag ratios; however, an expected maximum of L/D $\approx$ 6.0 has not been obtained. Since the caret-wing (wave-rider shape) is known for optimum aerodynamic efficiency in regards to lift/drag, additional tests should be conducted with the model design adhering to the wave rider concept.

The lack of roll stability for all configurations has been experimentally verified and reinforces the need for designing future models to overcome this deficiency.

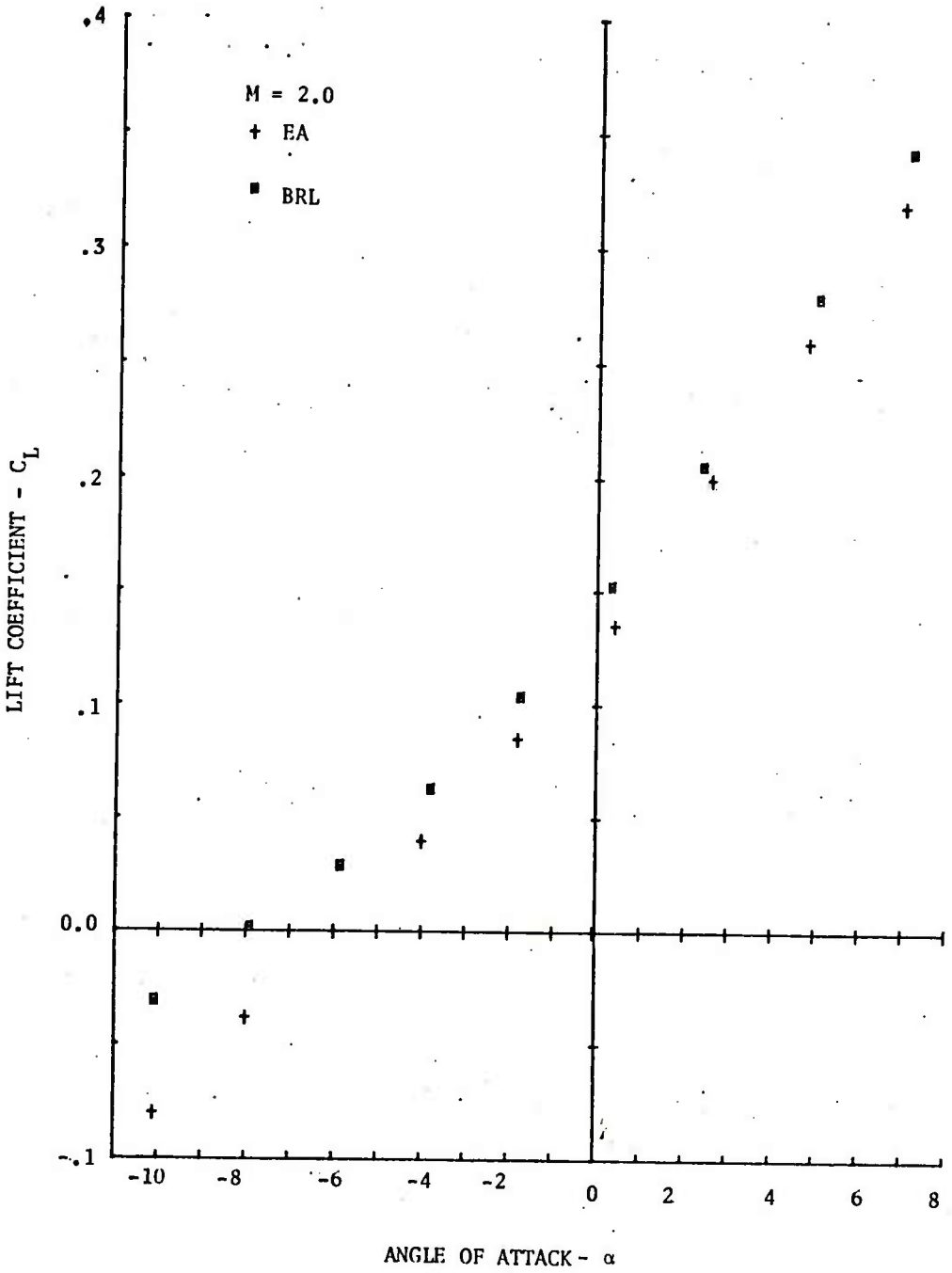

Figure 4. Comparison of Edgewood Arsenal and Ballistic Research Laboratories Lift Data, C_L, for Configuration 972.0

a. Mach 2.0

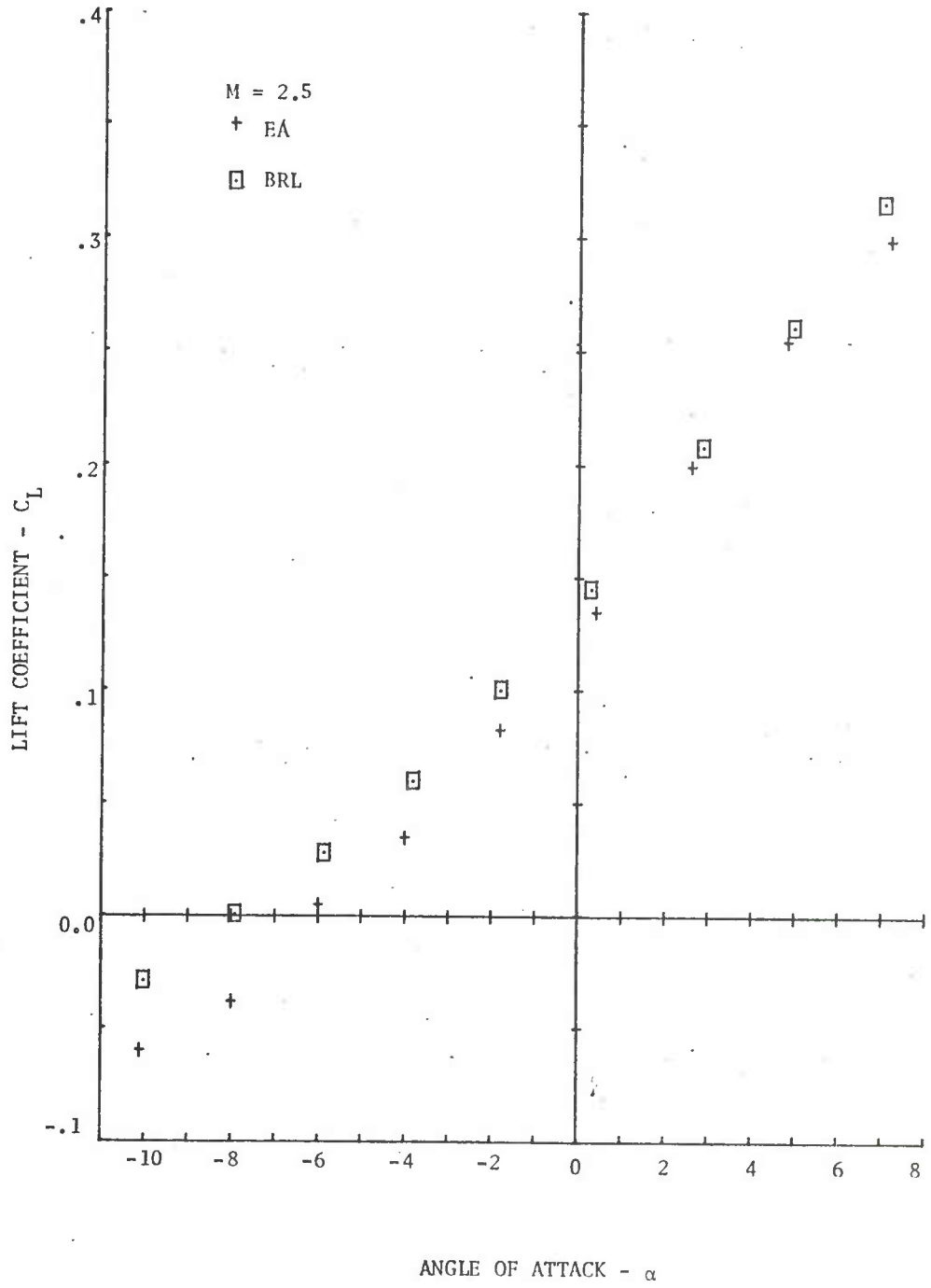

Figure 4. Continued

b. Mach 2.5

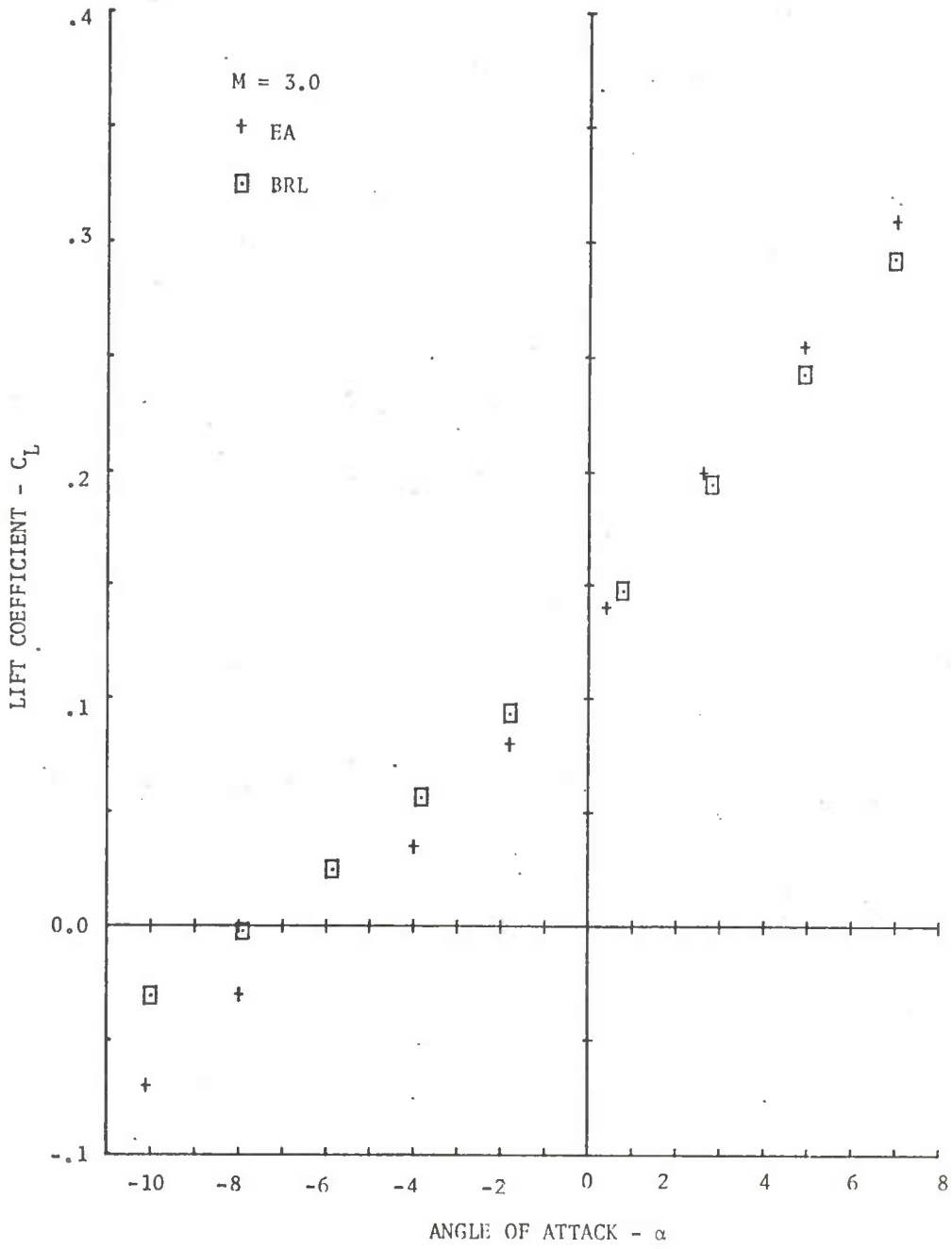

Figure 4. Continued

c. Mach 3.0

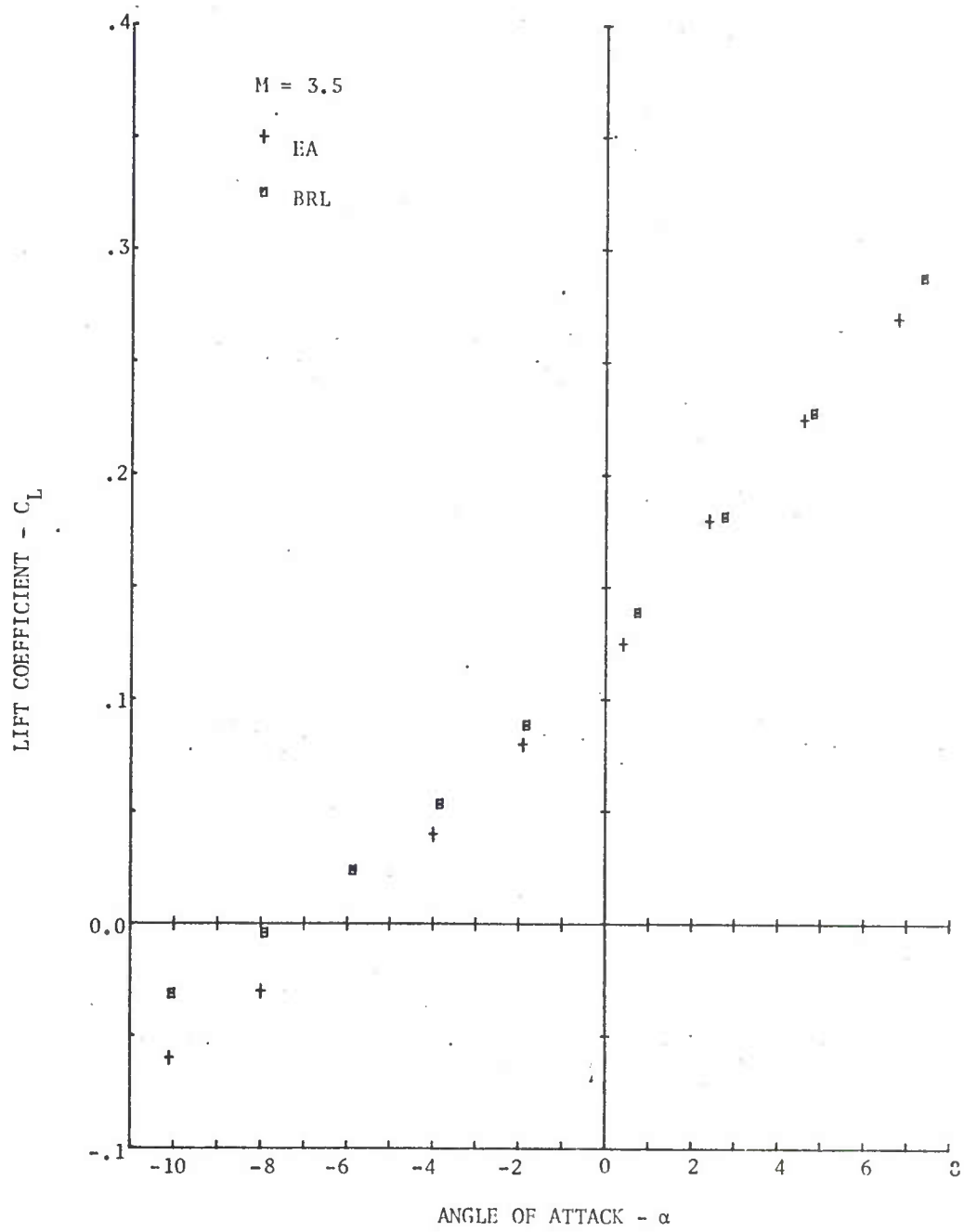

Figure 4. Concluded

d. Mach 3.5

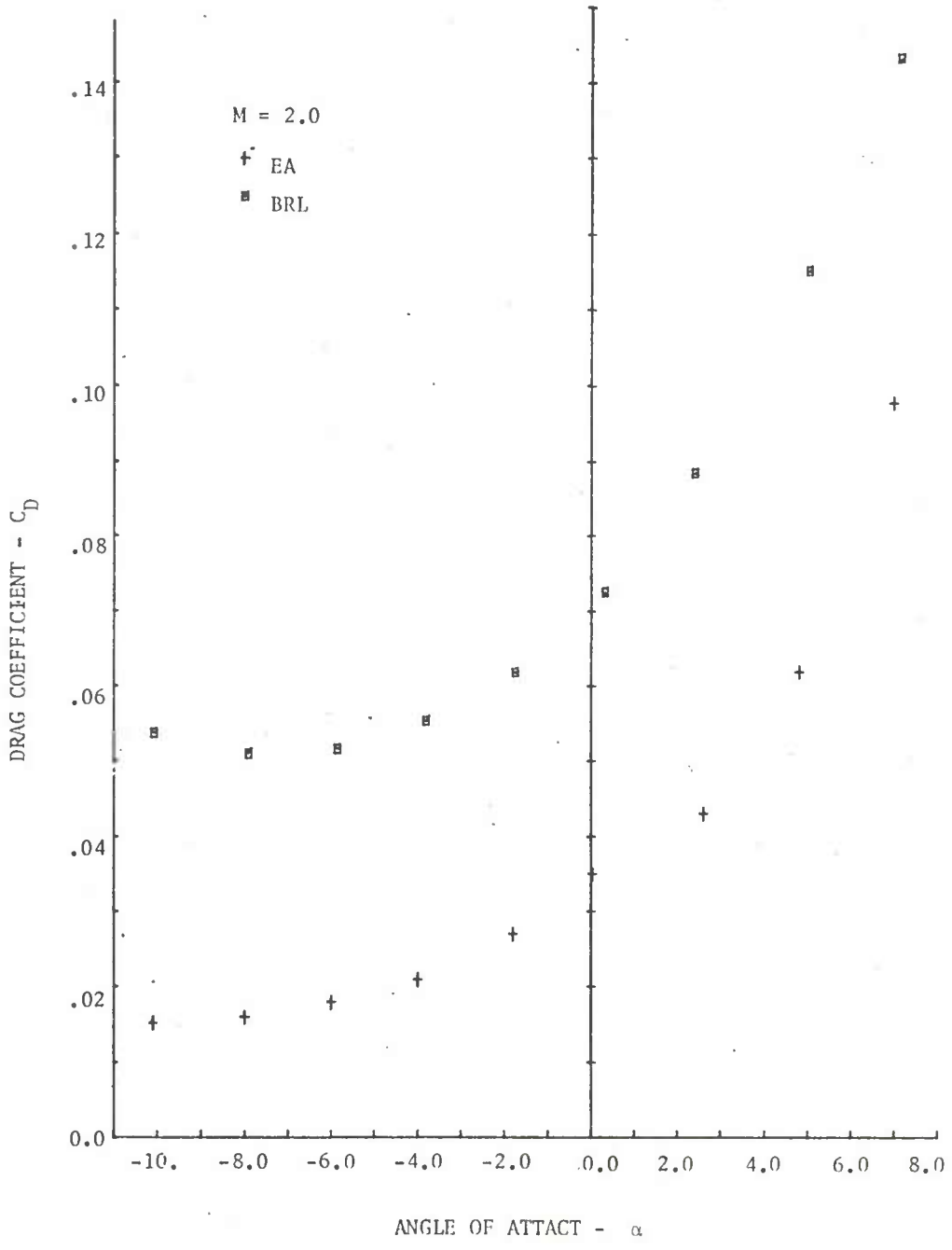

Figure 5. Comparison of Edgewood Arsenal and Ballistic Research Laboratories Drag Data, C_D, for Configuration 972.0

a. Mach 2.0

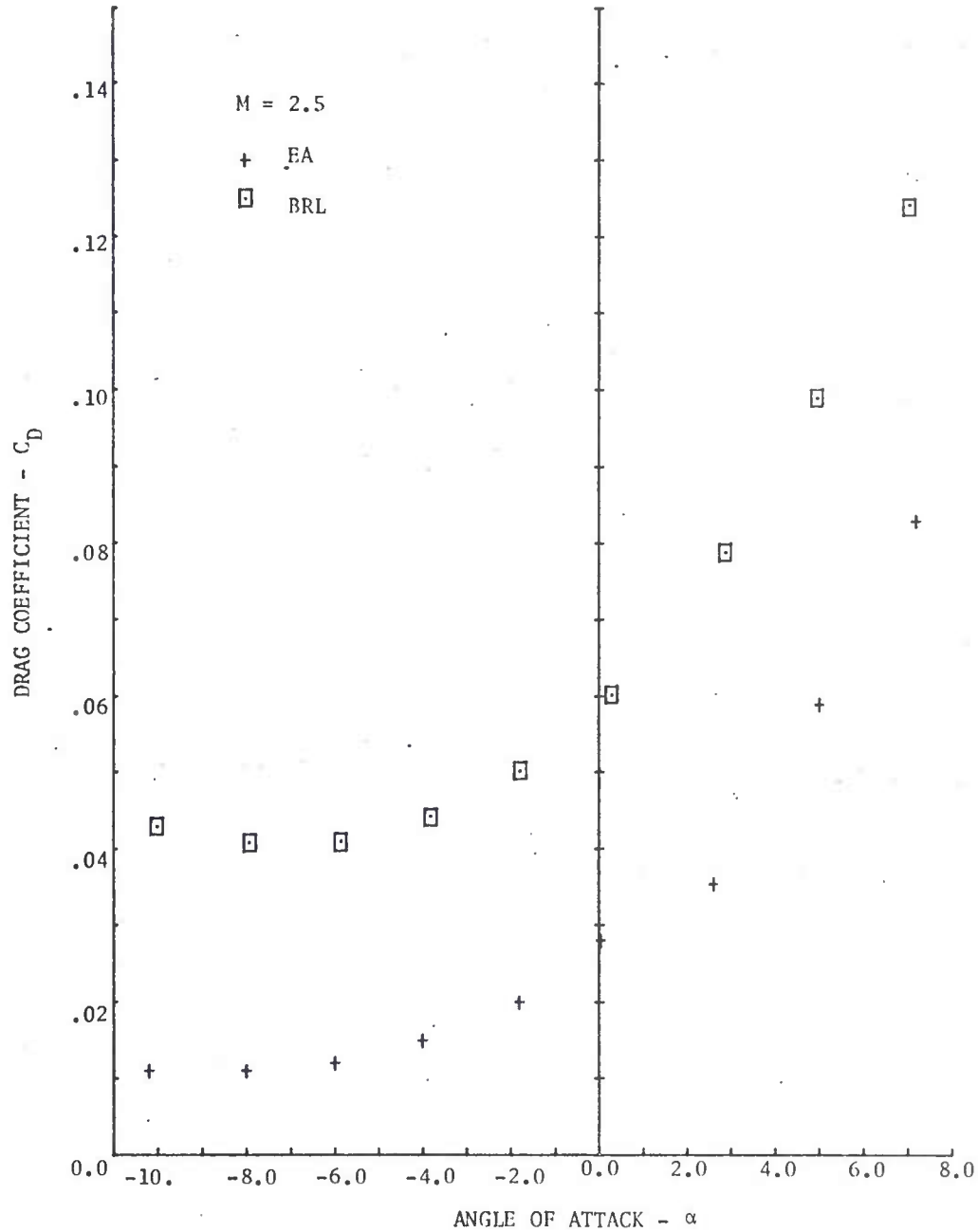

Figure 5. Continued

b. Mach 2.5

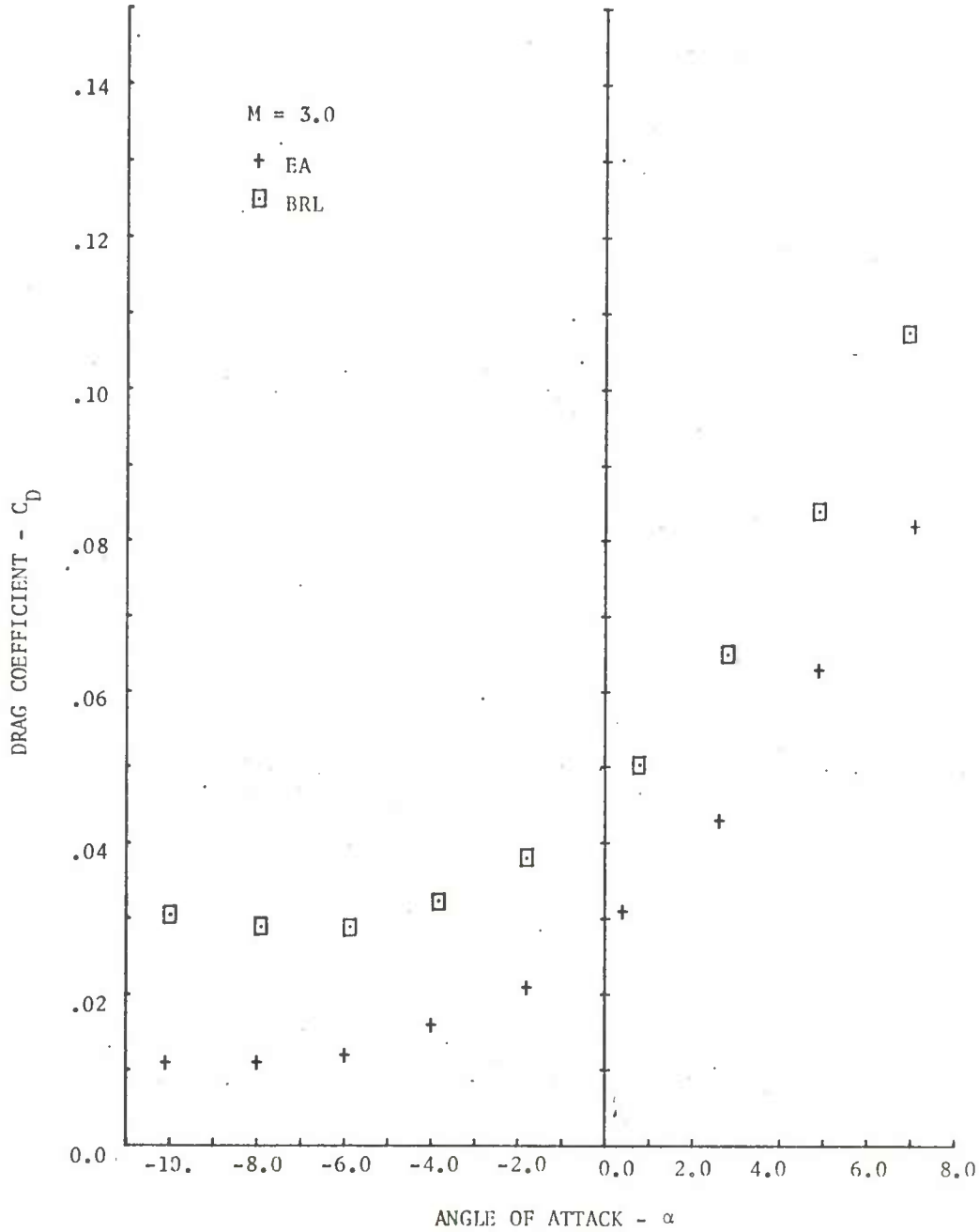

Figure 5. Continued

c. Mach 3.0

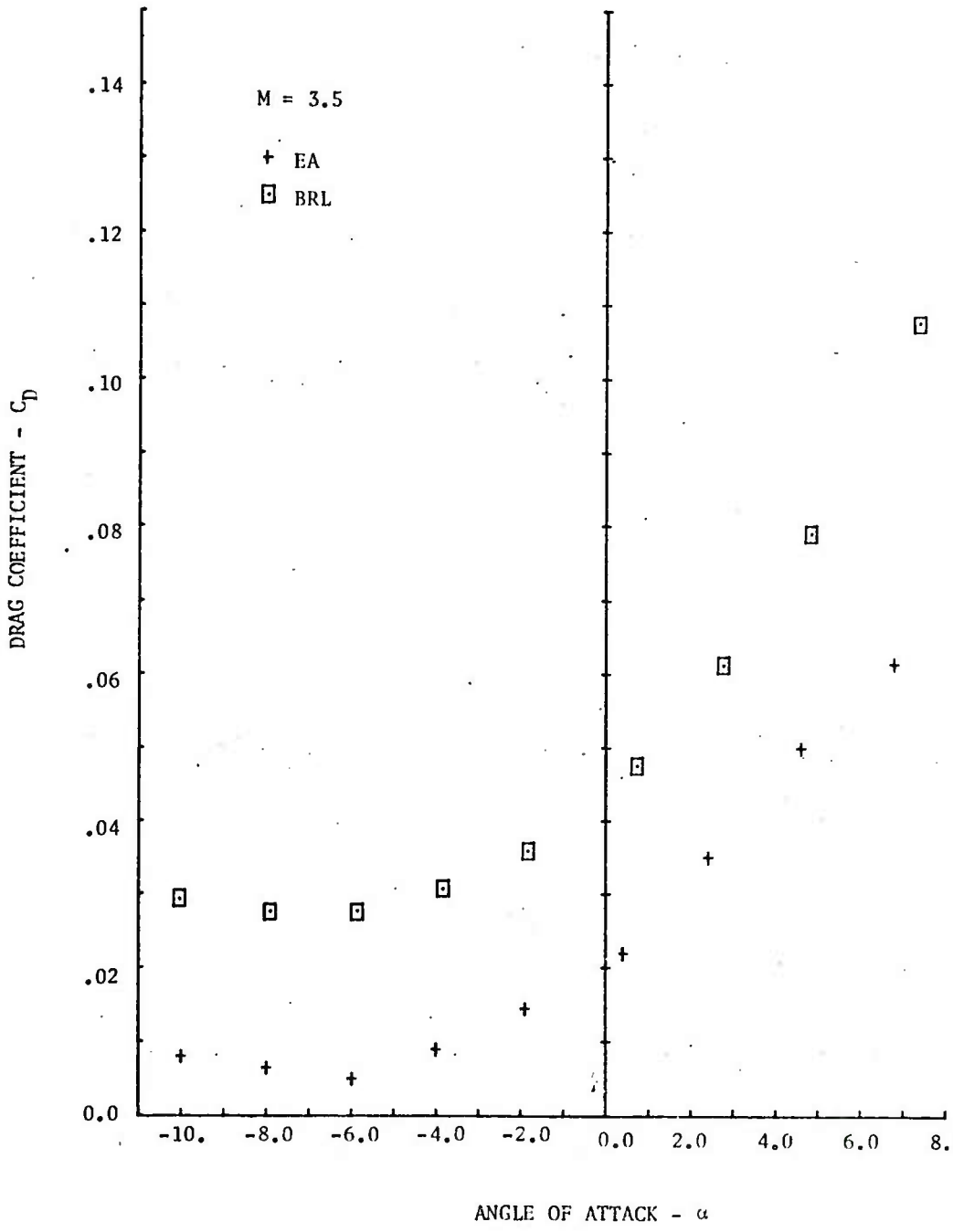

Figure 5. Concluded

d. Mach 3.5

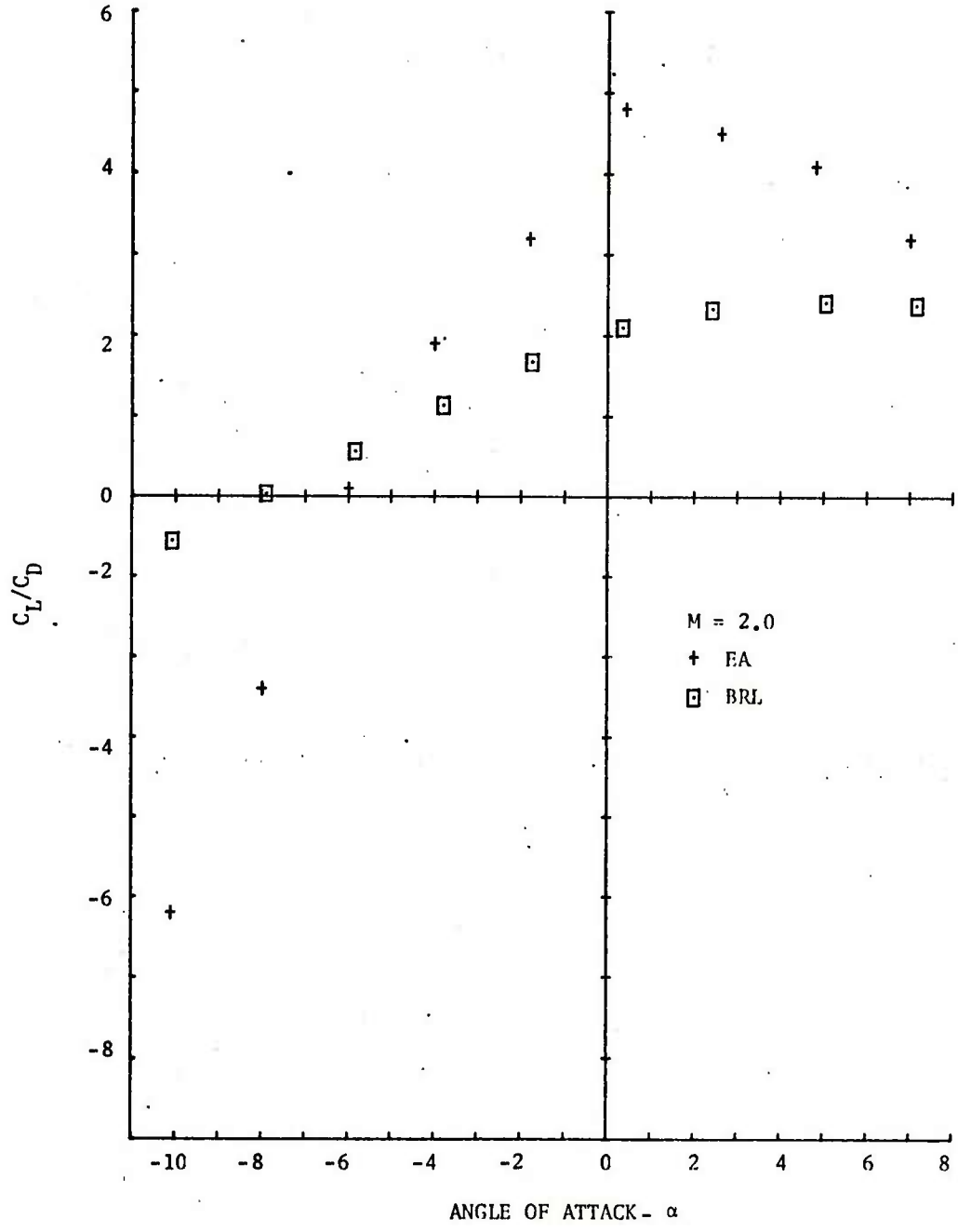

Figure 6. Comparison of Edgewood Arsenal and Ballistic Research Laboratories Lift/Drag Data, C_L/C_D, for Configuration 972.0

a. Mach 2.0

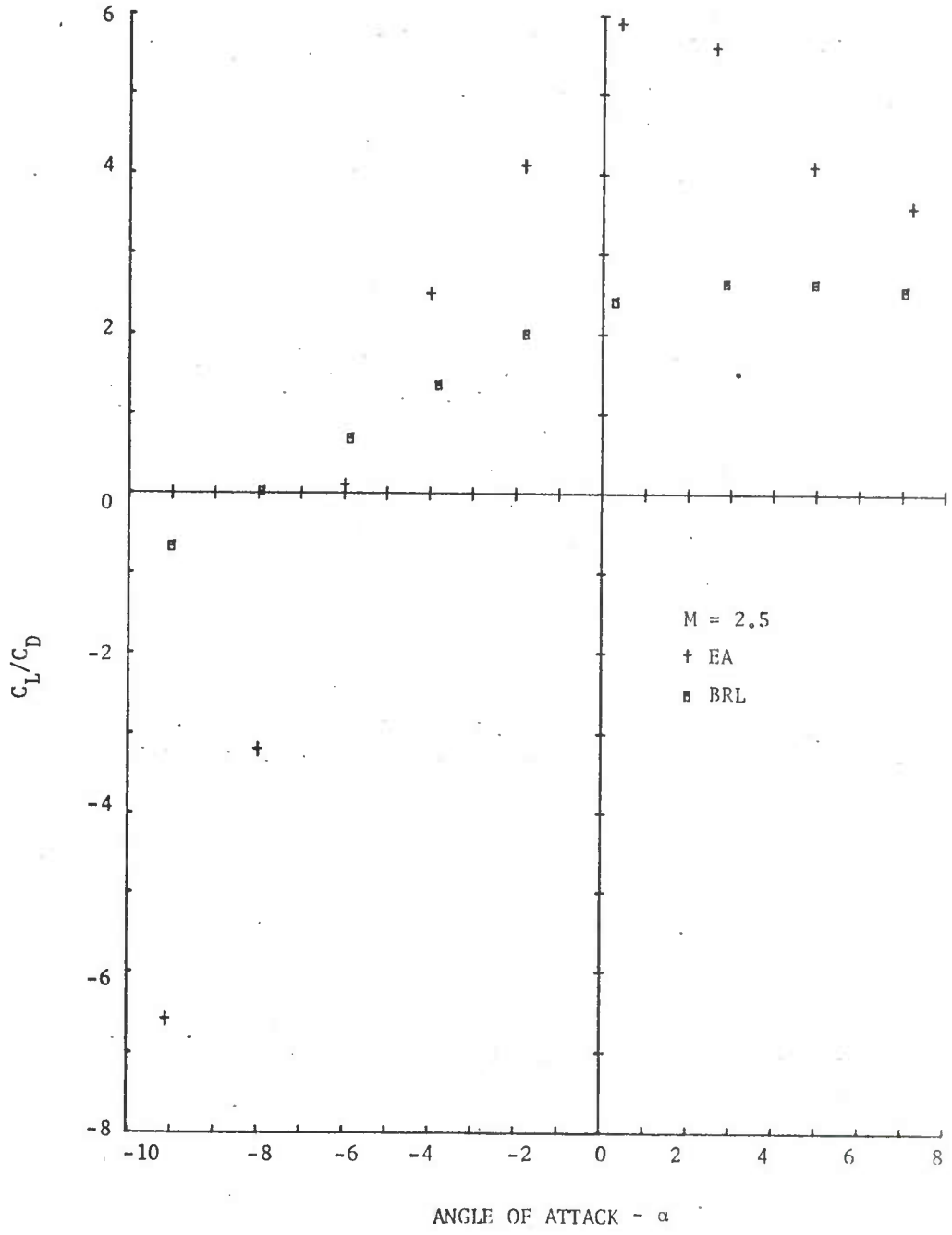

Figure 6. Continued

b. Mach 2.5

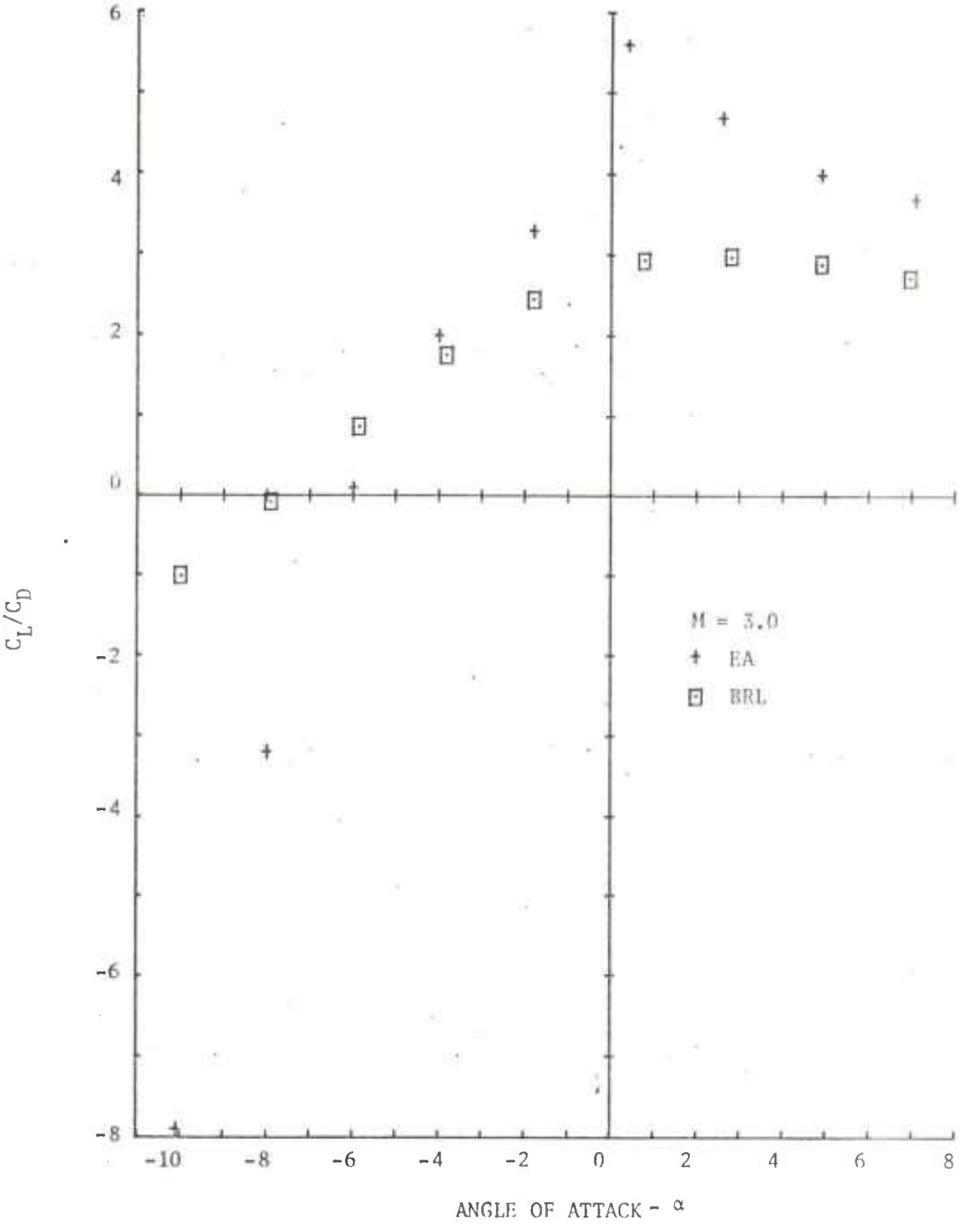

Figure 6. Continued

c. Mach 3.0

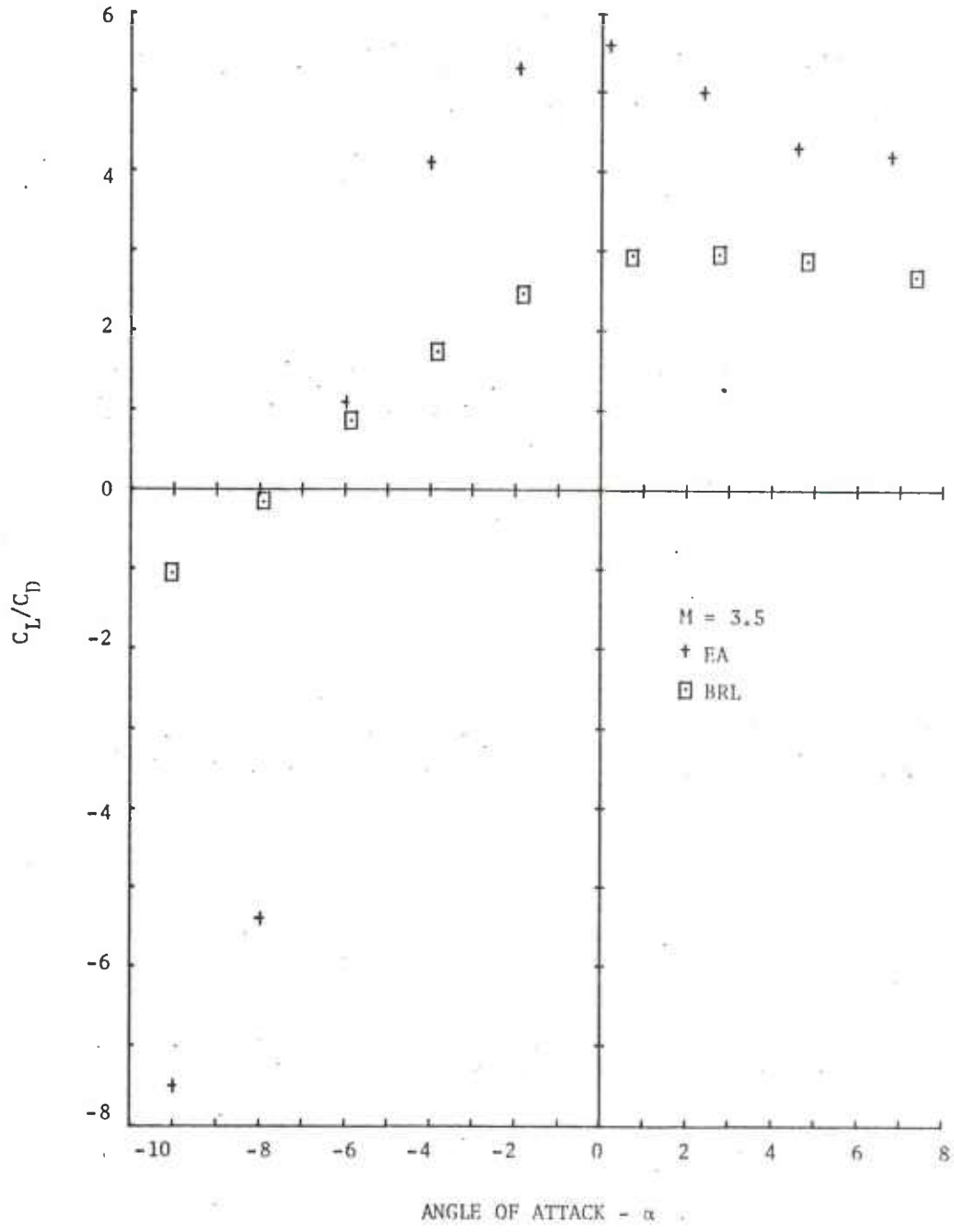

Figure 6. Concluded

d. Mach 3.5

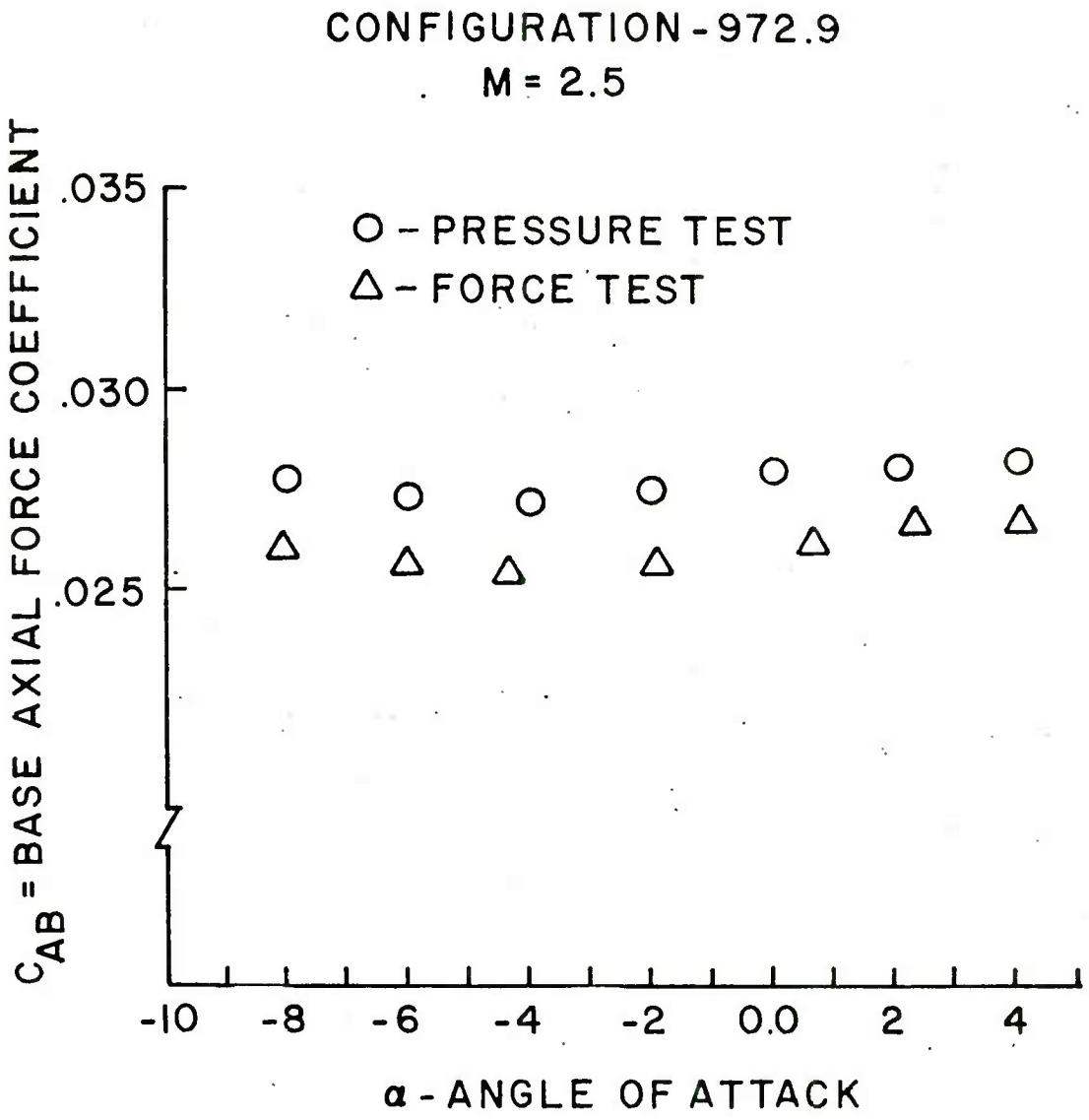

Figure 7. Comparison of Base Axial Force Between Independent Force and Pressure Tests

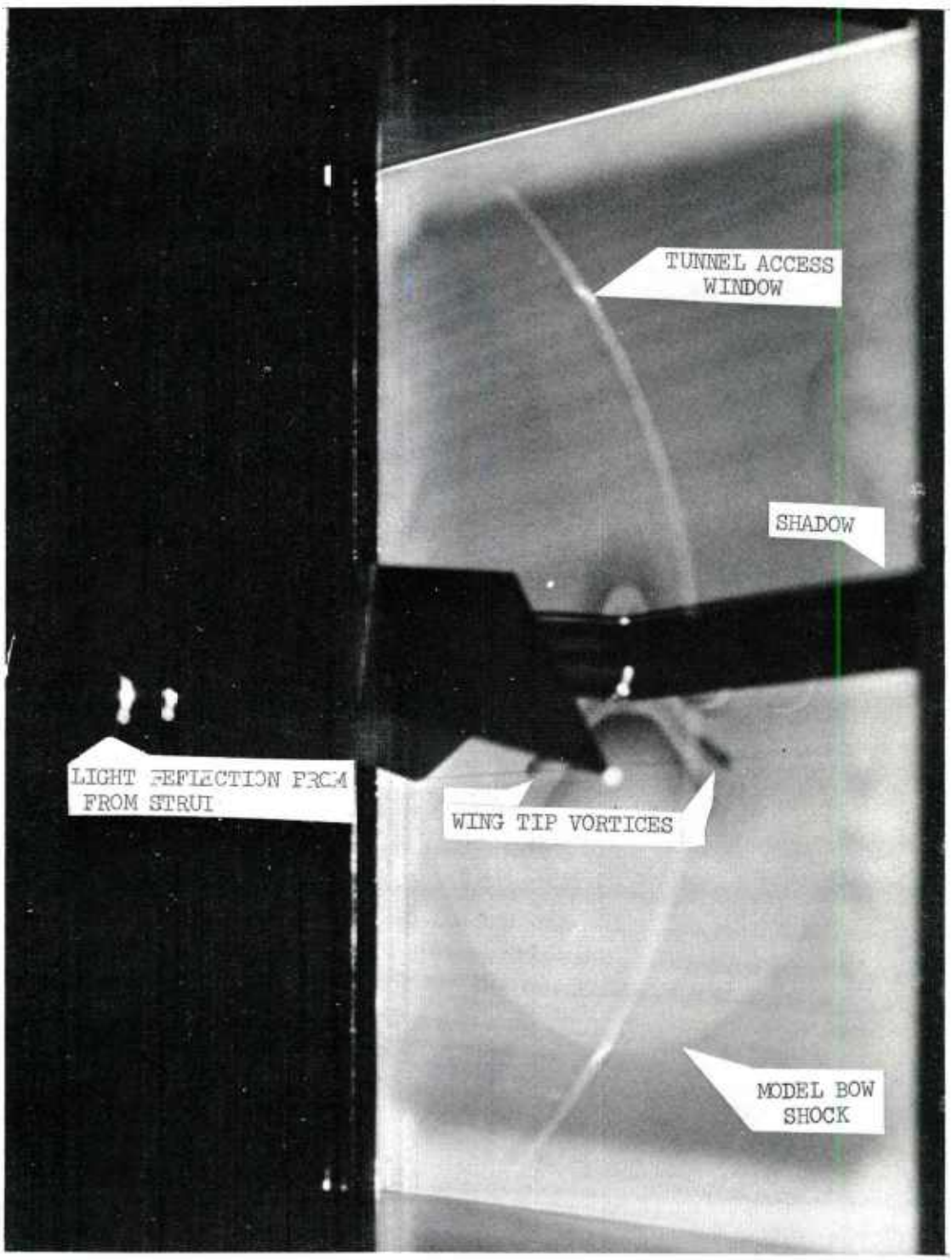

Figure 8. Vapor Screen Photograph of Configuration 972.9 at $\alpha = 0°$, M = 2.5

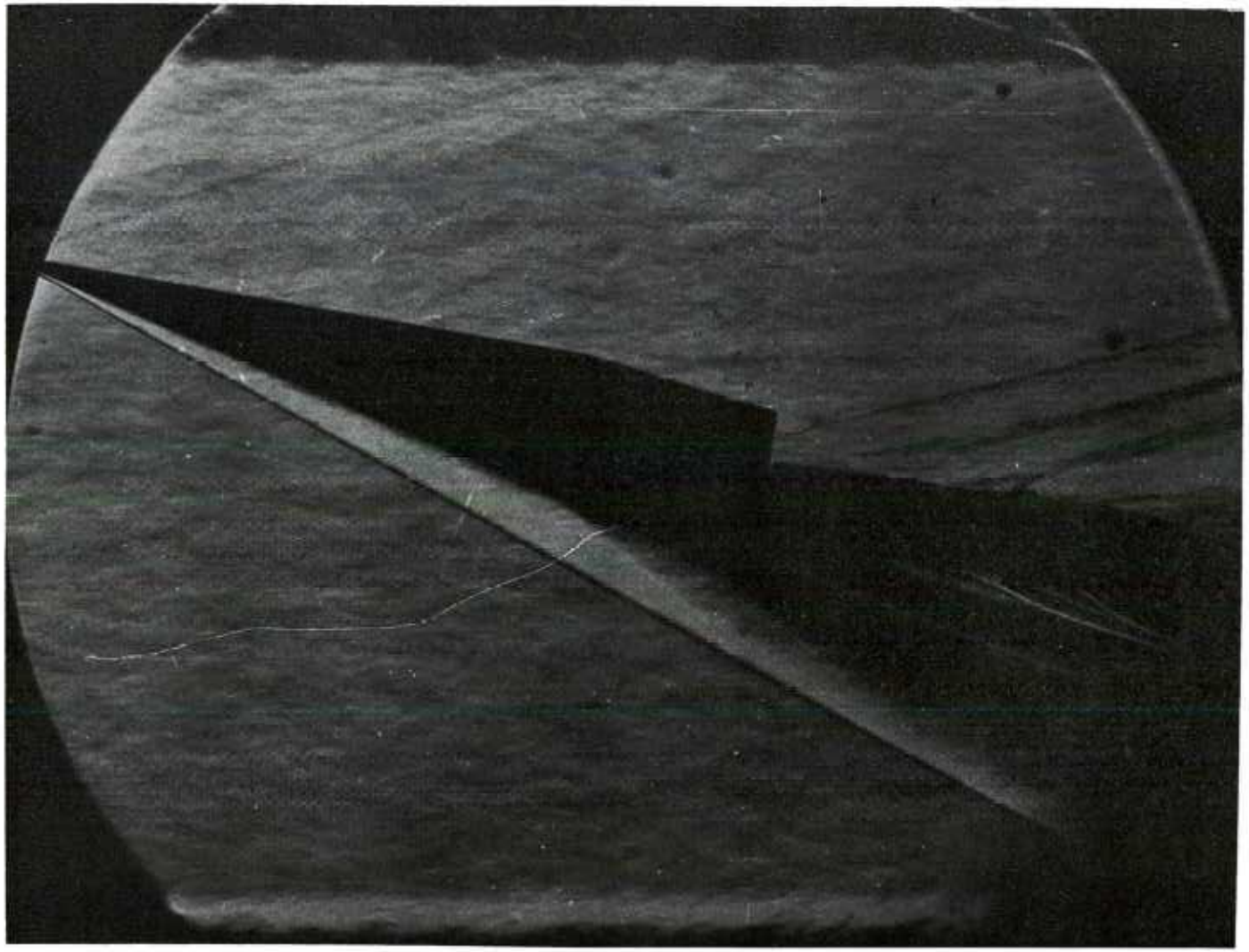

Figure 9. Schlieren Photograph of Configuration 972.7 at α = +9°, M = 3.5

APPENDIX

Static Aerodynamic Coefficients

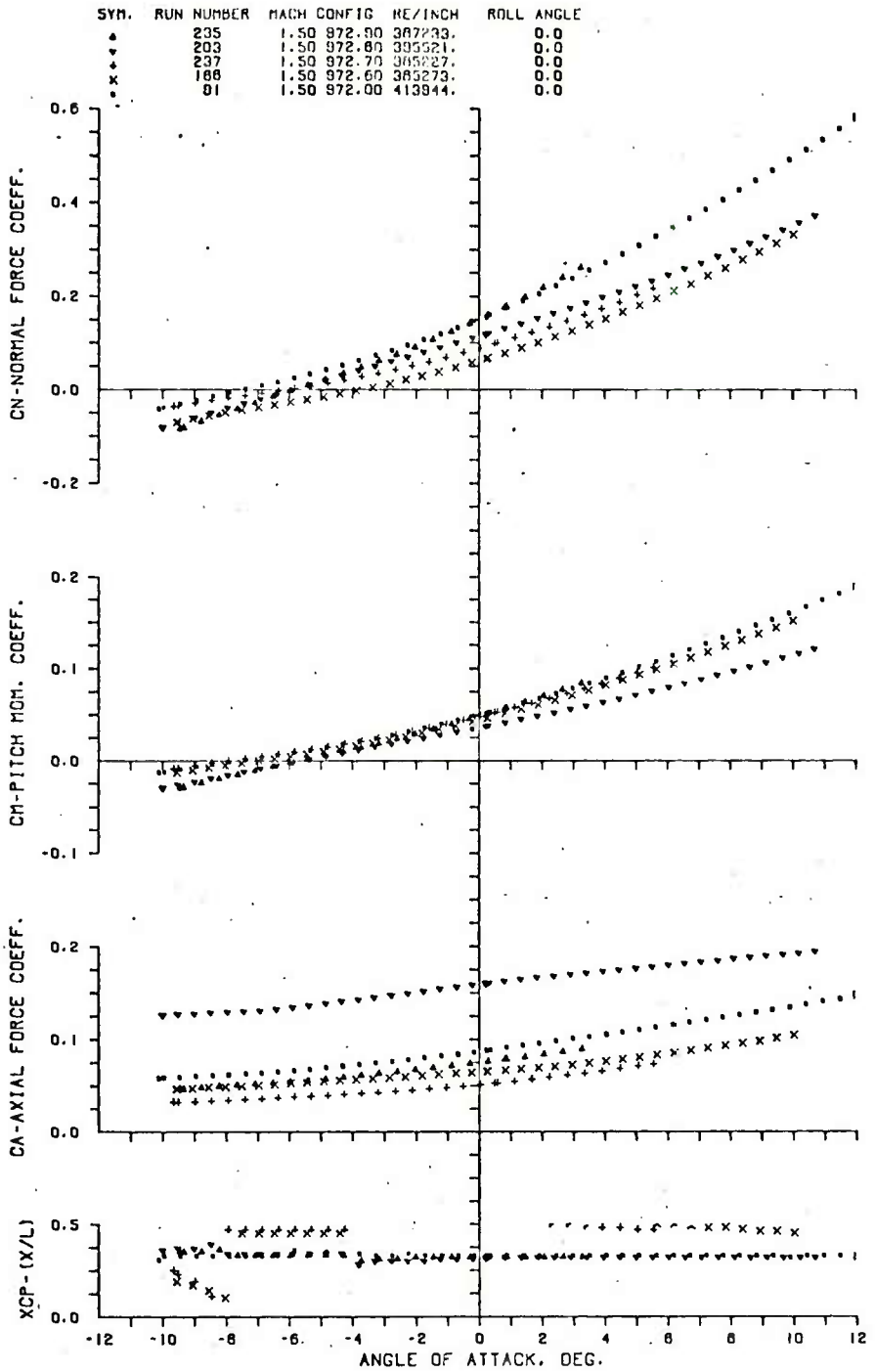

Figure A1. Variation of C_N, C_m, C_A, X_{CP} With Configuration at Constant Mach Number

a. Mach 1.5

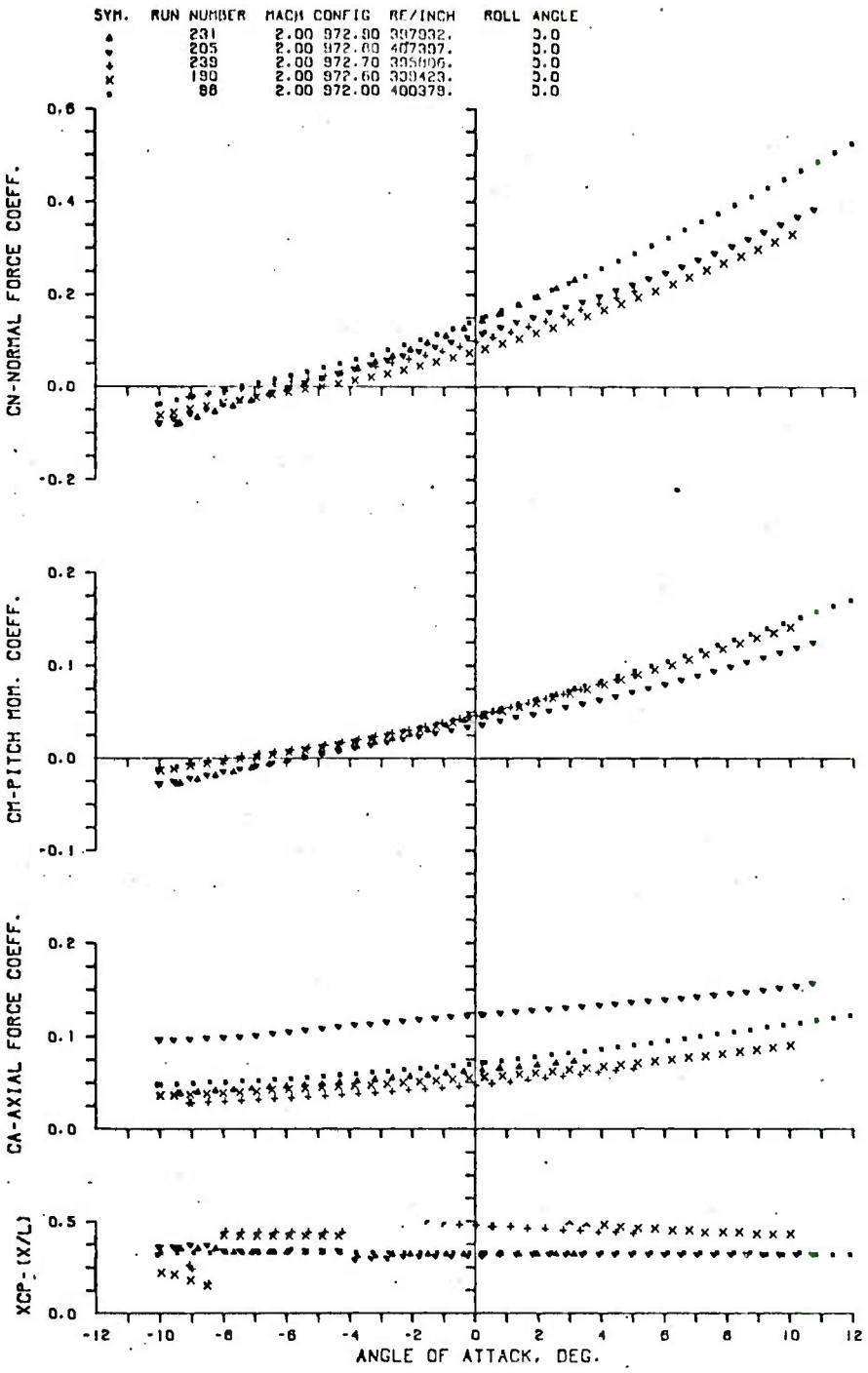

Figure A1. Continued

b. Mach 2.0

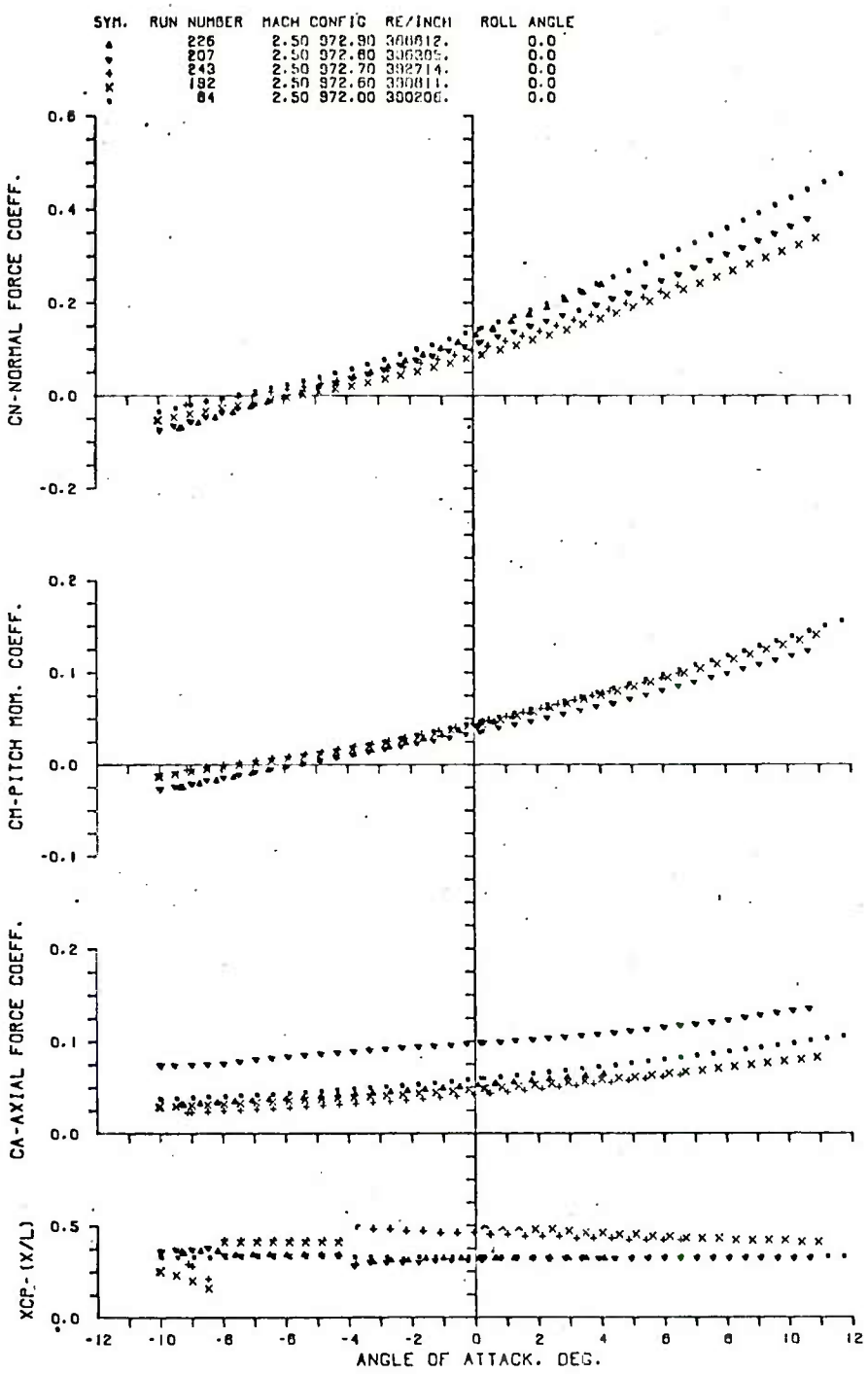

Figure A1. Continued

c. Mach 2.5

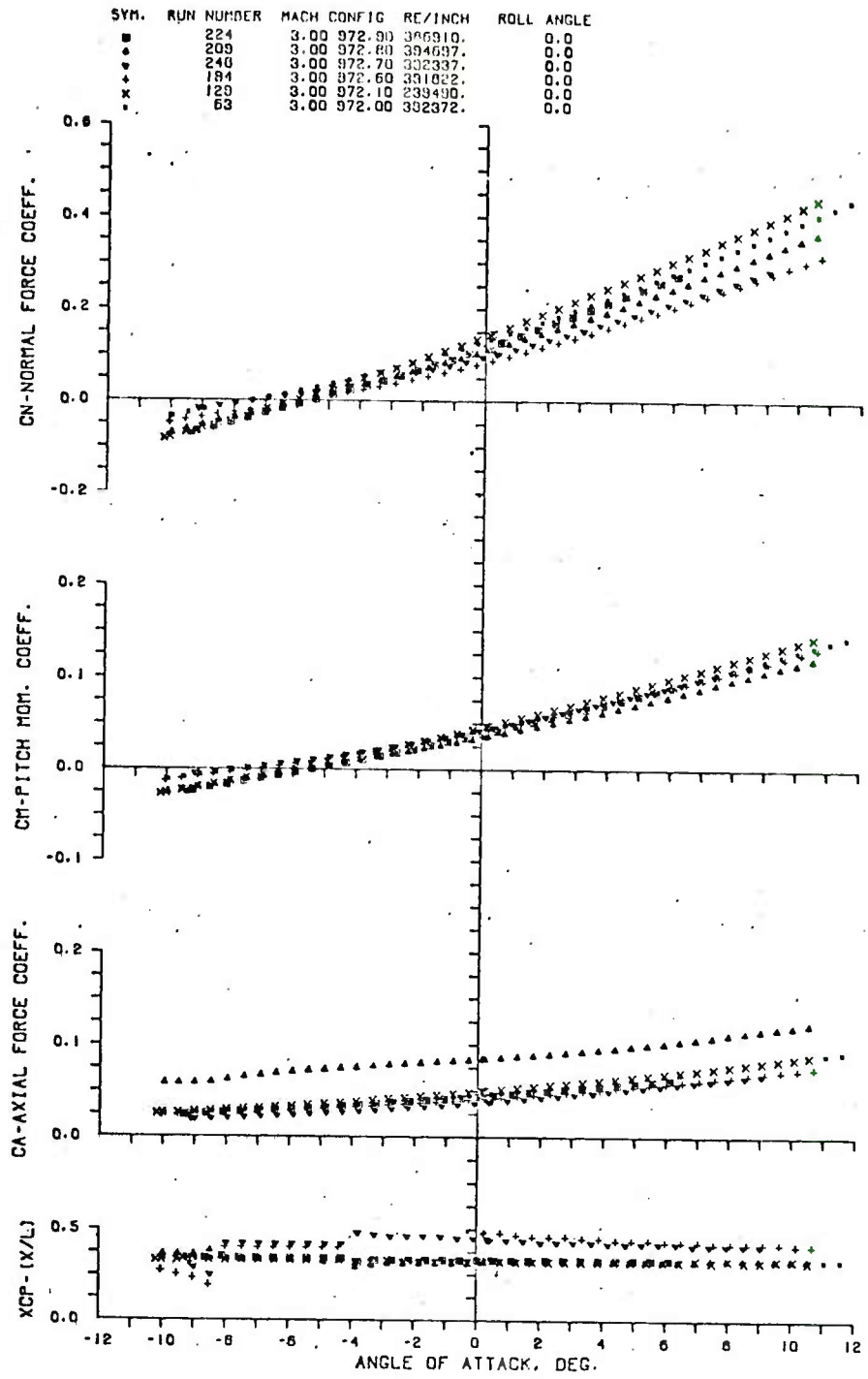

Figure A1. Continued

d. Mach 3.0

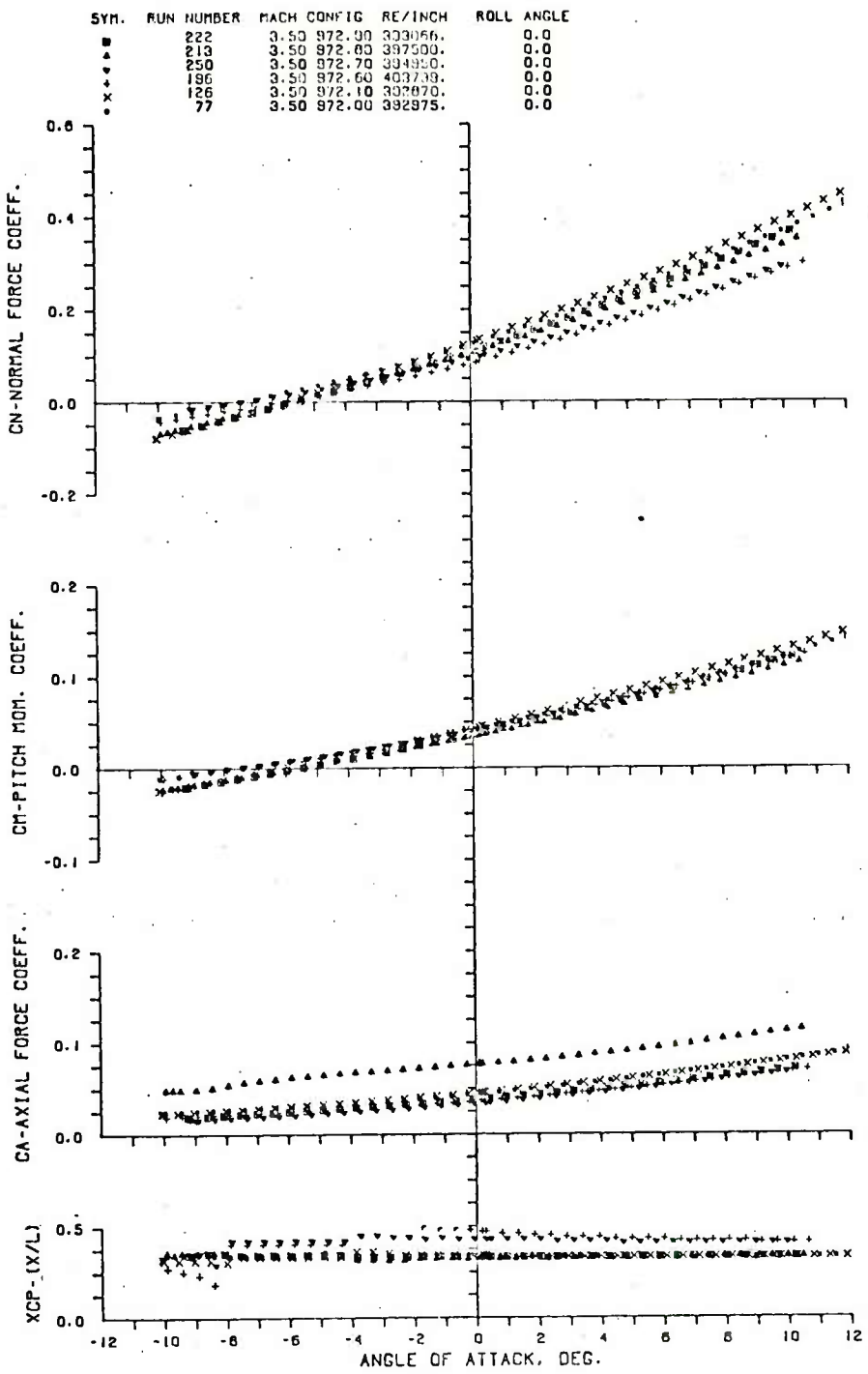

Figure A1. Continued

e. Mach 3.5

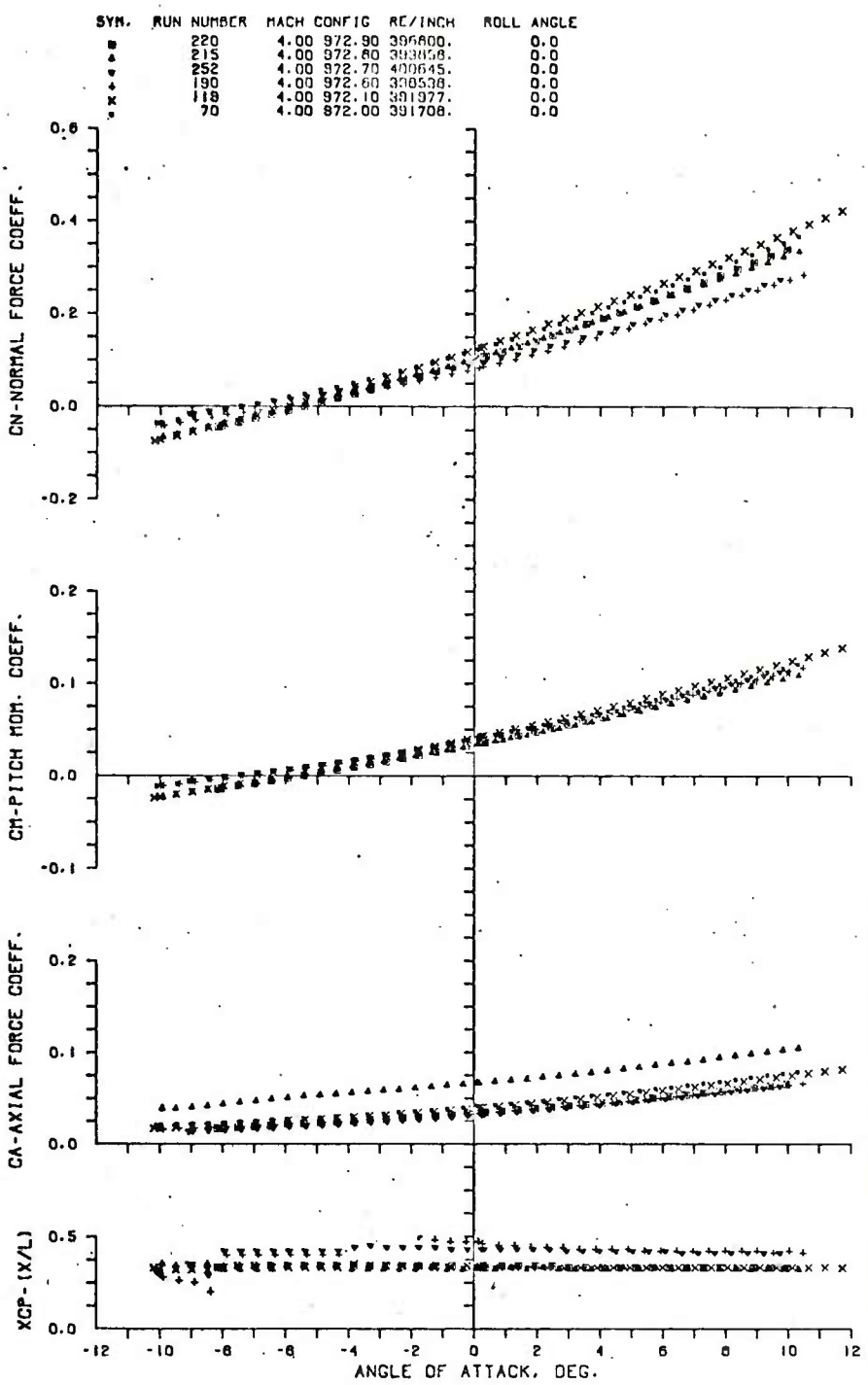

Figure A1. Concluded

f. Mach 4.0

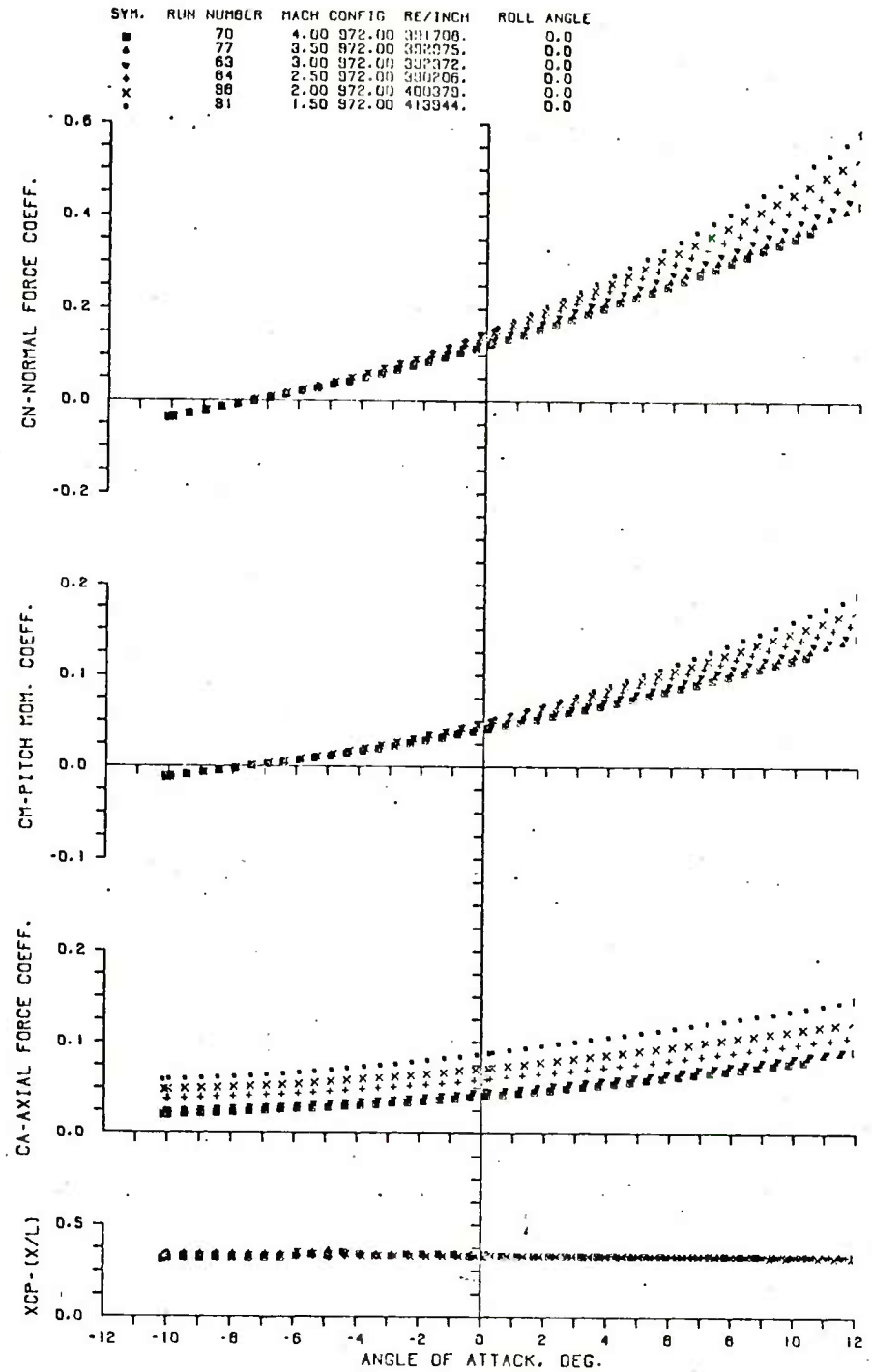

Figure A2. Variation of C_N, C_m, C_A, X_{CP} With Mach Number for Each Configuration

a. Configuration 972.0

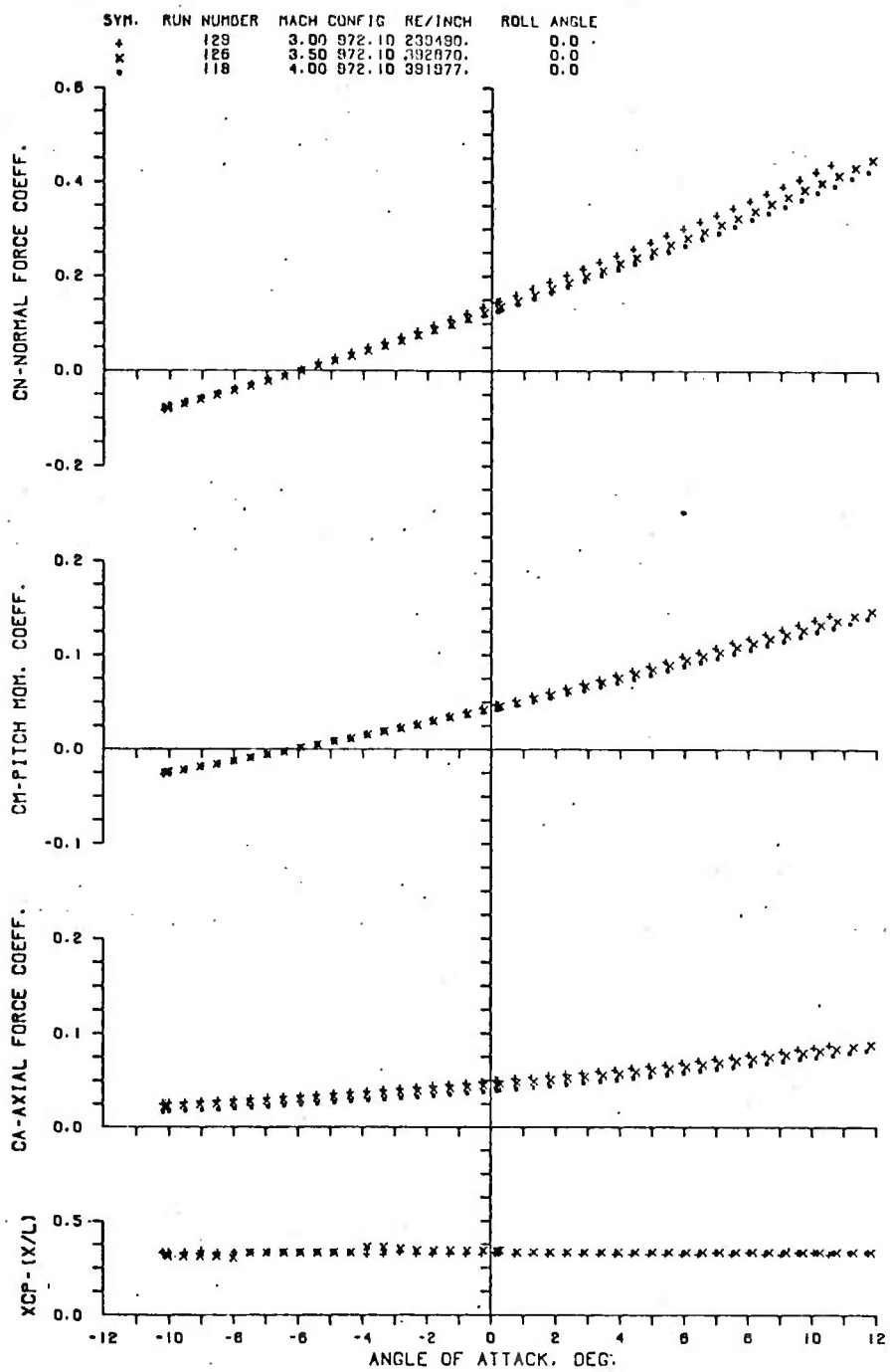

Figure A2. Continued

b. Configuration 972.1

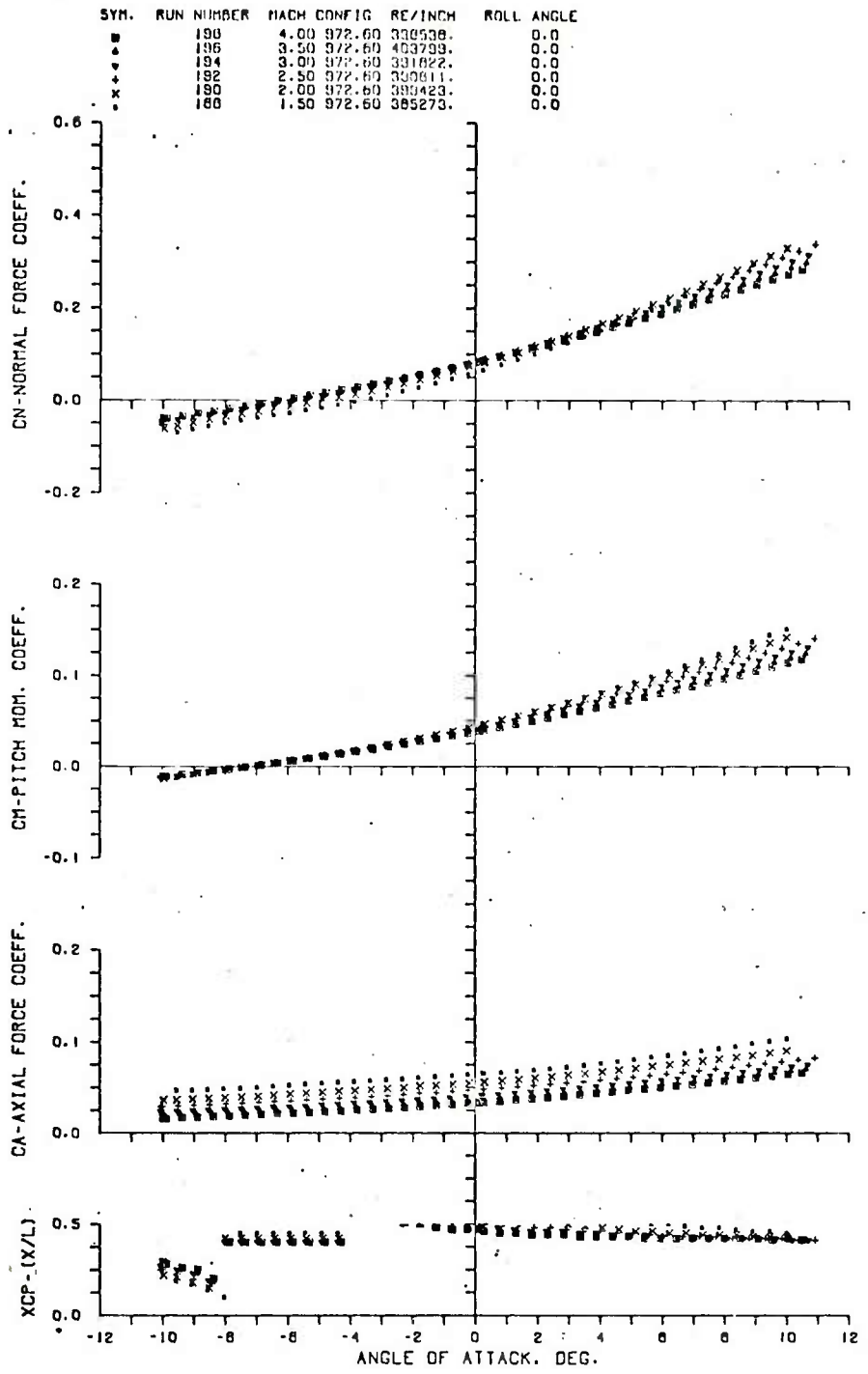

Figure A2. Continued

c. Configuration 972.6

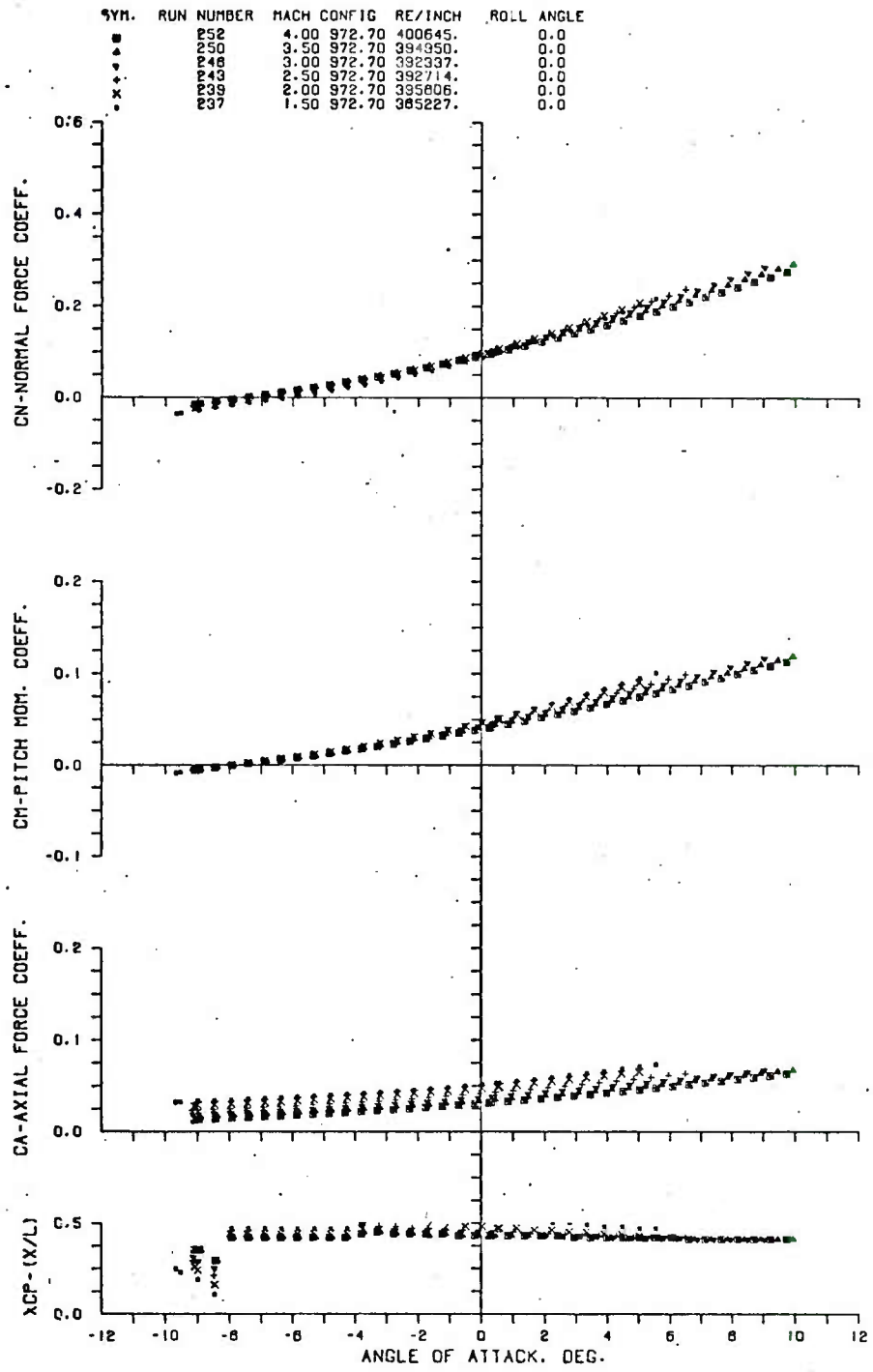

Figure A2. Continued

d. Configuration 972.7

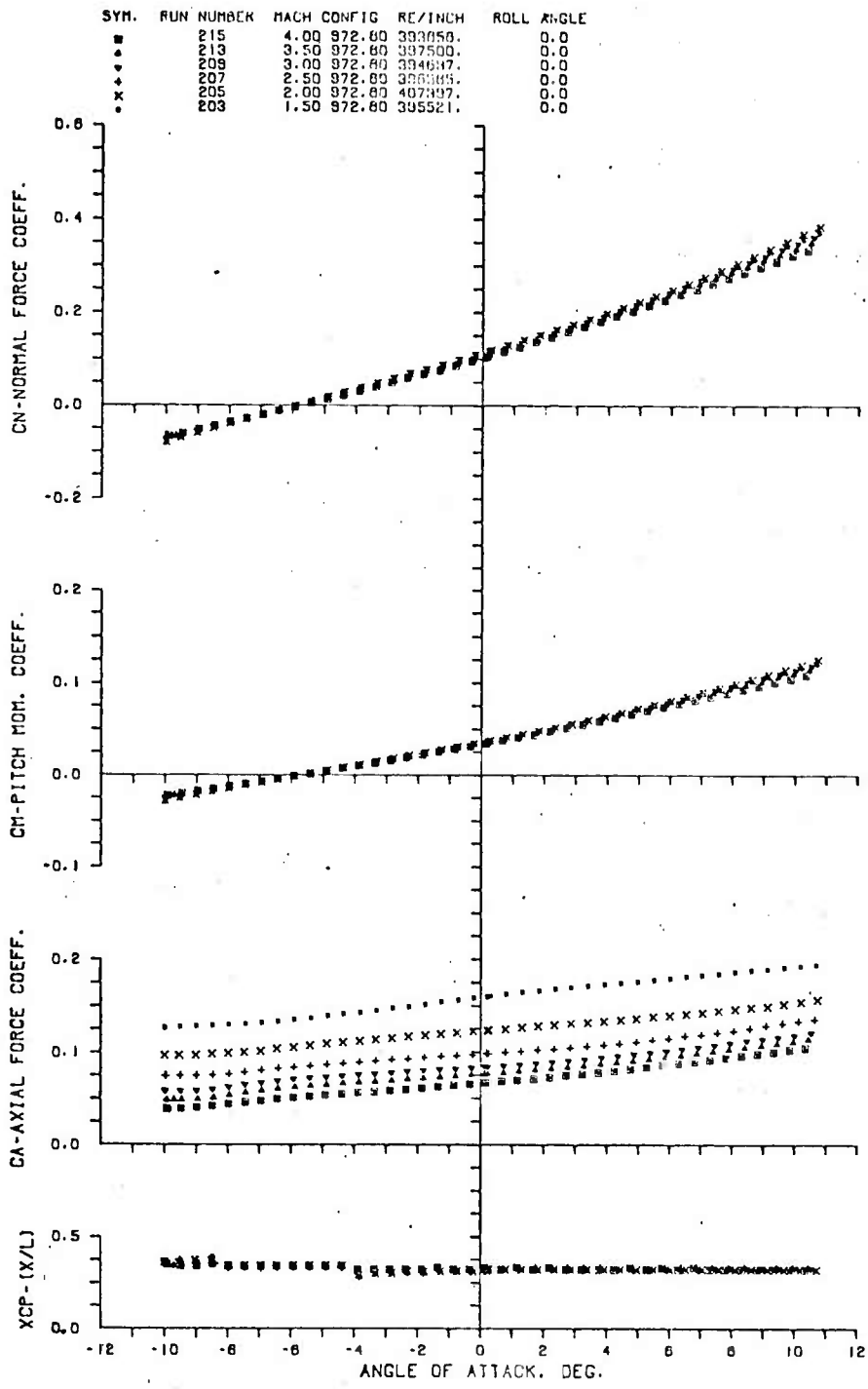

Figure A2. Continued

e. Configuration 972.8

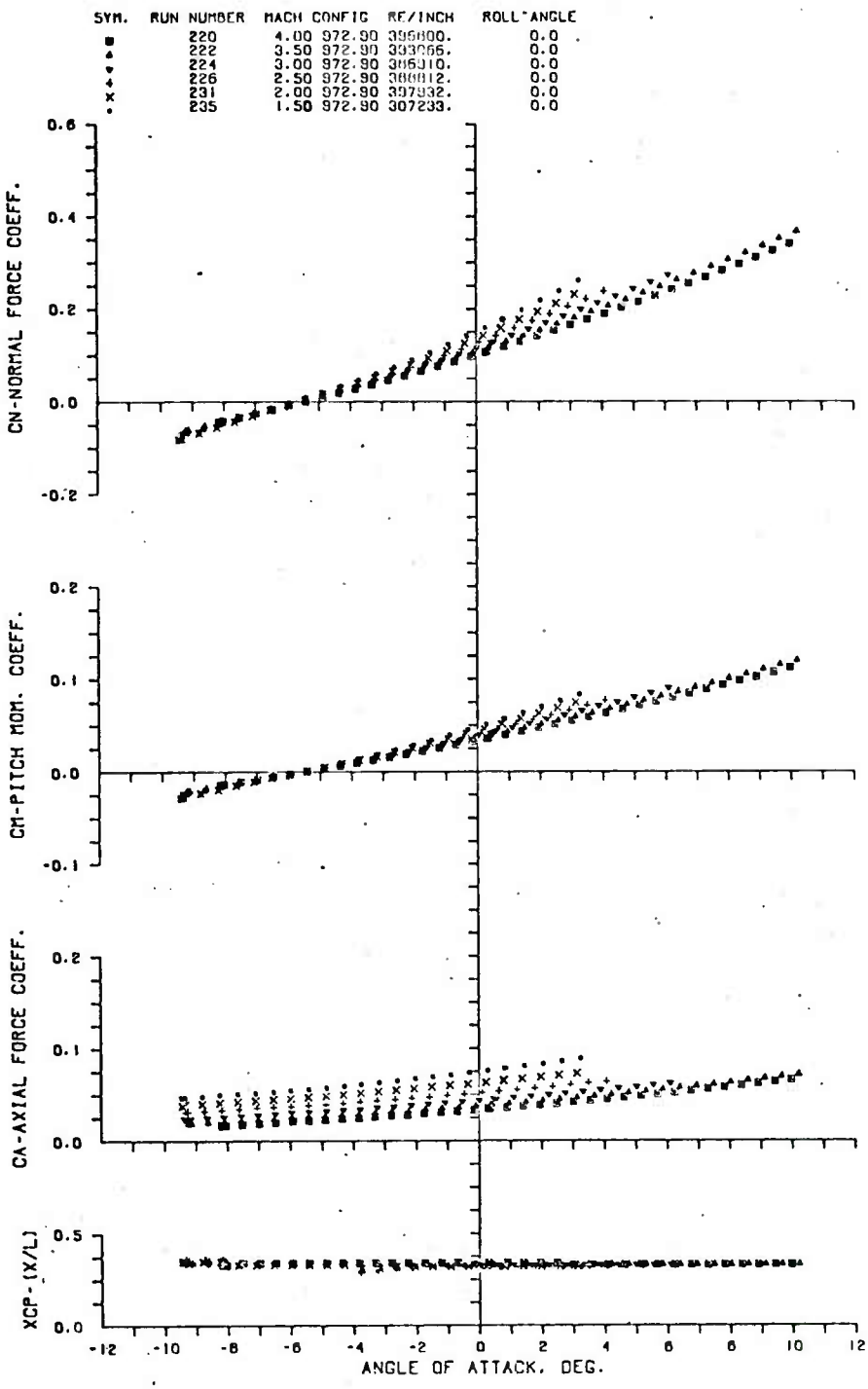

Figure A2. Concluded

f. Configuration 972.9

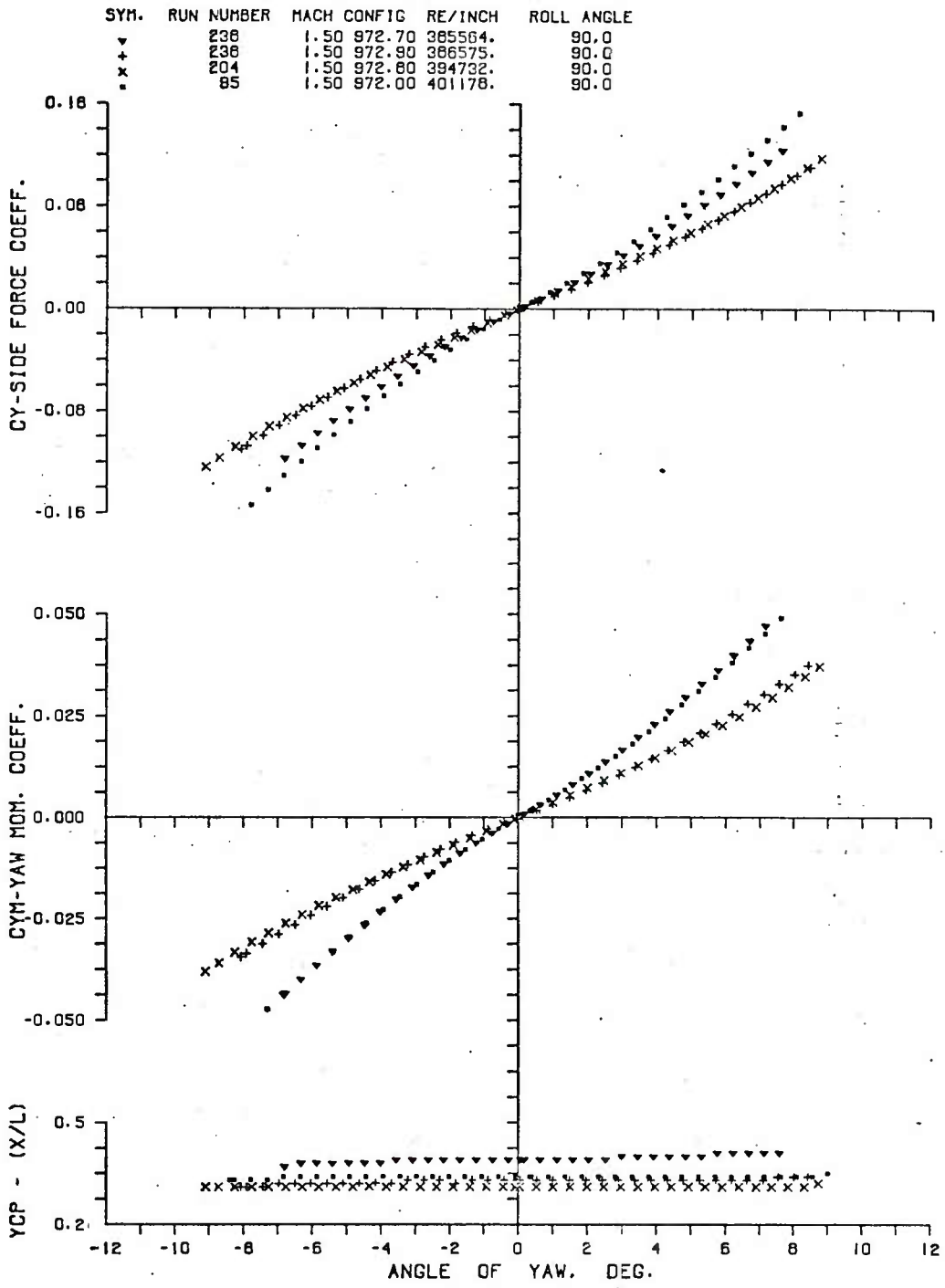

Figure A3. Variation of C_Y, C_n, Y_{CP} With Configuration at Constant Mach Number

a. Mach 1.5

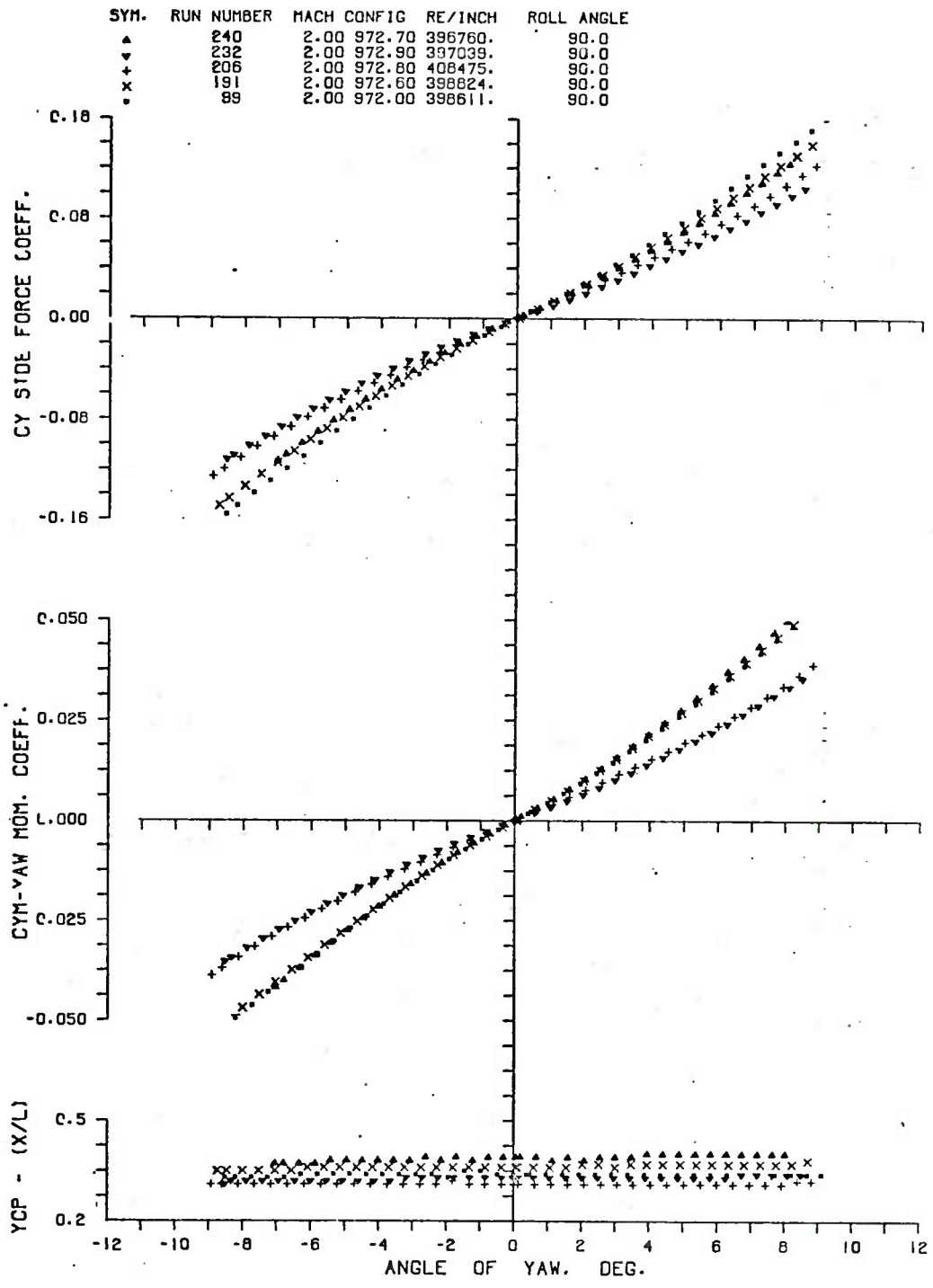

Figure A3. Continued

b. Mach 2.0

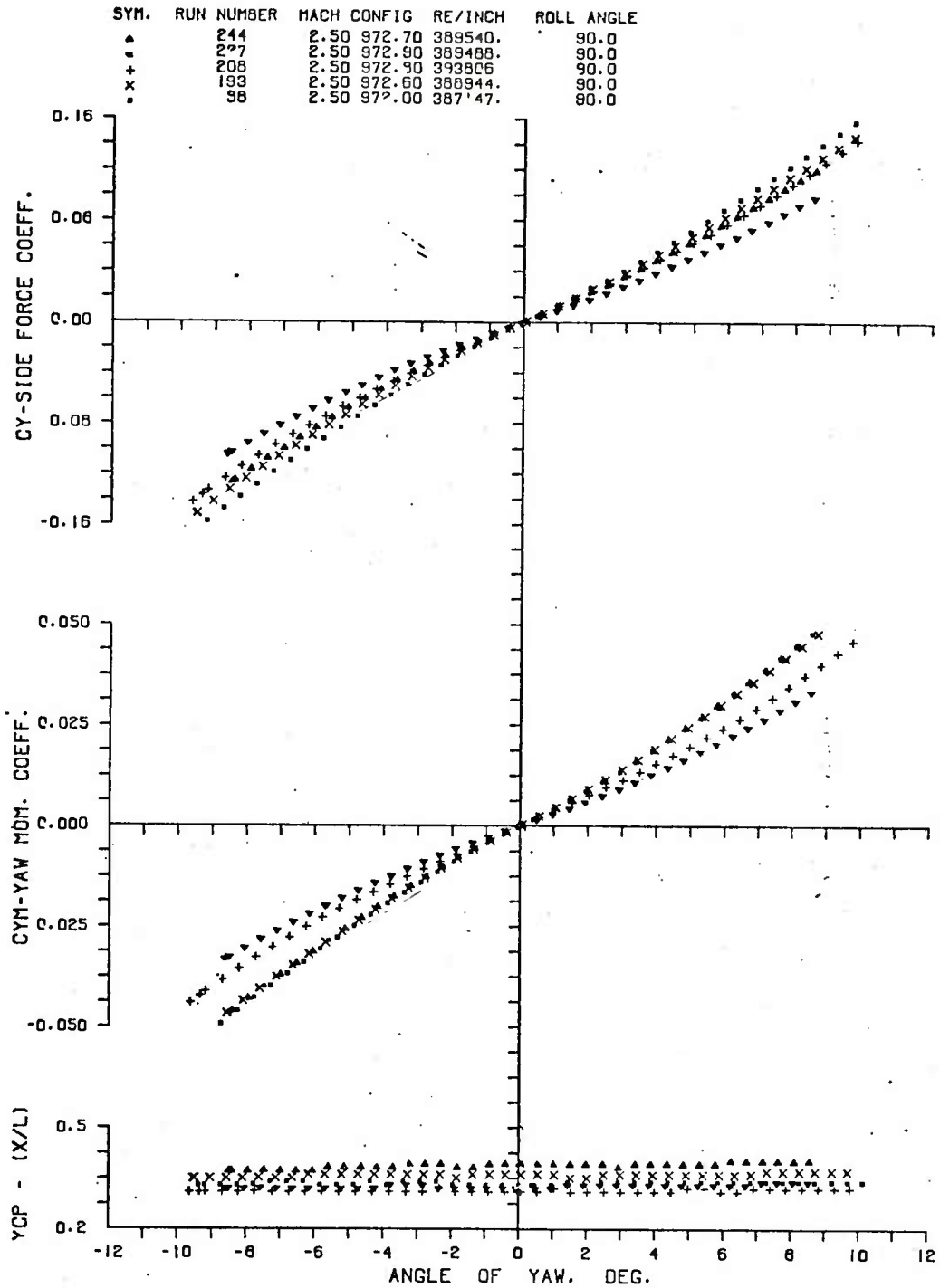

Figure A3. Continued

c. Mach 2.5

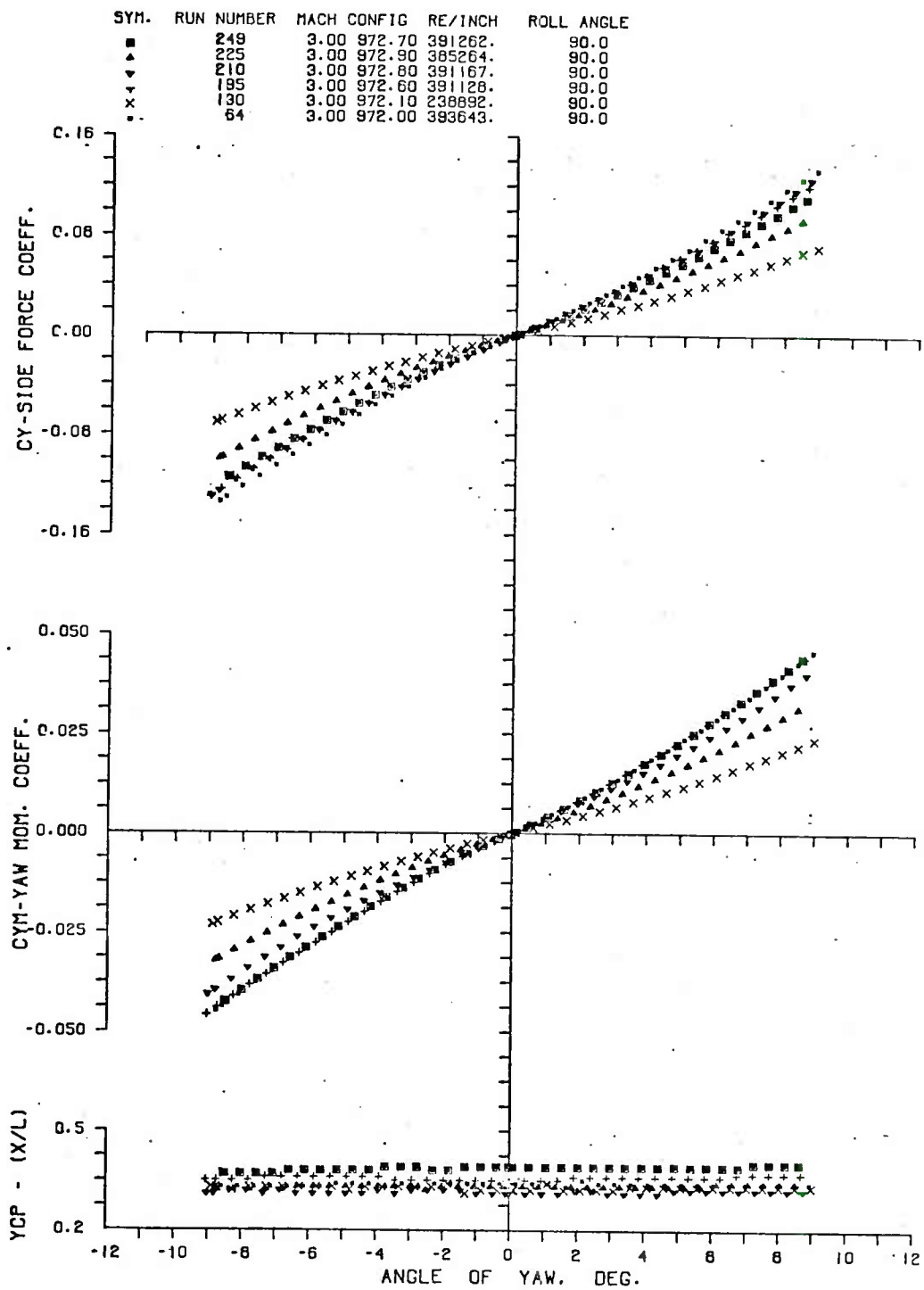

Figure A3. Continued

d. Mach 3.0

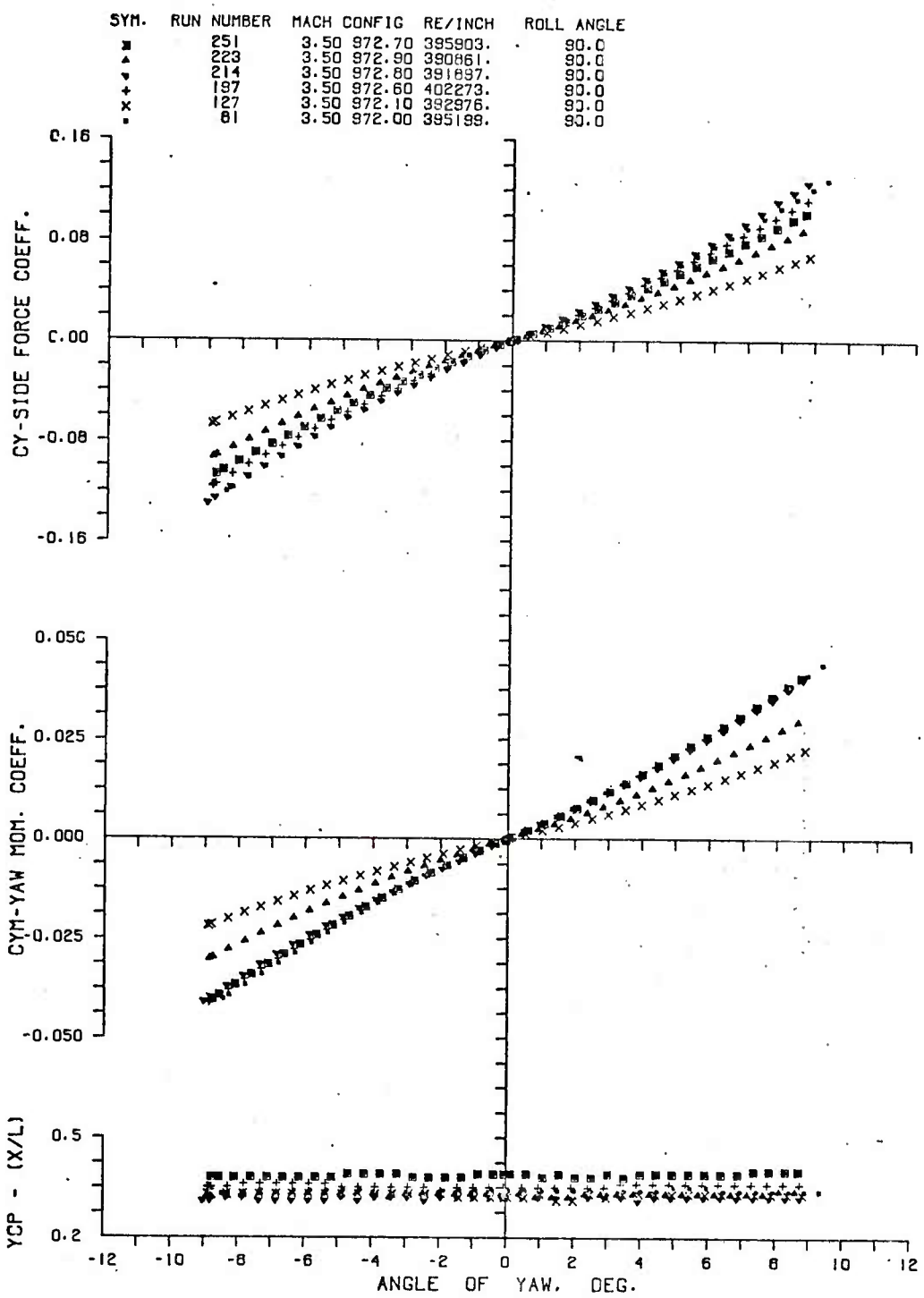

Figure A3. Continued

e. Mach 3.5

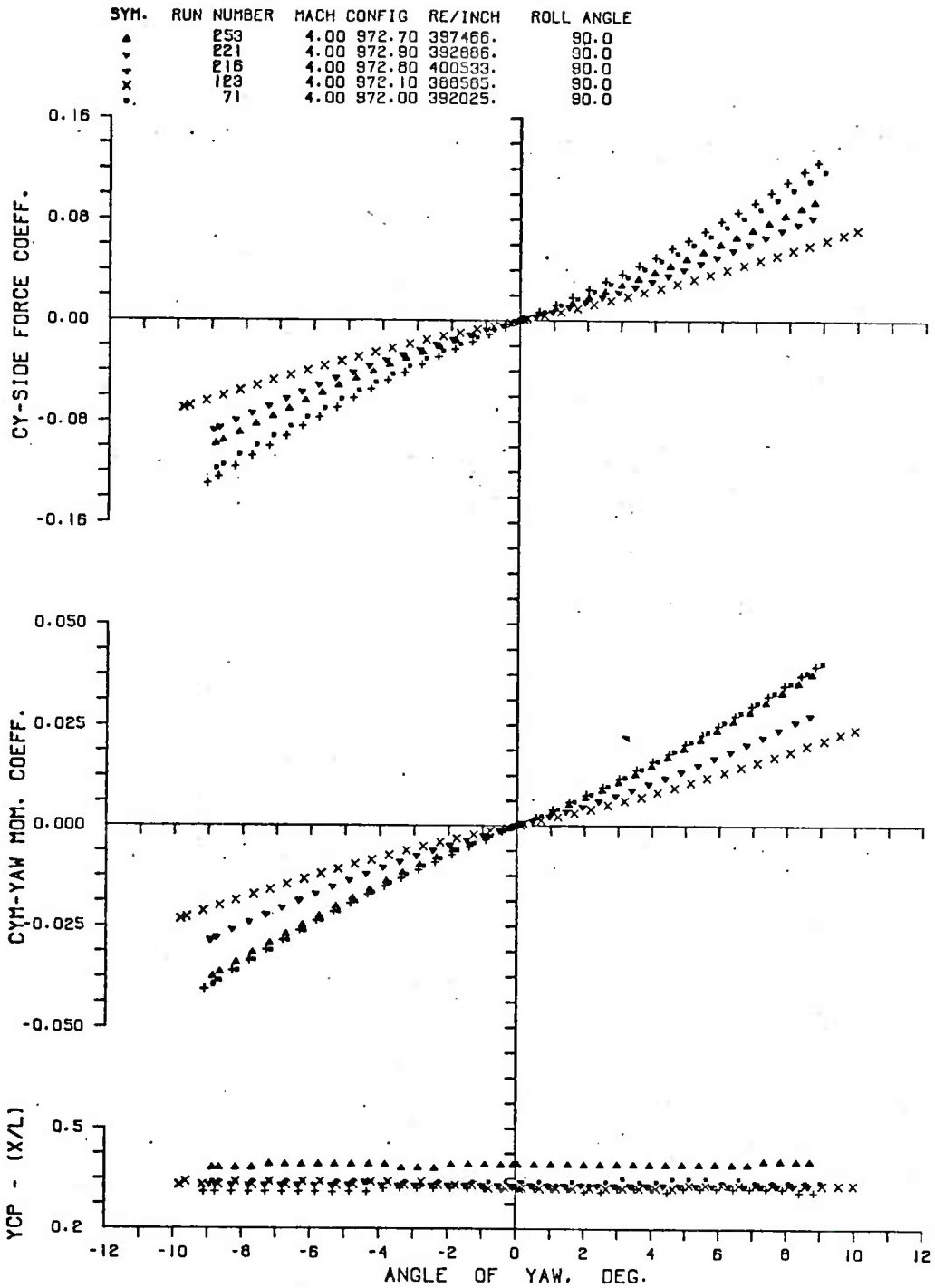

Figure A3. Concluded

f. Mach 4.0

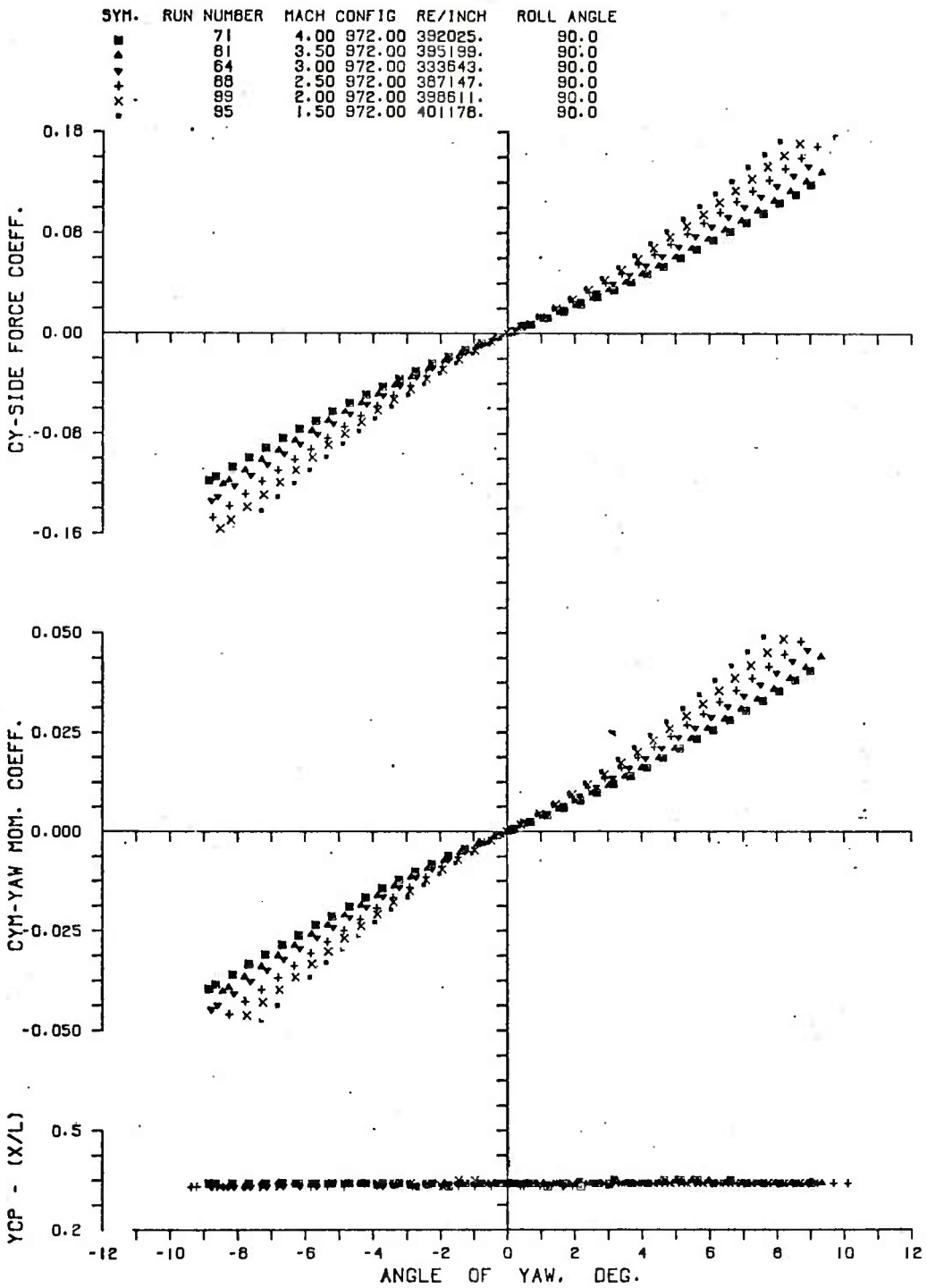

Figure A4. Variation of C_Y, C_n, Y_{CP} With Mach Number for Each Configuration

a. Configuration 972.0

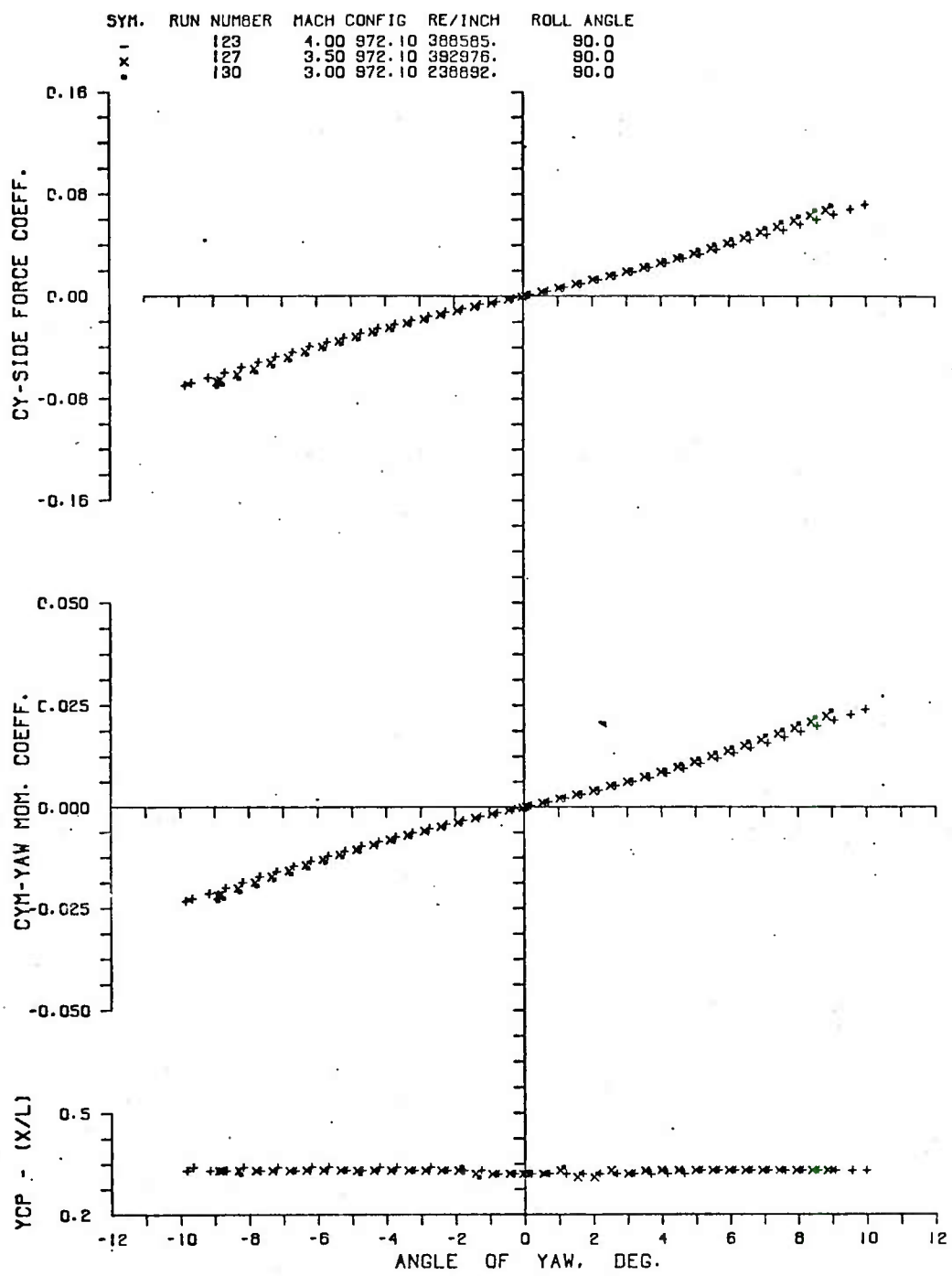

Figure A4. Continued

b. Configuration 972.1

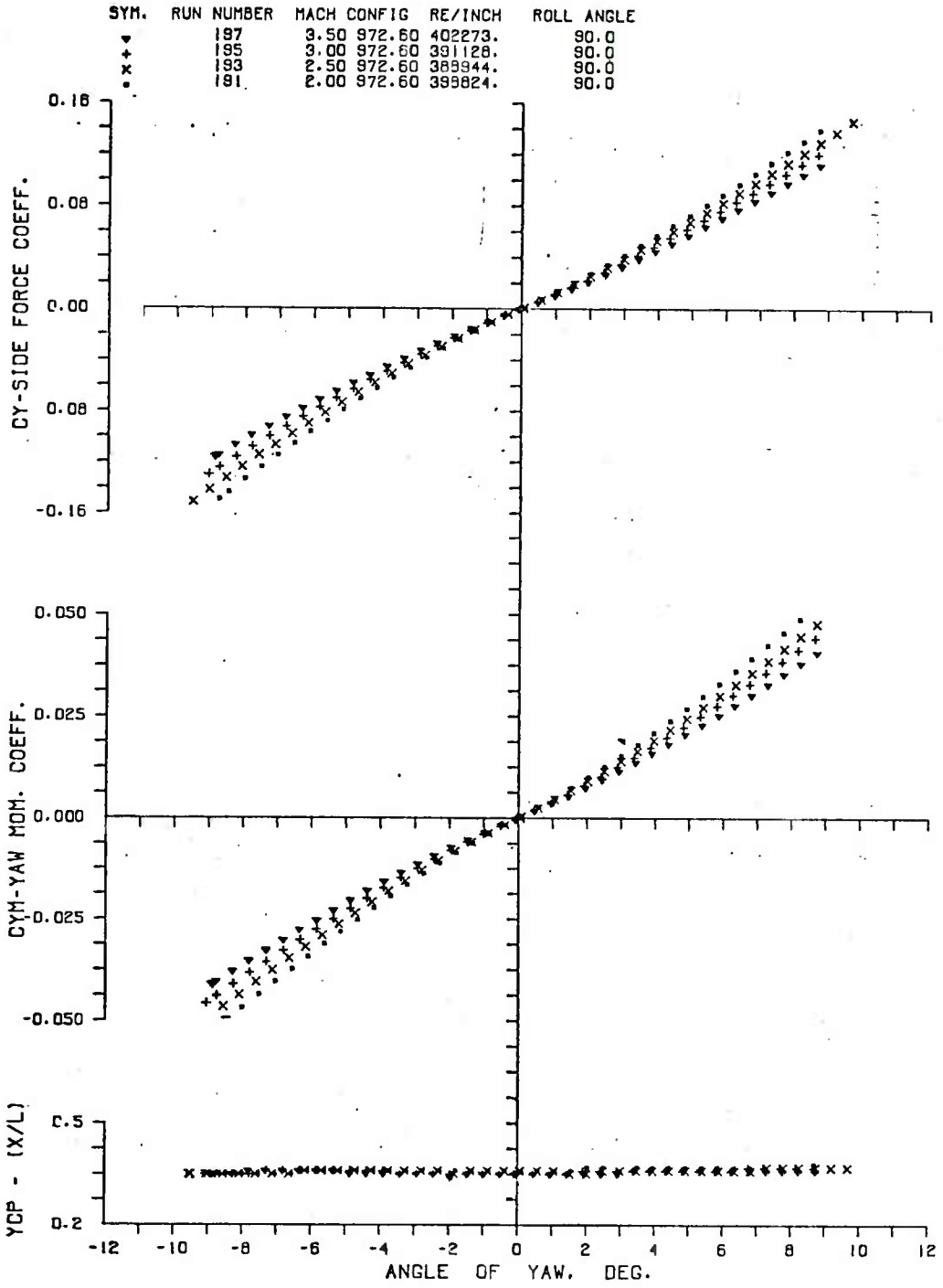

Figure A4. Continued

c. Configuration 972.6

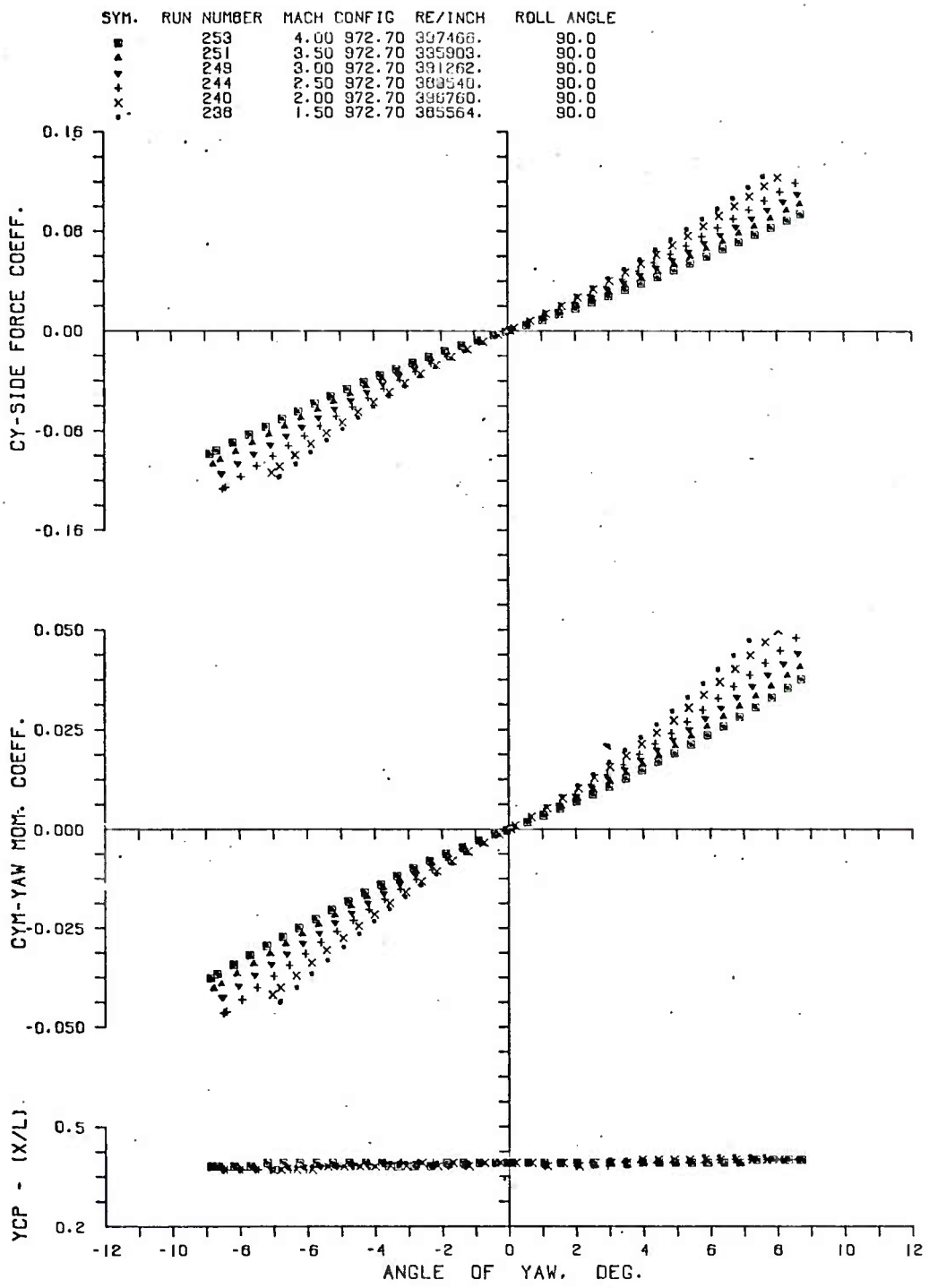

Figure A4. Continued

d. Configuration 972.7

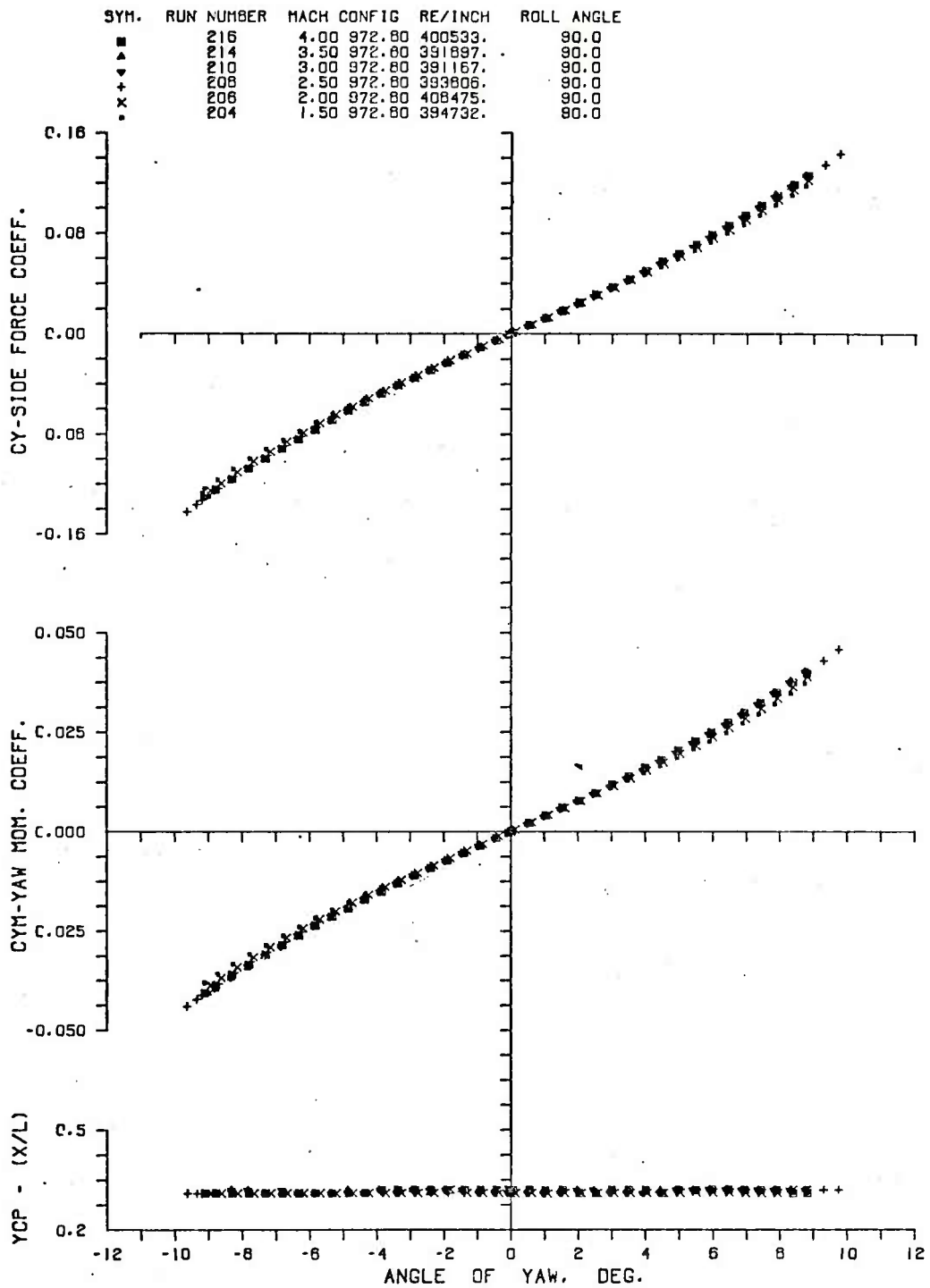

Figure A4. Continued

e. Configuration 972.8

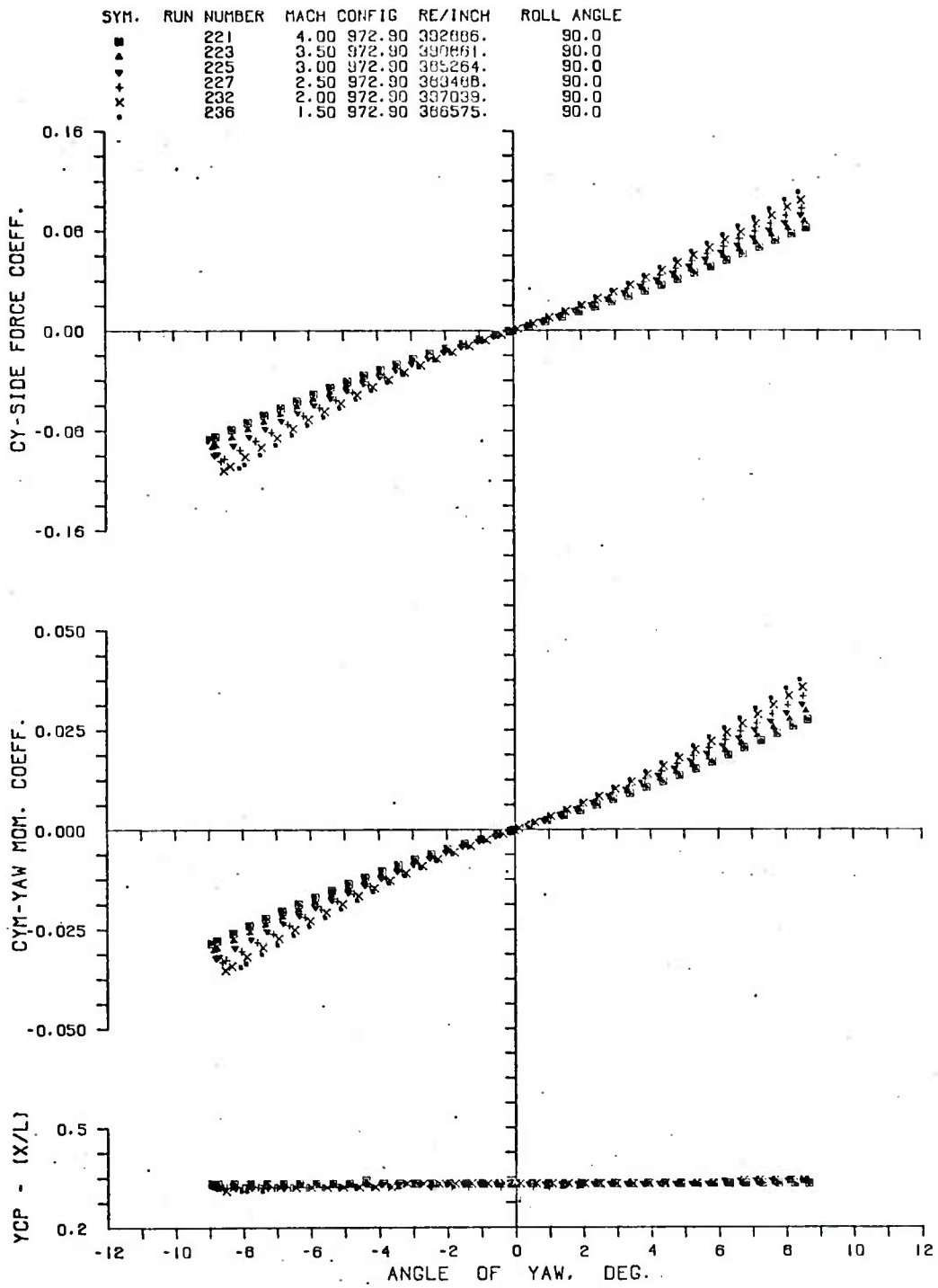

Figure A4. Concluded

f. Configuration 972.9

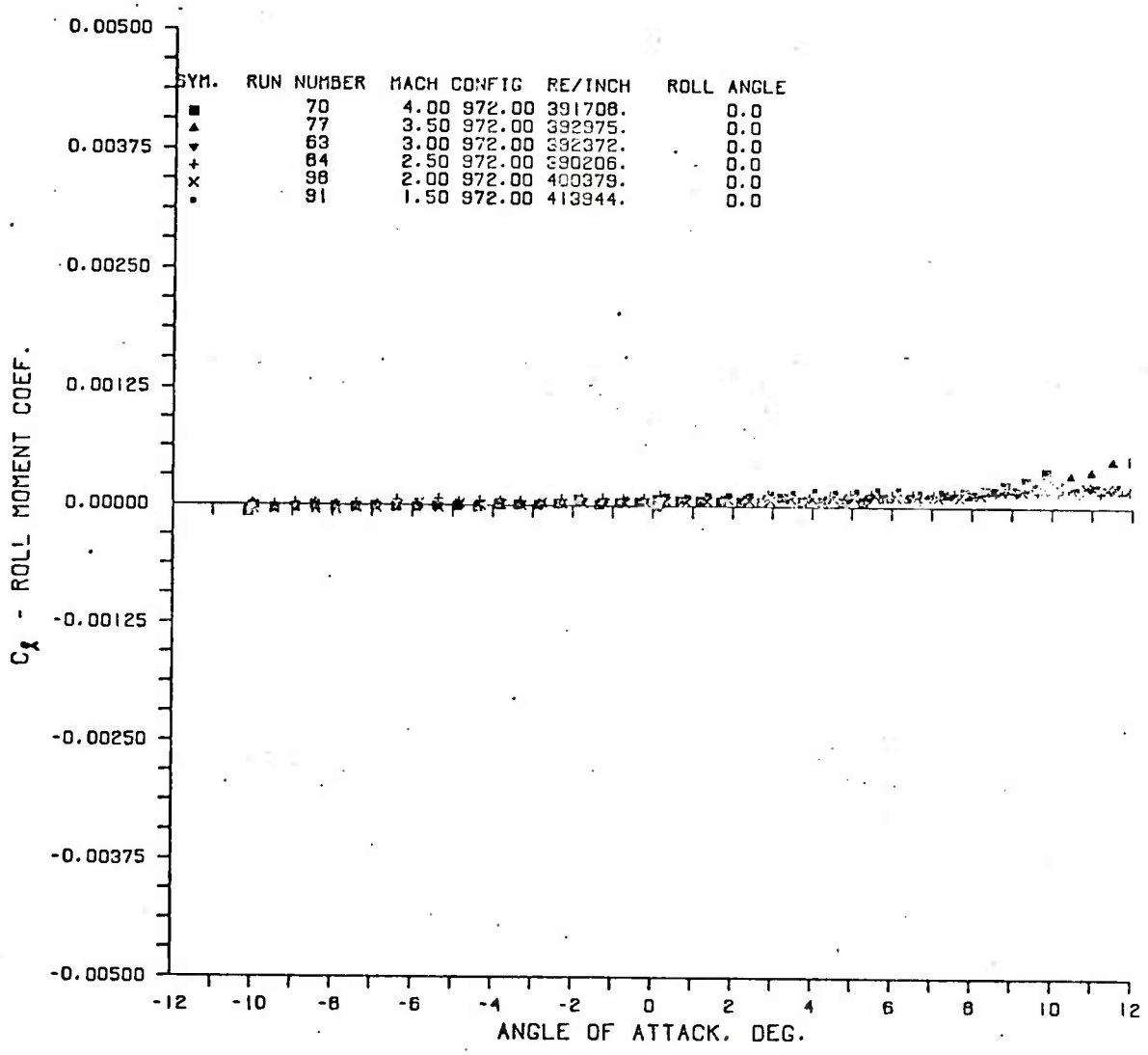

Figure A5. Variation of Roll Moment Coefficient, C_ℓ, With Mach Number for Given Roll Angles for Configuration 972.0

a. 0°

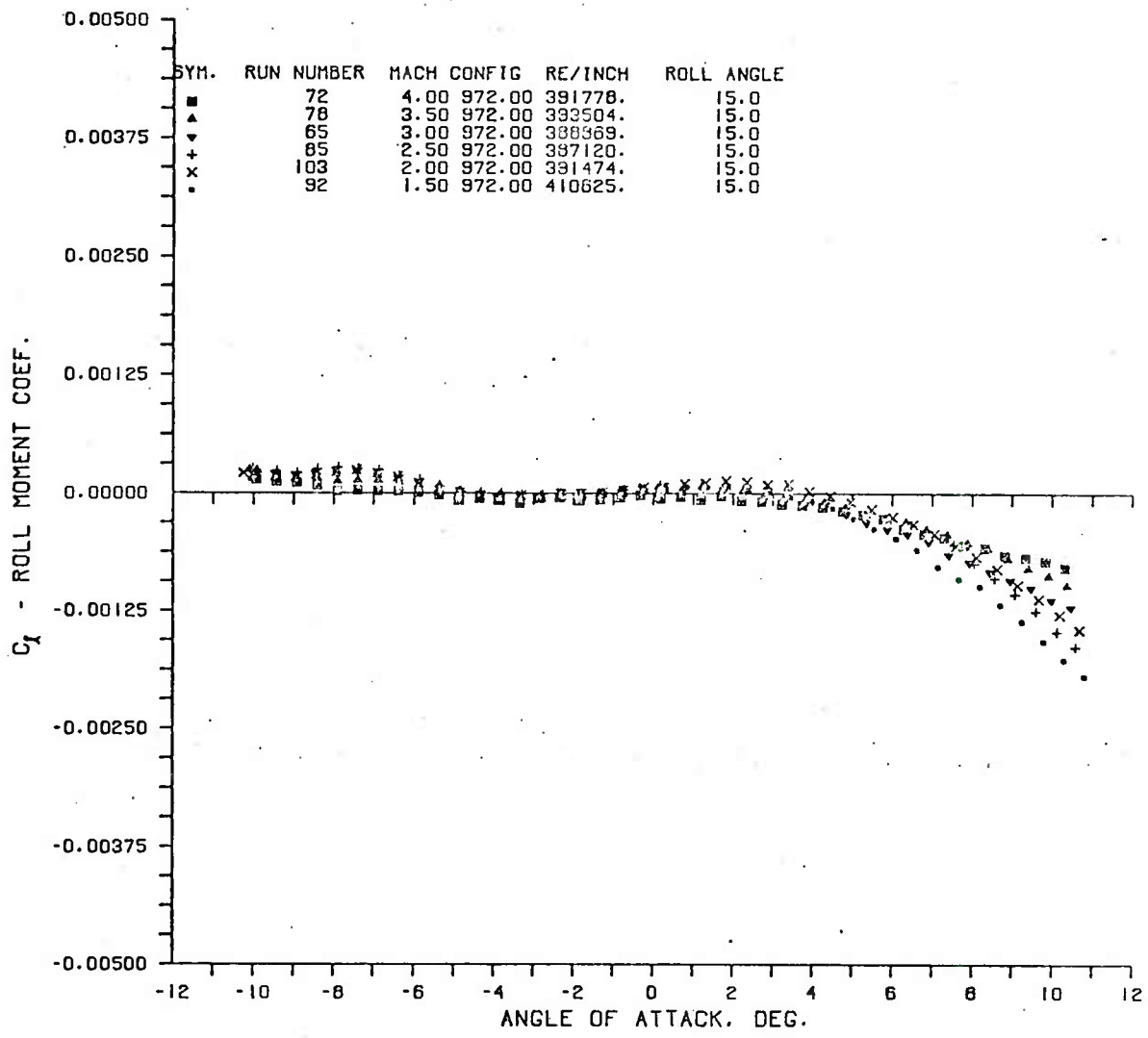

Figure A5. Continued

b. 15°

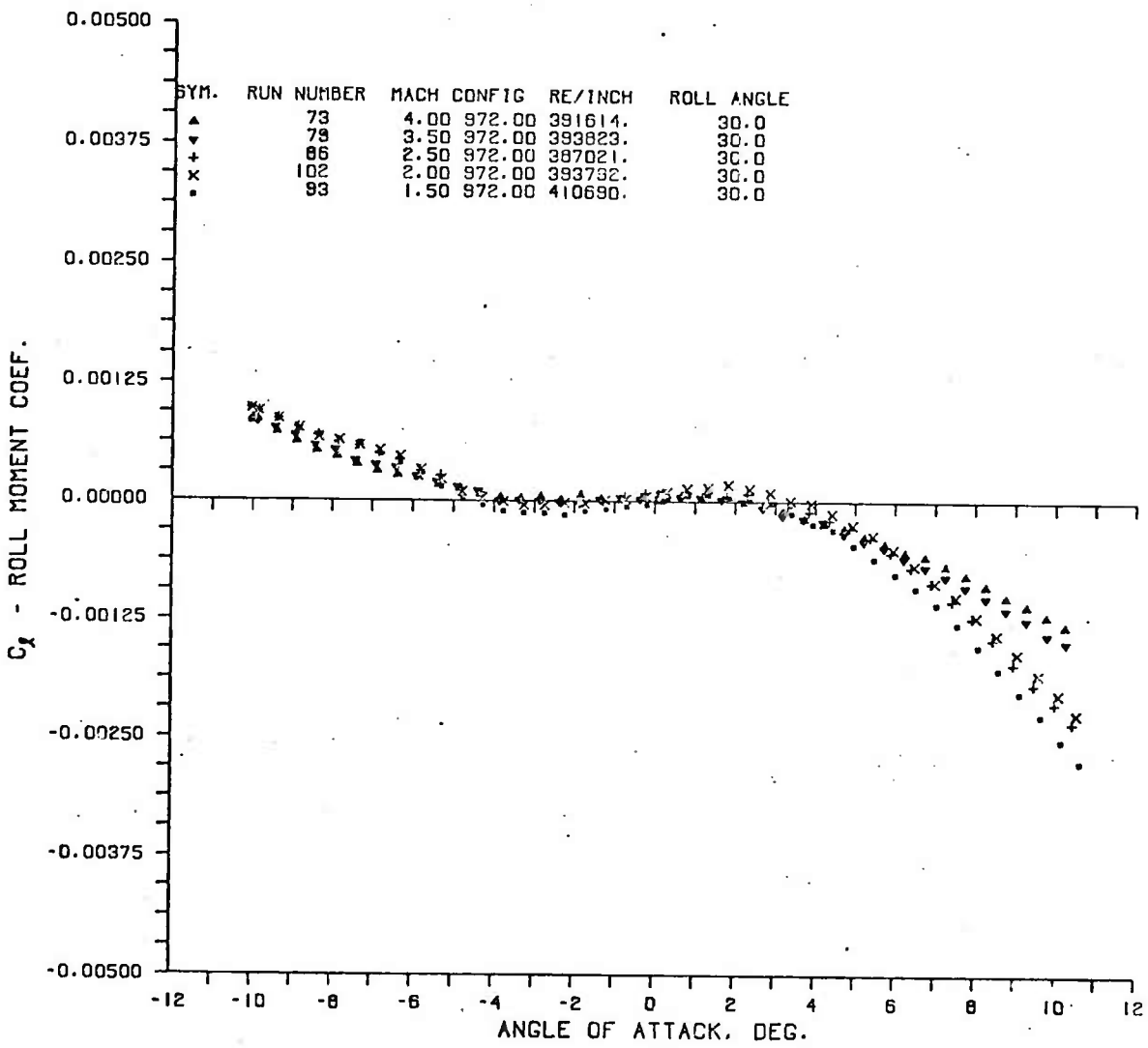

Figure A5. Continued

c. 30°

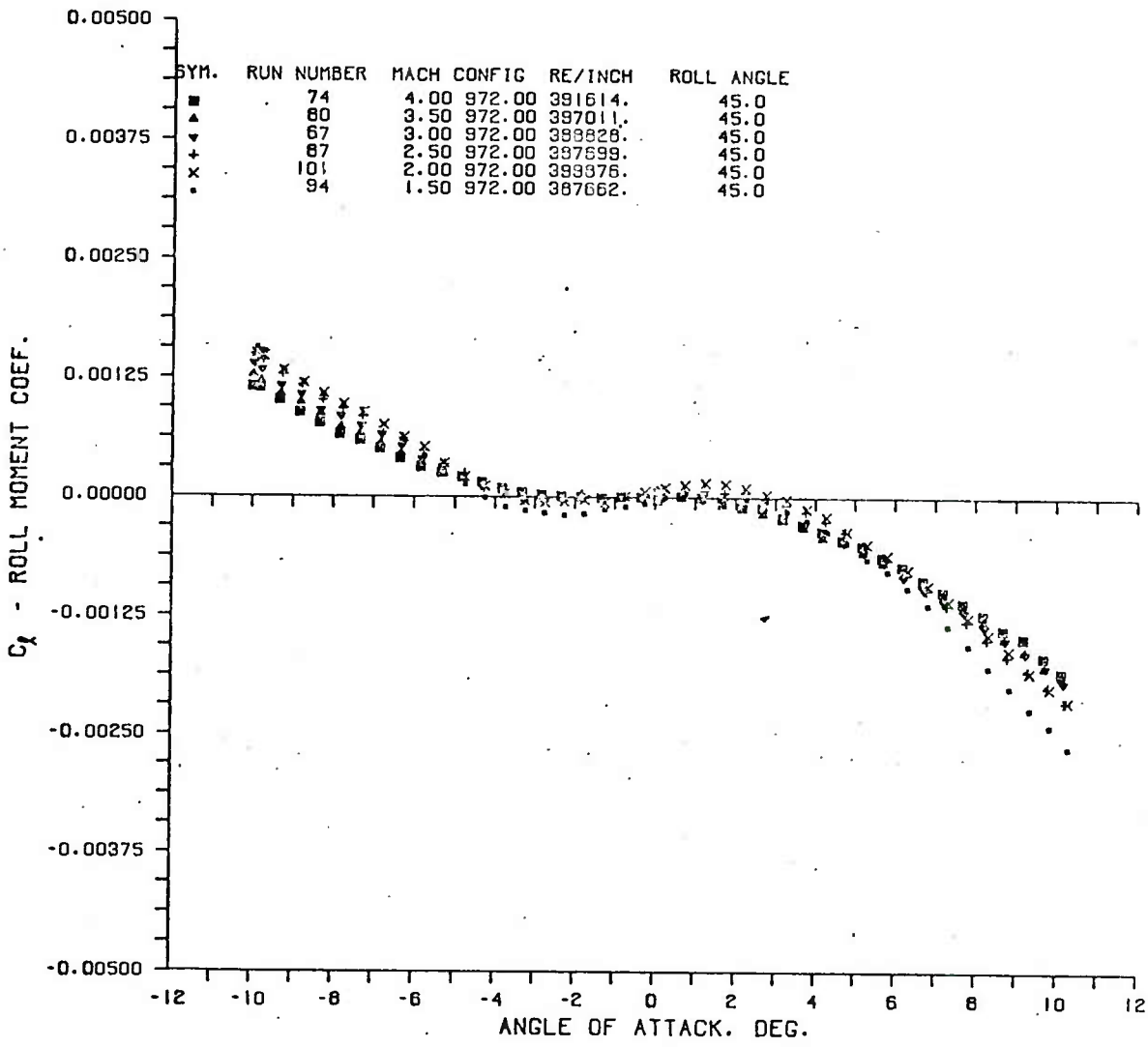

Figure A5. Continued

d. 45°

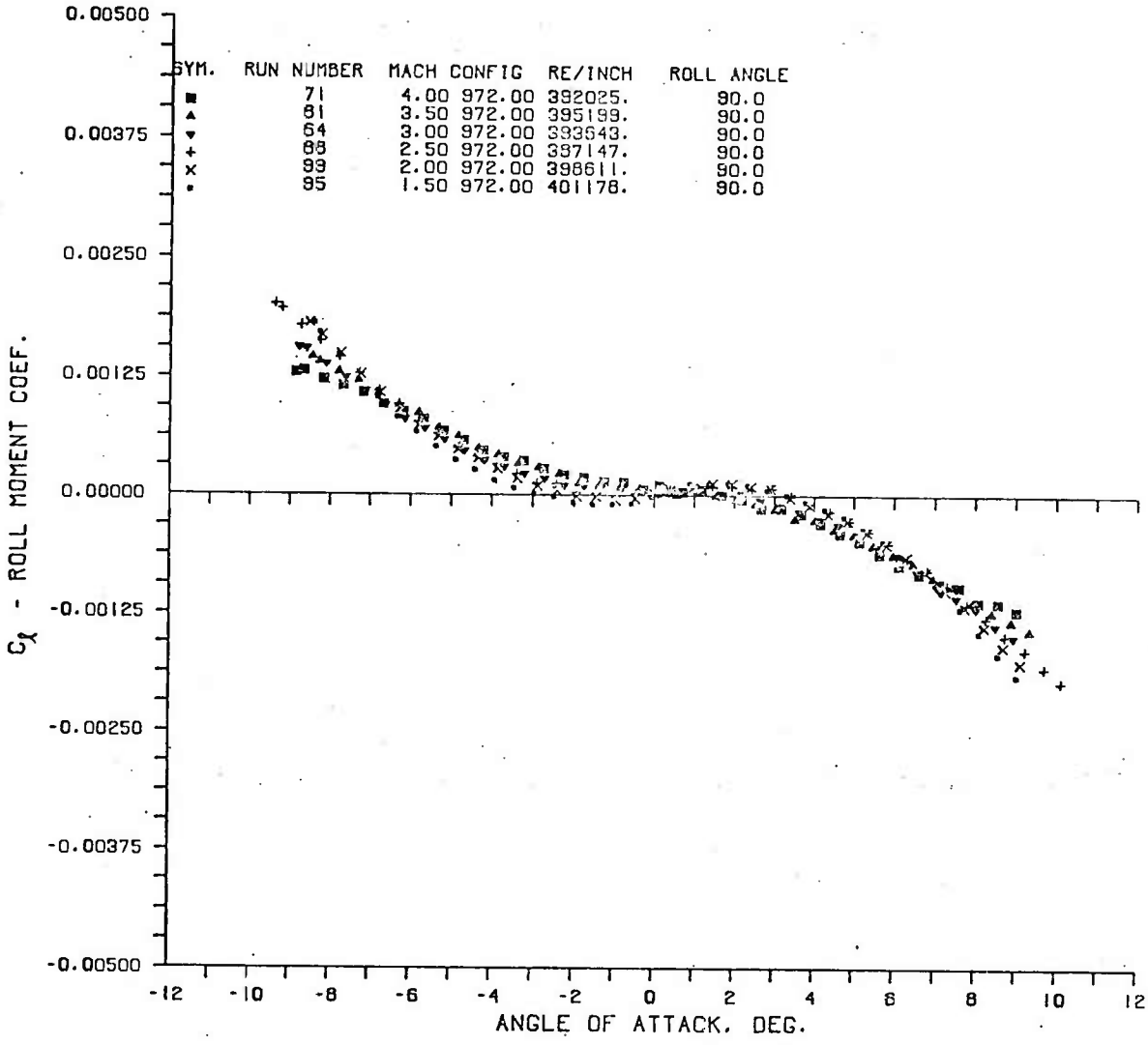

Figure A5. Continued

e. 90°

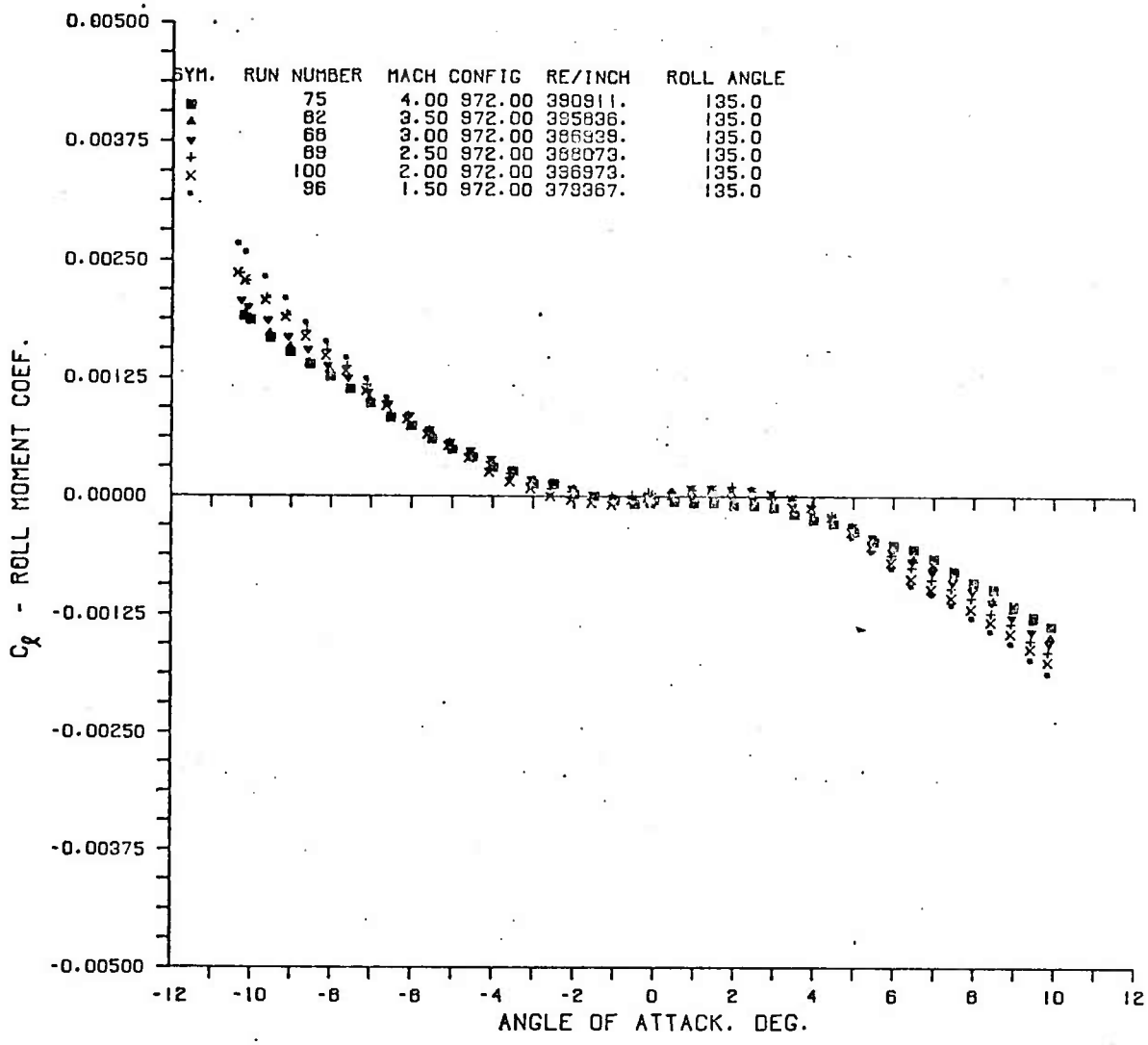

Figure A5. Continued

f. 135°

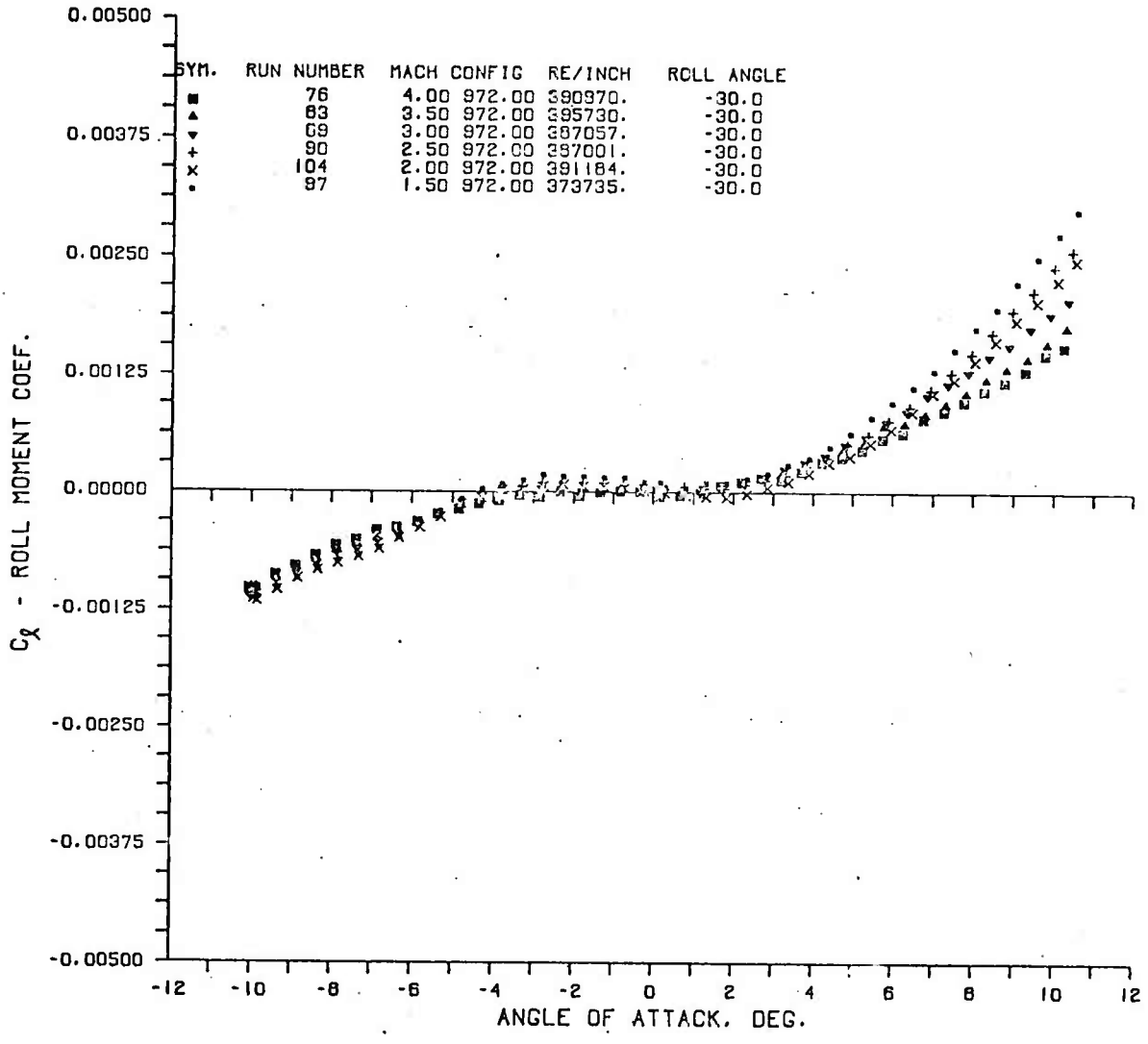

Figure A5. Concluded

g. -30°

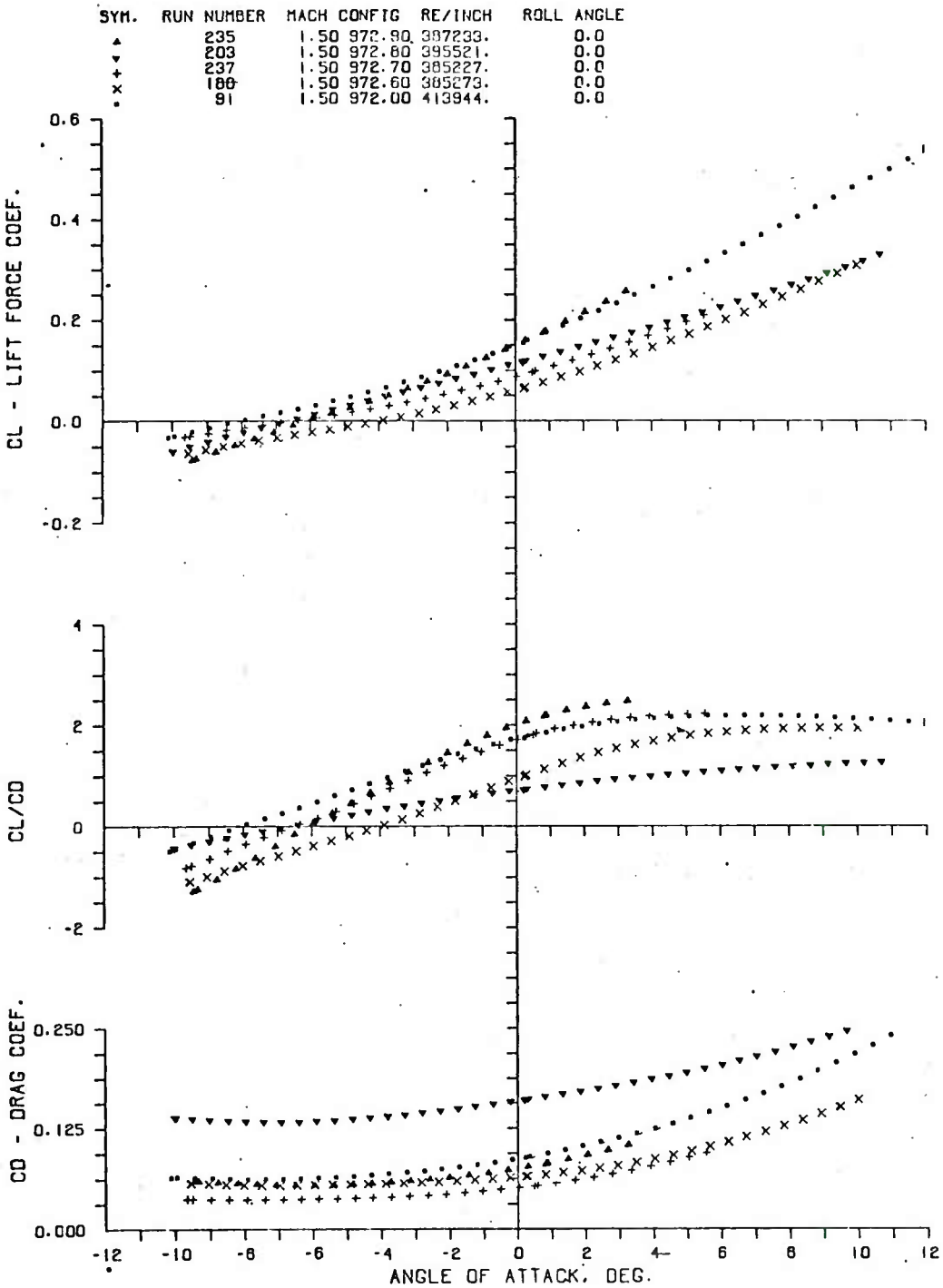

Figure A6. Variation of C_L, C_D, C_L/C_D With Configuration at Constant Mach Number

a. Mach 1.5

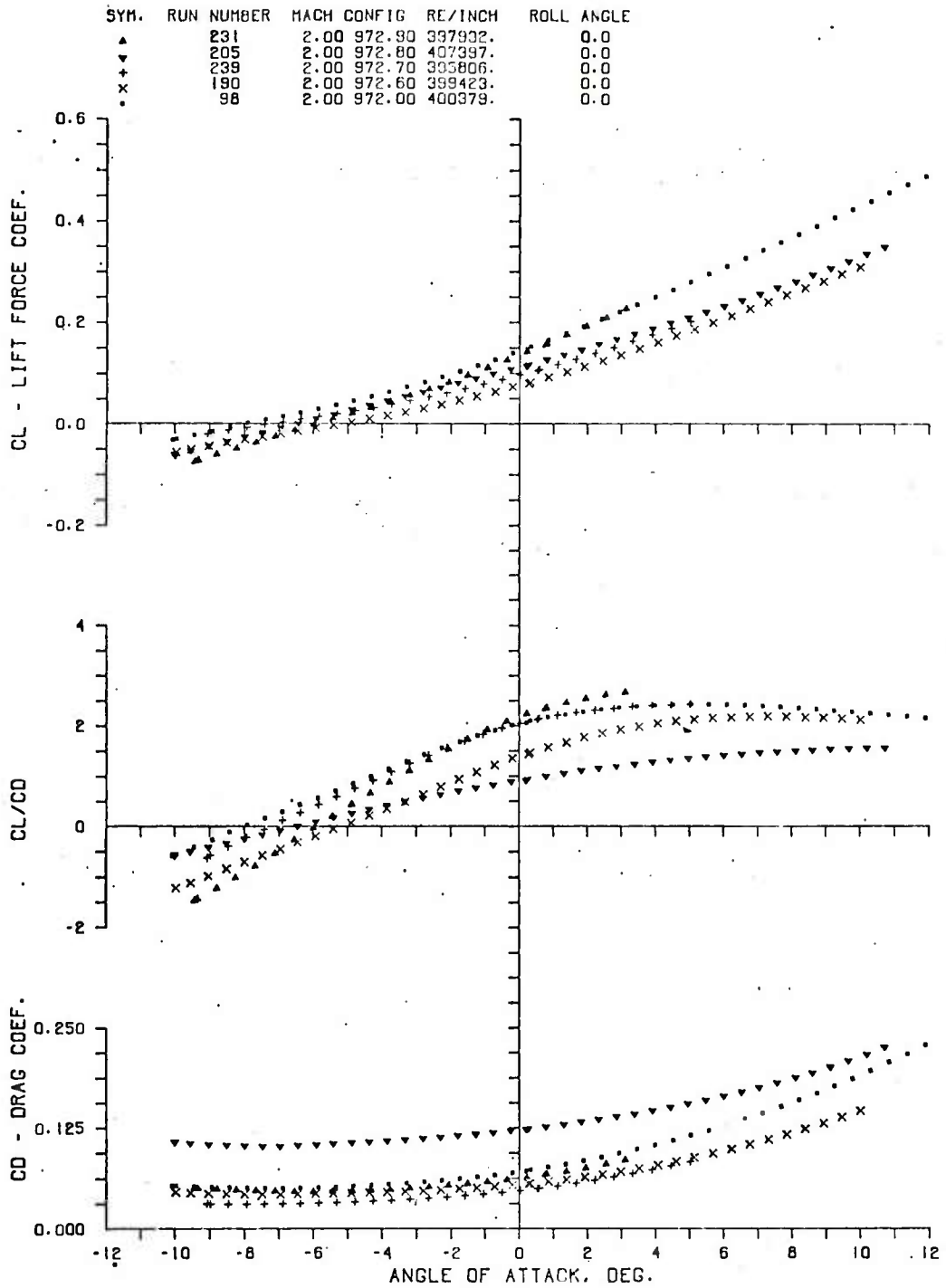

Figure A6. Continued

b. Mach 2.0

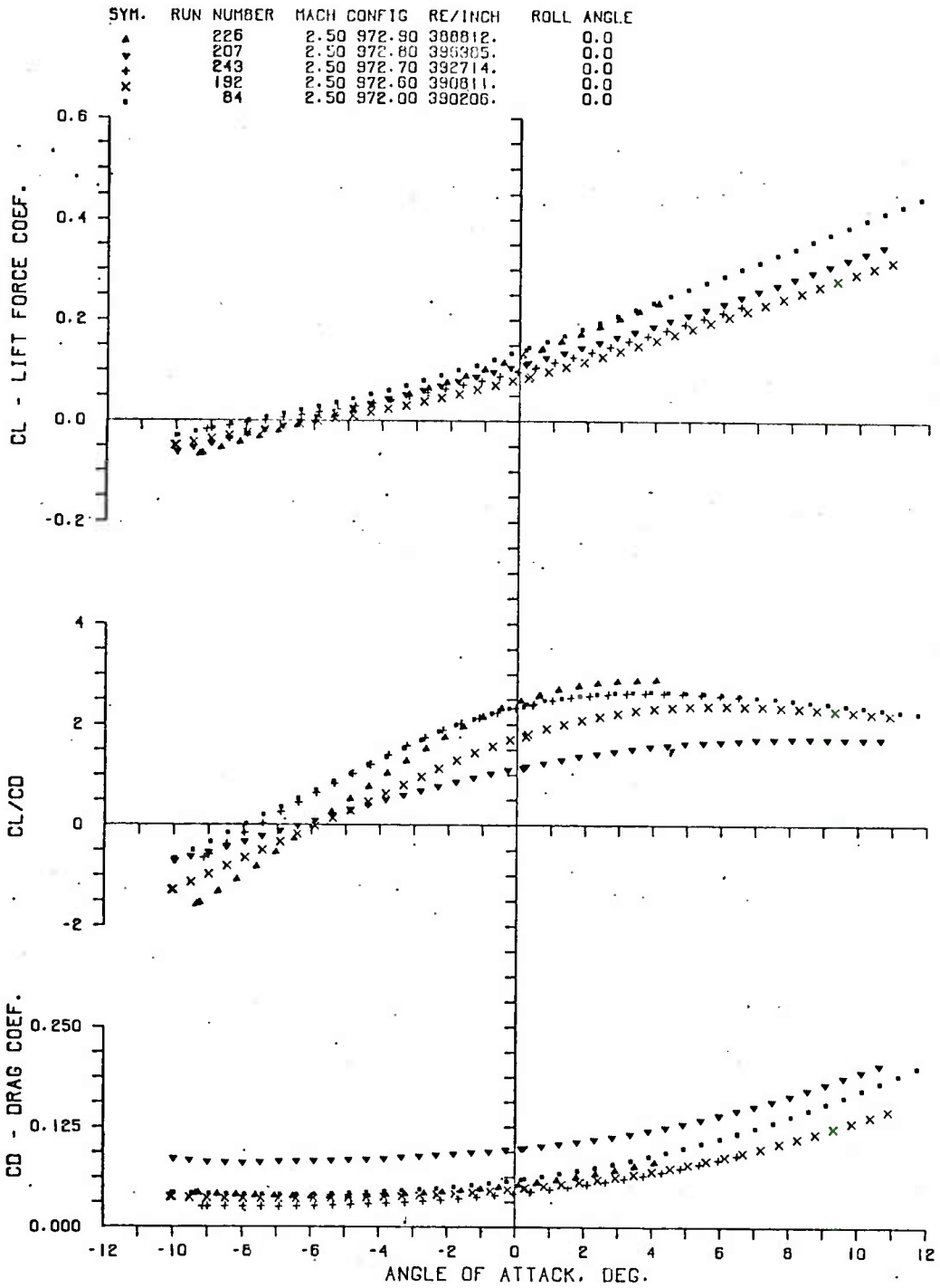

Figure A6. Continued

c. Mach 3.0

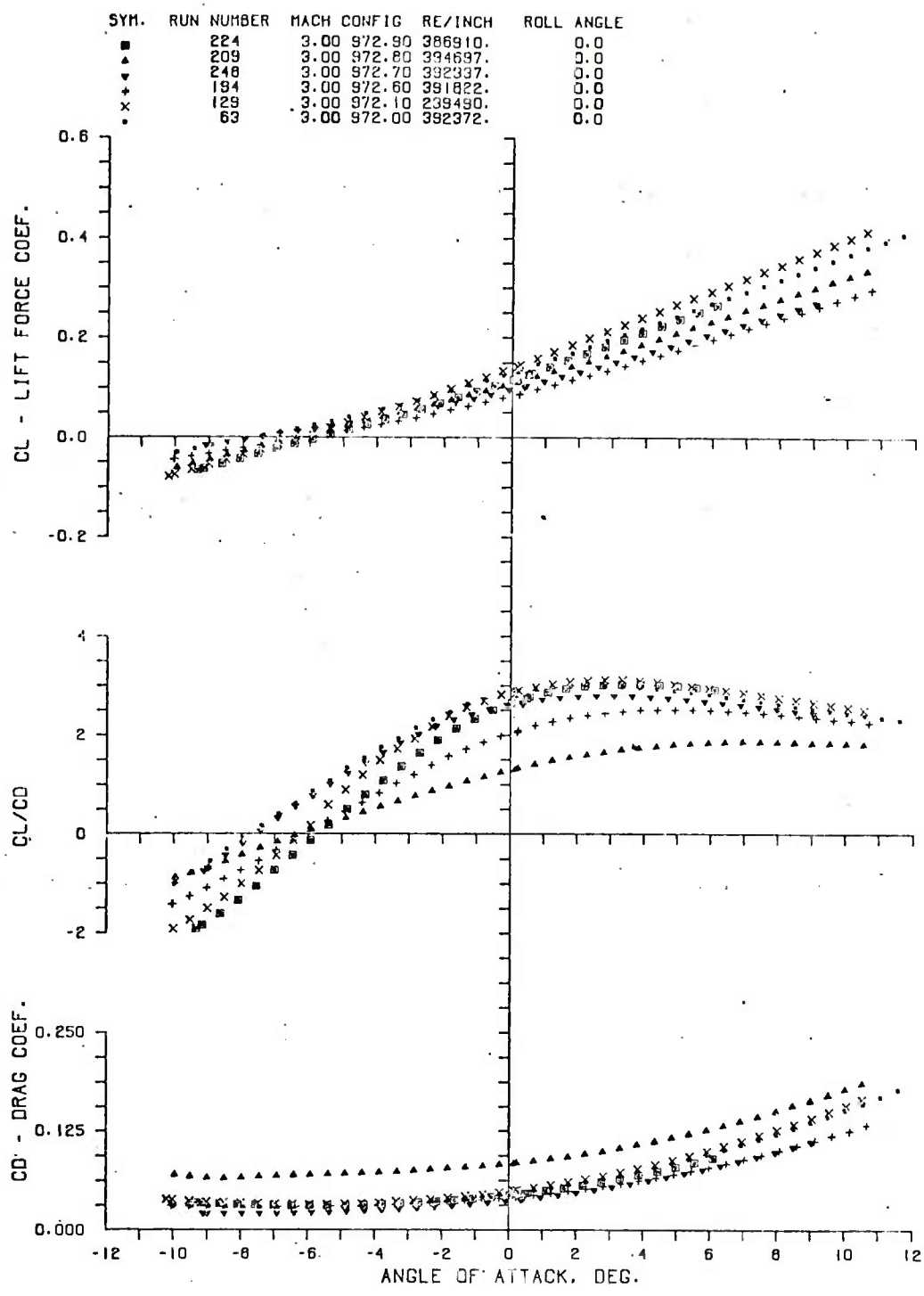

Figure A6. Continued

d. Mach 3.0

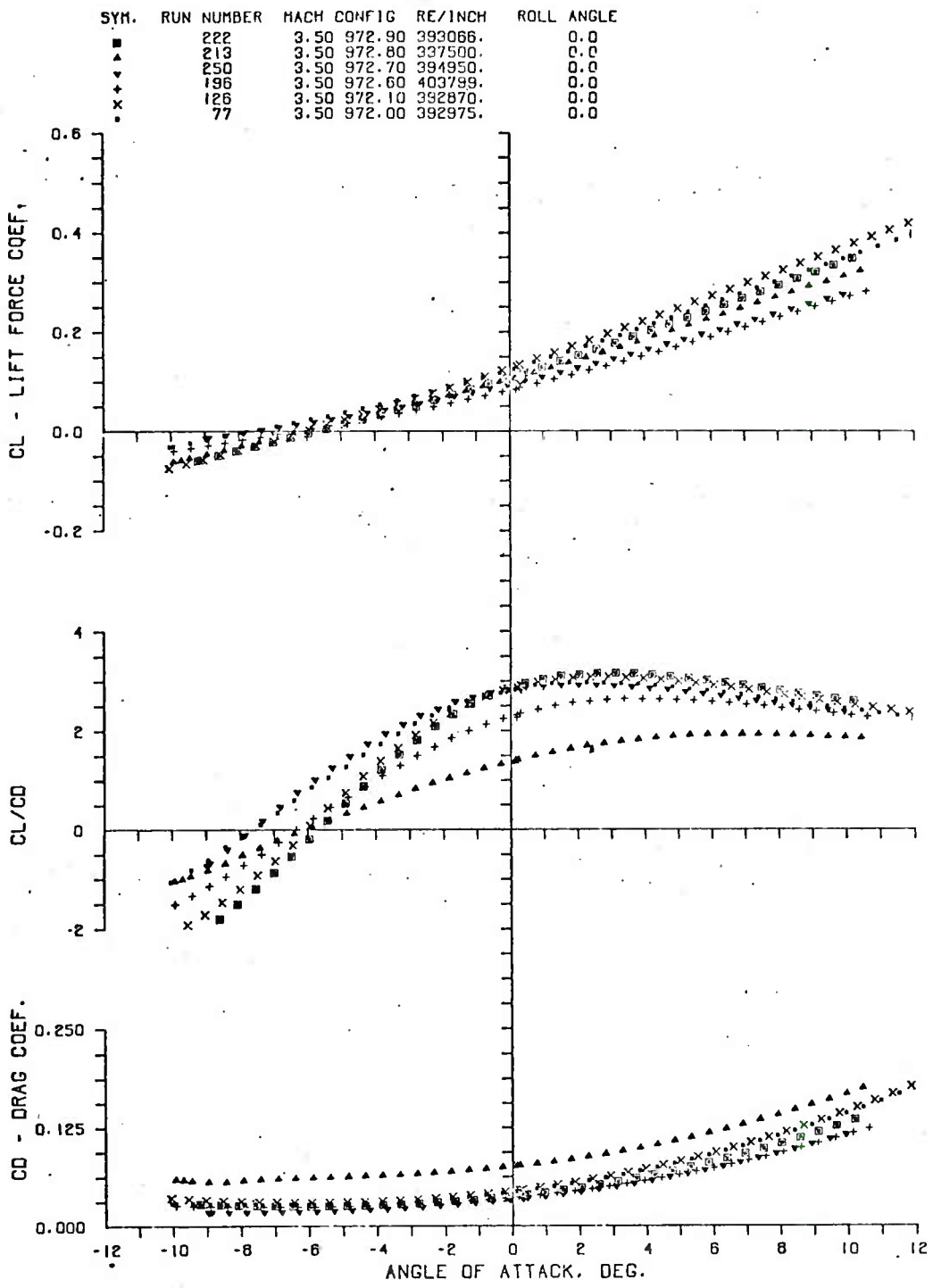

Figure A6. Continued

e. Mach 3.5

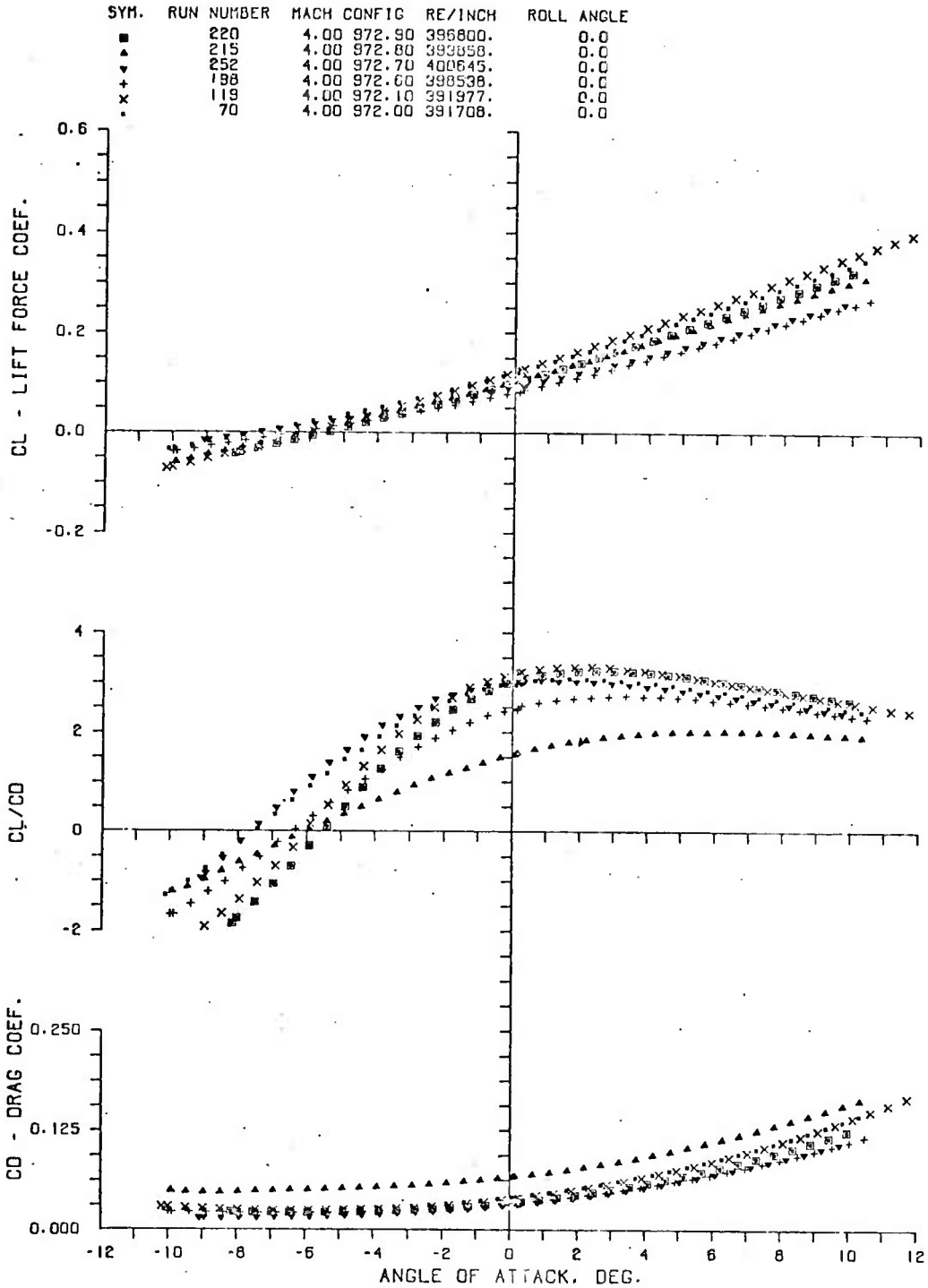

Figure A6. Concluded

f. Mach 4.0

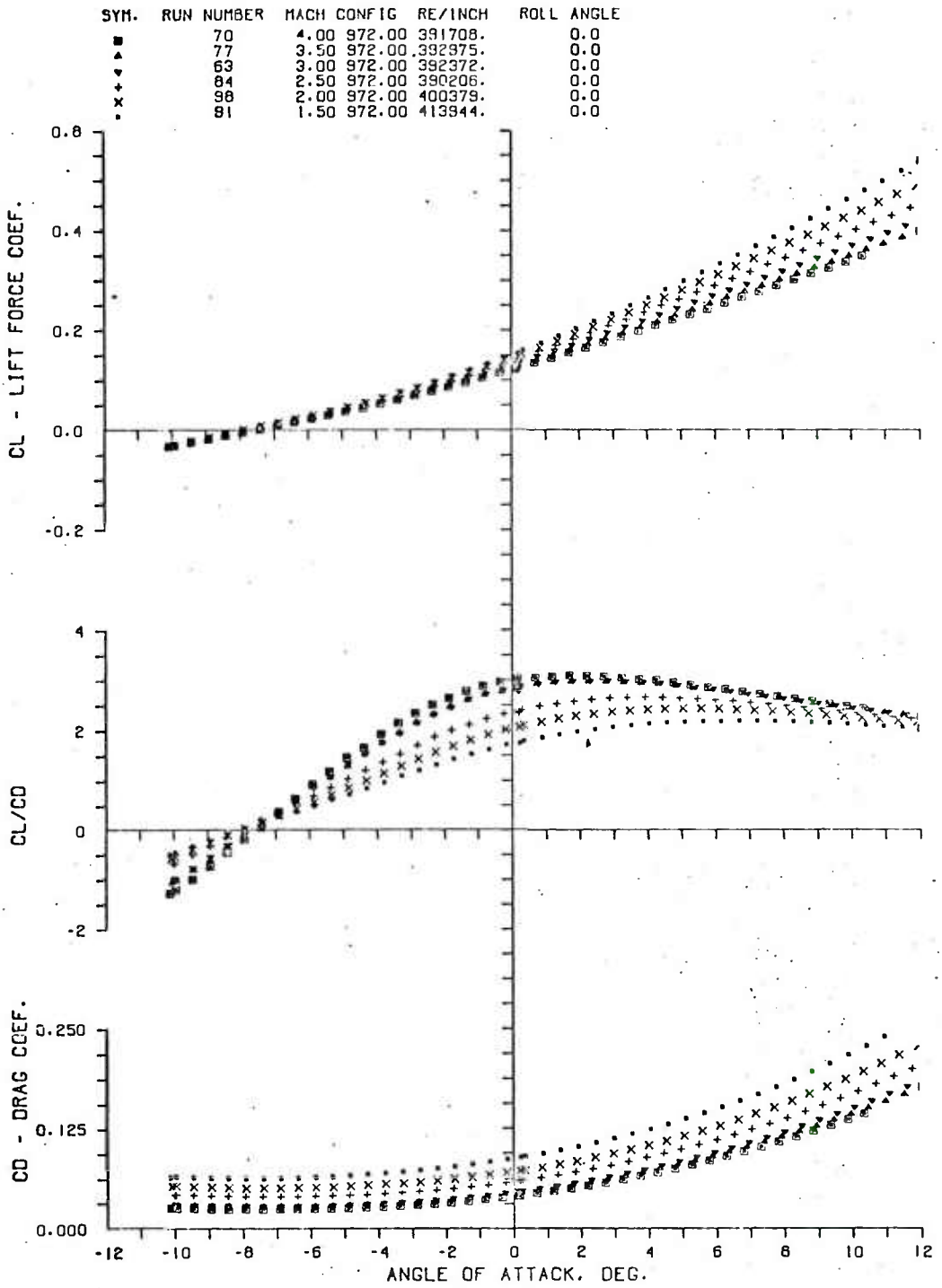

Figure A7. Variation of C_L, C_D, C_L/C_D With Mach Number for Each Configuration

a. Configuration 972.0

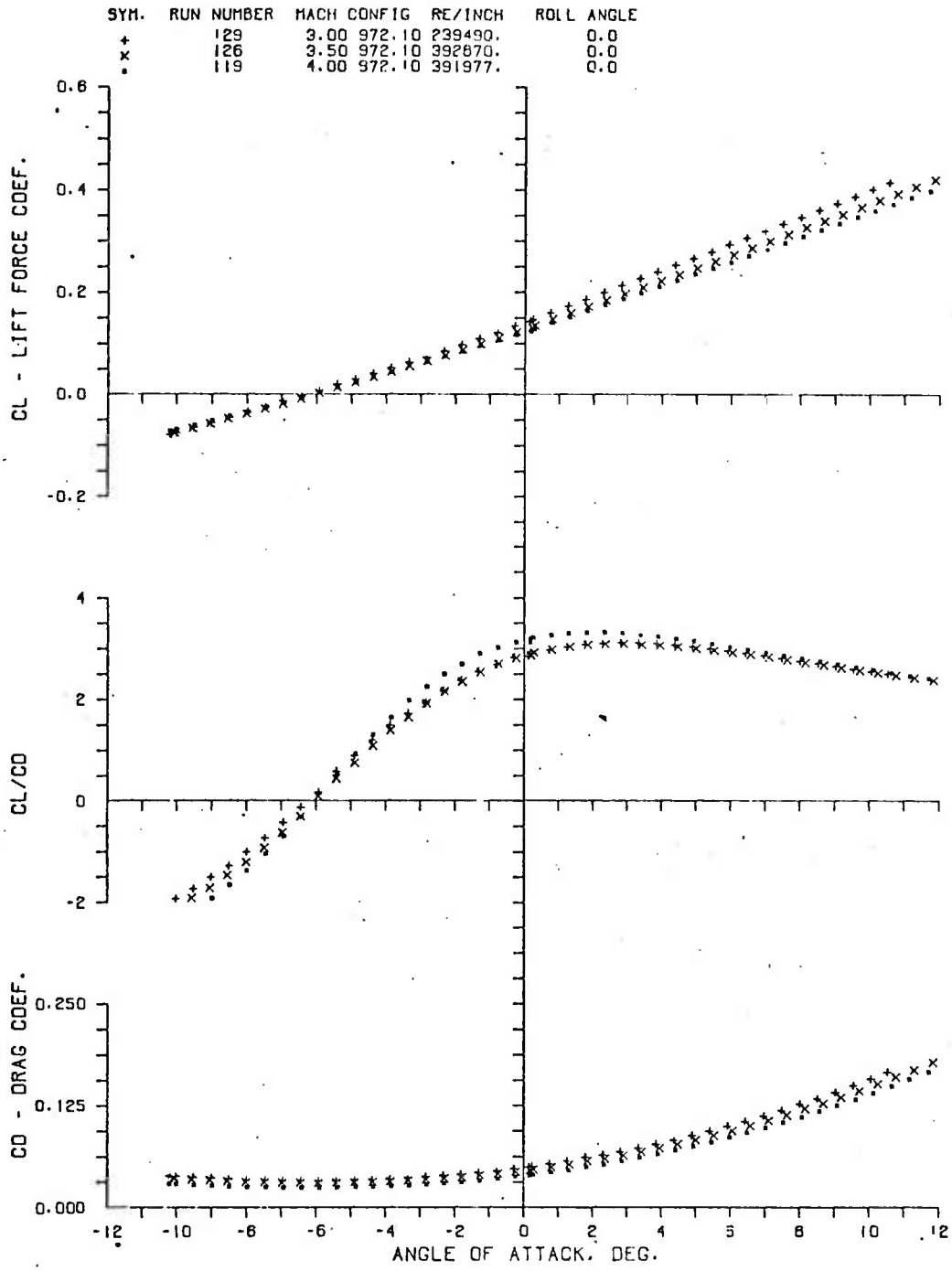

Figure A7. Continued

b. Configuration 972.1

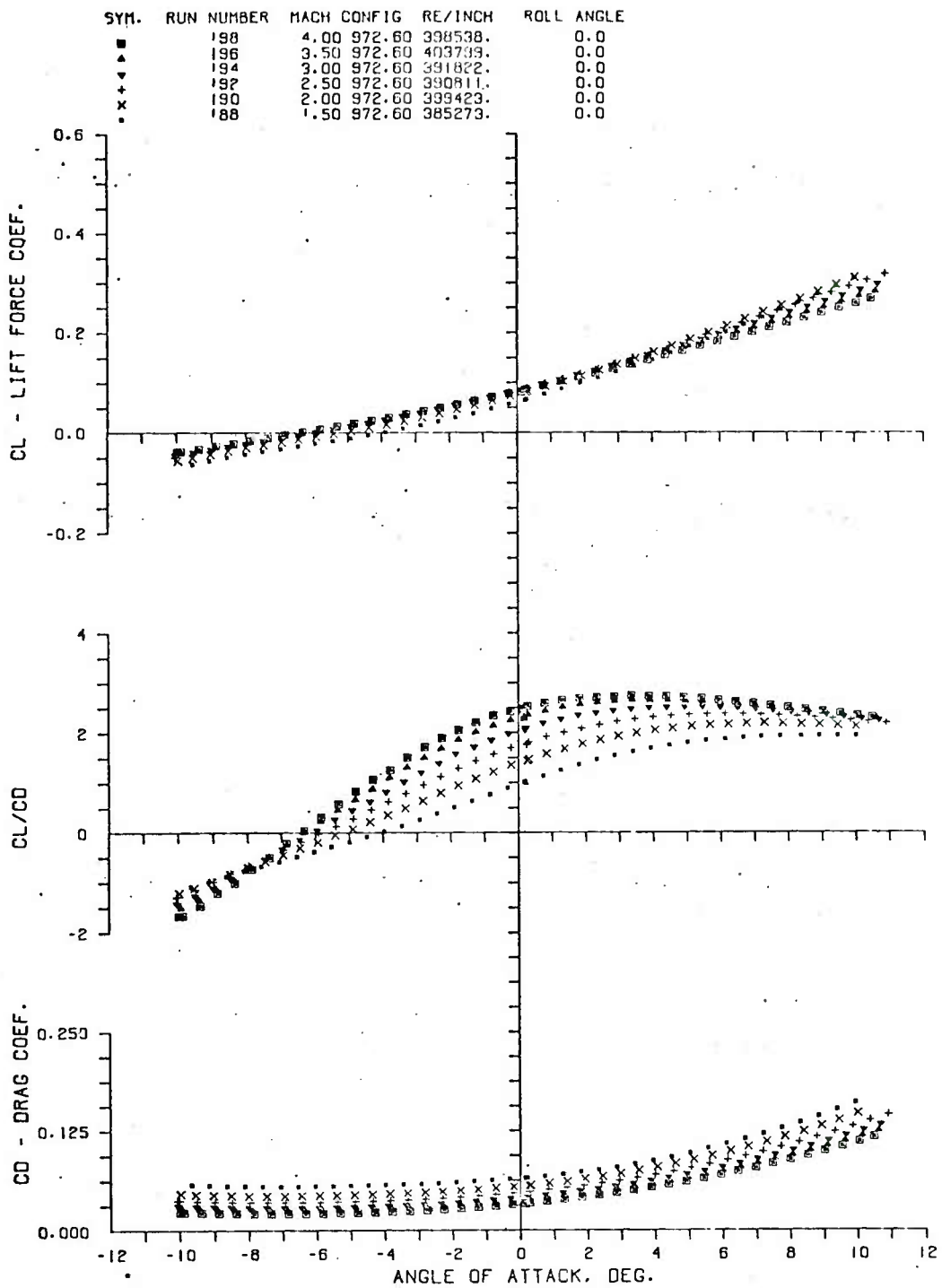

Figure A7. Continued

c. Configuration 972.6

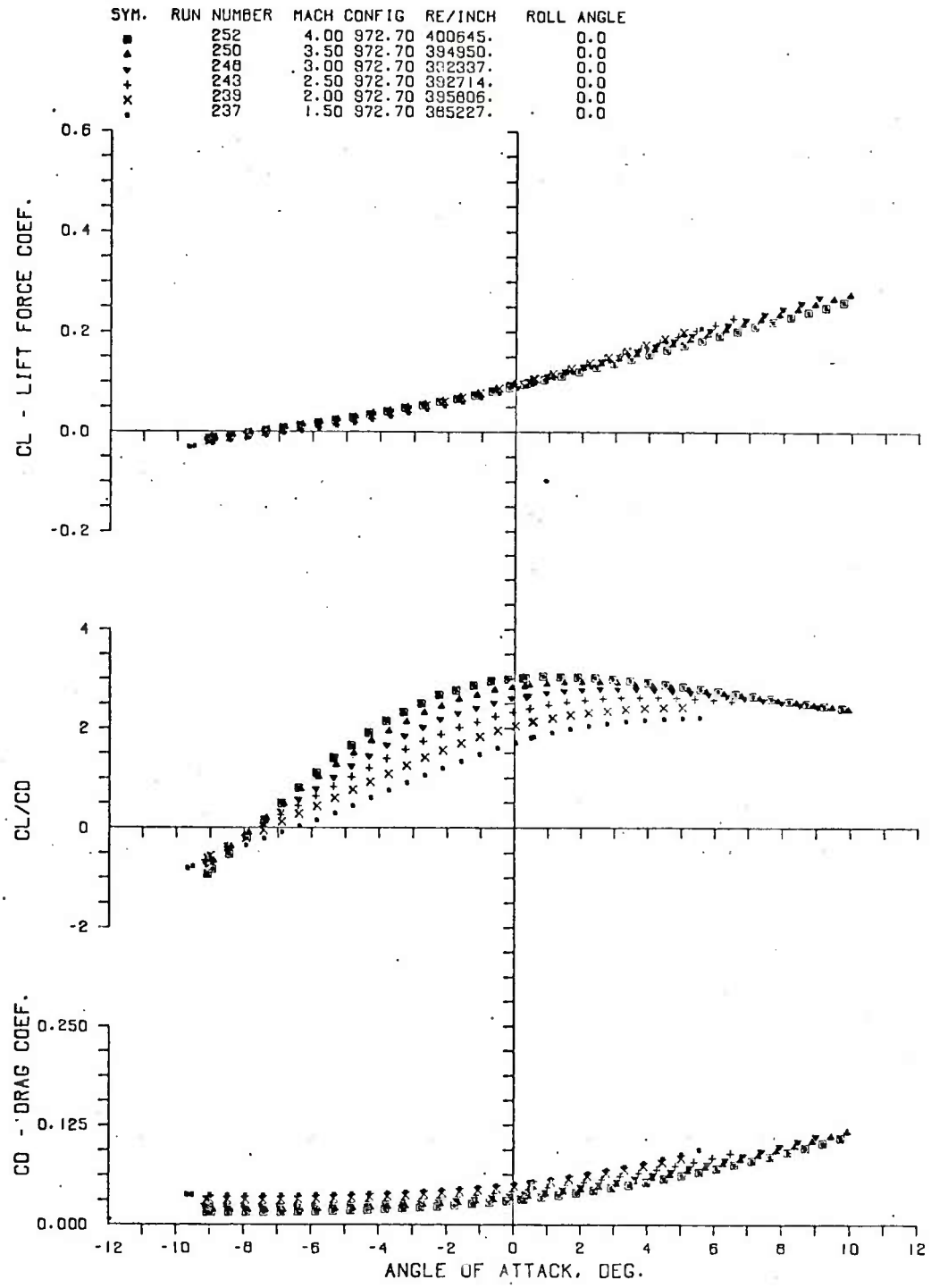

Figure A7. Continued

d. Configuration 972.7

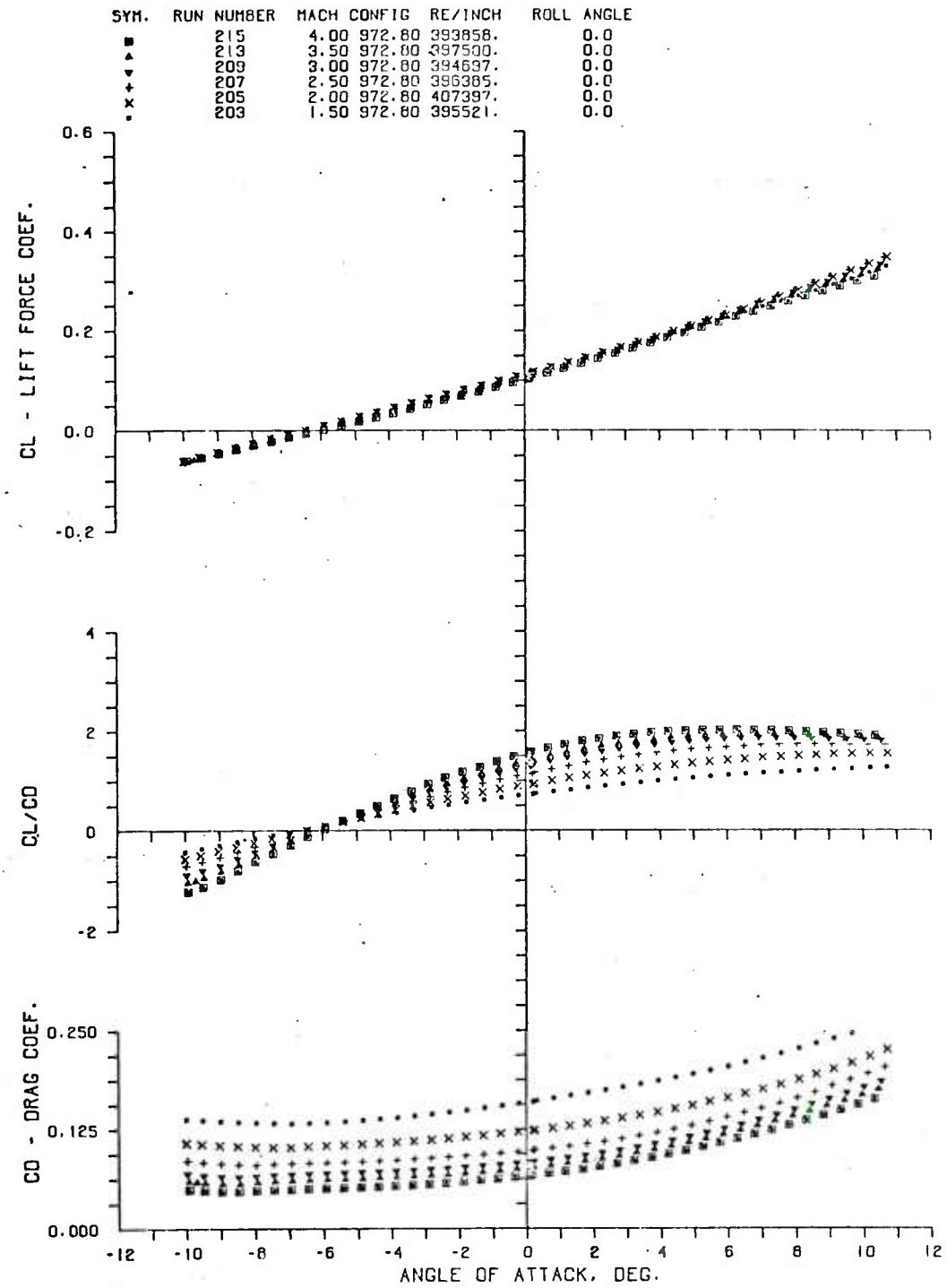

Figure A7. Continued

e. Configuration 972.8

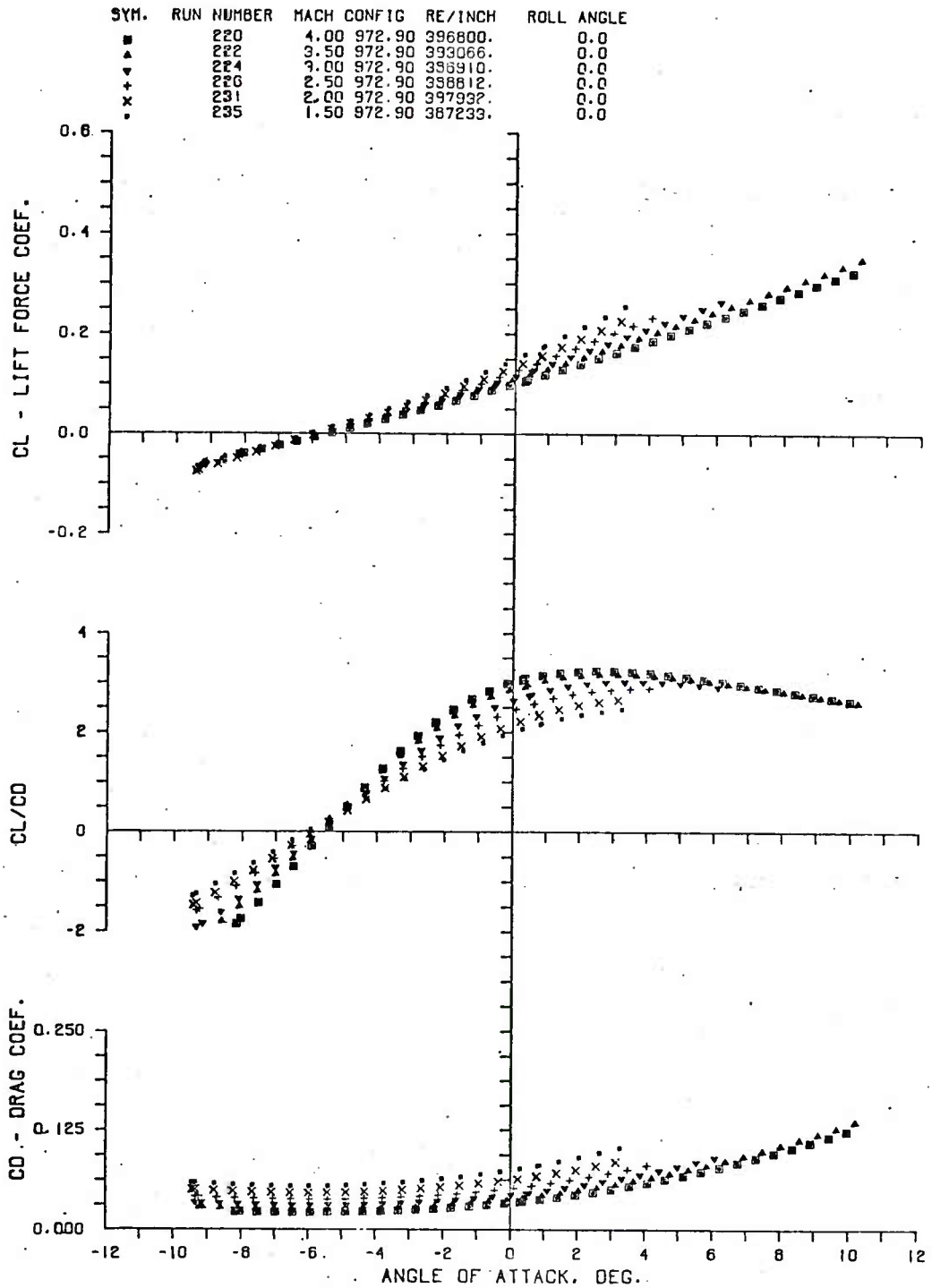

Figure A7. Concluded

f. Configuration 972.9

LIST OF SYMBOLS

b	model base width
C_A	axial-force coefficient, $F_A/(qS)$
C_D	drag-force coefficient, $F_D/(qS)$
C_L	lift-force coefficient, $F_L/(qS)$
C_m	pitching-moment coefficient, $m/(qS\ell)$, reference at the model base
C_n	yawing-moment coefficient, $n/(qS\ell)$, reference at the model base
C_N	normal-force coefficient, $F_N/(qS)$
C_Y	side-force coefficient, $F_Y/(qS)$
F_A	axial-force
F_D	drag-force, $F_A \cos \alpha + F_N \sin \alpha$
F_L	lift-force, $F_N \cos \alpha - F_A \sin \alpha$
F_N	normal force
F_Y	side force
ℓ	model length
m	pitching moment
M	Mach number
n	yawing moment
q	free-stream dynamic pressure
Re	Reynolds number, based on free-stream conditions
S	reference planform area, $1/2[b\ell]$
X_{CP}	location of normal-force center of pressure, normalized with respect to model length, ℓ, and referenced at the model base

Y_{CP} location of side-force center of pressure, normalized with respect to model length, ℓ, and referenced at the model base

α angle of attack

ψ angle of yaw

DISTRIBUTION LIST

No. of Copies	Organization
12	Commander Defense Documentation Center ATTN: DDC-TCA Cameron Station Alexandria, VA 22314
2	Commander US Army Materiel Command ATTN: AMCDMA Mr. N. Klein Mr. J. Bender 5001 Eisenhower Avenue Alexandria, VA 22333
1	Commander US Army Materiel Command ATTN: AMCRD, BG H.A. Griffith 5001 Eisenhower Avenue Alexandria, VA 22333
1	Commander US Army Materiel Command ATTN: AMCRD-T 5001 Eisenhower Avenue Alexandria, VA 22333
1	Commander US Army Materiel Command ATTN: AMCRD-MT 5001 Eisenhower Avenue Alexandria, VA 22333
1	Commander US Army Aviation Systems Command ATTN: AMSAV-E 12th & Spruce Streets St. Louis, MO 63166
1	Director US Army Air Mobility Research and Development Laboratory ATTN: SAVDL-D, Mr. P. Yaggy Ames Research Center Moffett Field, CA 94035
2	Commander US Army Electronics Command ATTN: AMSEL-CT/L, B. Louis AMSEL-RD Fort Monmouth, NJ 07703
1	Commander US Army Jefferson Proving Ground ATTN: STEJP-TD-D Madison, IN 47250
3	Commander US Army Missile Command ATTN: AMSMI-R AMSMI-RDK Mr. R. Deep Mr. R. Becht Redstone Arsenal, AL 35809
1	Commander US Army Tank Automotive Command ATTN: AMSTA-RHFL Warren, MI 48090
2	Commander US Army Mobility Equipment Research & Development Center ATTN: Tech Docu Cen, Bldg. 315 AMSME-RZT Fort Belvoir, VA 22060
1	Commander US Army Armament Command Rock Island, IL 61202
4	Commander US Army Picatinny Arsenal ATTN: SARPA-AD, S. Wasserman SARPA-FR-S-A Mr. A. Loeb Mr. D. Mertz Mr. E. Falkowski Dover, NJ 07801

DISTRIBUTION LIST

No. of Copies	Organization
1	Commander US Army Harry Diamond Laboratories ATTN: AMXDO-TI 2800 Powder Mill Road Adelphi, MD 20783
1	Commander US Army Materials and Mechanics Research Center ATTN: AMXMR-ATL Watertown, MA 02172
1	Commander US Army Natick Laboratories ATTN: AMXRE, Dr. D. Sieling Natick, MA 01762
1	Commander US Army Research Office (Durham) ATTN: CRD-AA-EH Box CM, Duke Station Durham, NC 27706
3	Commander US Naval Air Systems Command ATTN: AIR-604 Washington, DC 20360
3	Commander US Naval Ordnance Systems Command ATTN: ORD-0632 ORD-035 ORD-5524 Washington, DC 20360
1	Commander US Naval Ship Research and Development Center ATTN: Dr. S. de los Santos Aerodynamics Lab Washington, DC 20007
2	Commander US Naval Weapons Center ATTN: Code 503, W. Haseltine Code 5115, A. Charters China Lake, CA 93555
3	Commander US Naval Ordnance Laboratory ATTN: Code 031, Mr. K. Lobb Code 312, S. Hastings Mr. F. Regan Silver Spring, MD 20910
2	Commander US Naval Weapons Laboratory ATTN: Dr. W. Kemper Mr. C. Wingo Dahlgren, VA 22448
1	AFATL (DLR) Eglin AFB, FL 32542
1	AFATL (DLRD) Eglin AFB, FL 32542
1	AFATL (DLRV) Eglin AFB, FL 32542
1	Director Jet Propulsion Laboratory ATTN: Mr. B. Dayman 4800 Oak Grove Drive Pasadena, CA 91103
1	Calspan Corporation ATTN: Mr. J. Andes, Head Transonic Tunnel Dept P. O. Box 235 Buffalo, NY 14221
1	Sandia Corporation ATTN: Division No. 9322 Mr. Warren Curry P. O. Box 5800 Albuquerque, NM 87115

DISTRIBUTION LIST

No. of Copies	Oranization
1	Space Research Corporation ATTN: Dr. G. Bull North Jay Road, Box 281 North Troy, VT 05859
2	Massachusetts Institute of Technology ATTN: Prof. E. Covert Prof. C. Haldeman 77 Massachusetts Avenue Cambridge, MA 02139
1	MIT/Lincoln Laboratories ATTN: Dr. Milan Vlajinac Mail Stop D-382 P. O. Box 73 Lexington, MA 02173

No. of Copies	Organization
1	University of Virginia Department of Aerospace Engineering and Engineering Physics ATTN: Prof. I. Jacobson Charlottesville, VA 22904

Aberdeen Proving Ground

Dir, USAMSAA
Cdr, USAEA
ATTN: SAREA-DE-W
Mr. A. Flatau
Mr. J. Huerta